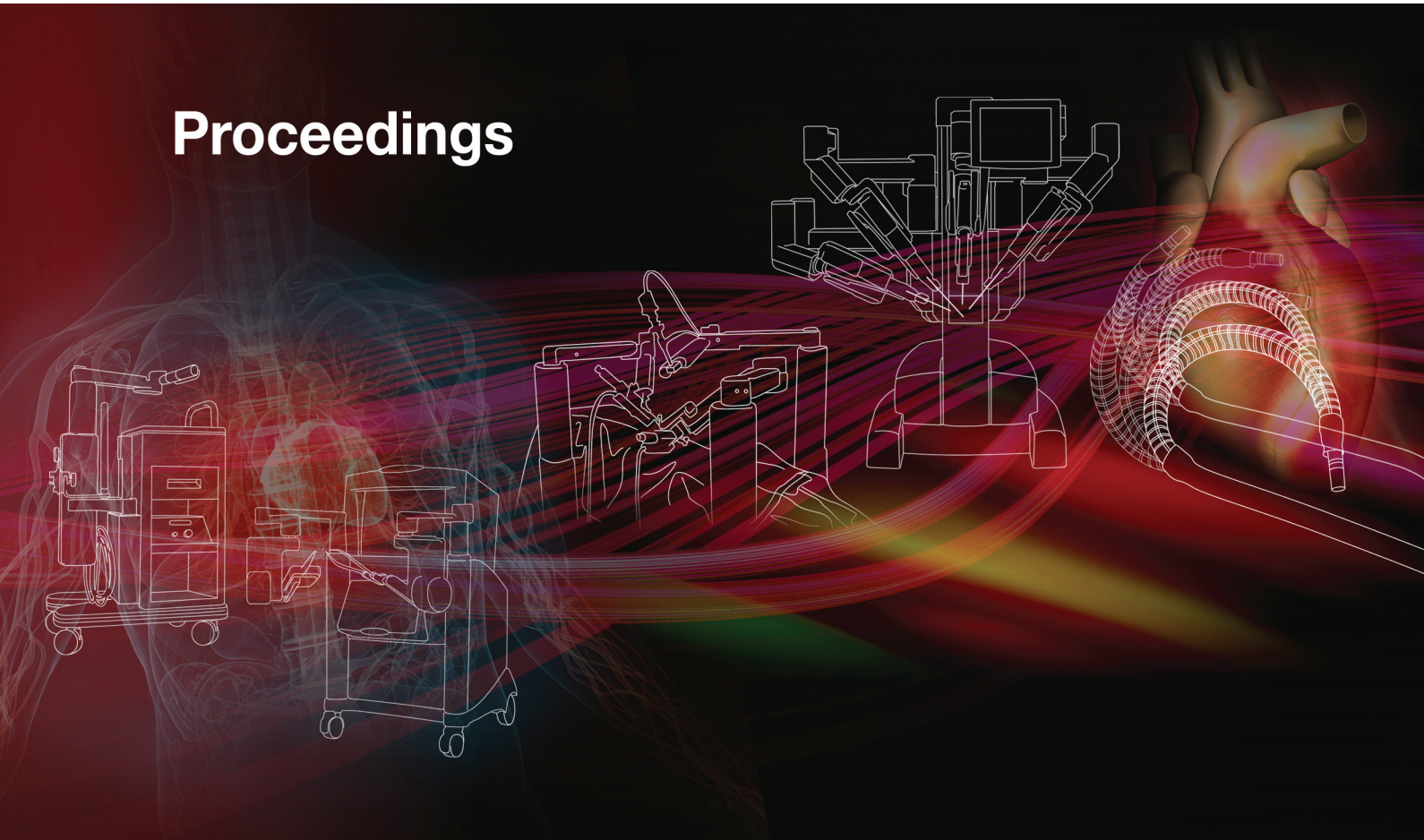


GZ Yang and A Darzi (Eds.)

Proceedings



The Hamlyn Symposium on Medical Robotics

25 May, The Royal Society, London UK

Proceedings

Guang-Zhong Yang and Ara Darzi (Eds.)

The Hamlyn Symposium on Medical Robotics

25 May 2010

The Royal Society, London, UK

Proceedings of
The Hamlyn Symposium on Medical Robotics
25 May, 2010, The Royal Society
London, UK
ISBN: 978-0-9563776-1-6

Preface

The 3rd Hamlyn Symposium on Medical Robotics was held at the Royal Society in London, UK on 25th May, 2010. Medical robotics and computer assisted surgery are used in a growing number of operating rooms around the world. The need to perform delicate surgical procedures safely in tight spaces where the surgeon cannot see directly has created a growing demand for devices that act as extensions of the surgeon's eyes and hands. This creates a unique opportunity to develop new robotic devices that build on the latest advances in imaging, sensing, mechatronics, and machine vision.

The Hamlyn Symposium grew out of Imperial College's Cross Faculty Workshops on Medical Robotics funded by the Hamlyn Centre for Robotic Surgery. Establishing this centre was made possible through philanthropic support from both the Helen Hamlyn Trust and Lady Hamlyn personally. The focus of the symposium this year was to develop robotic technologies that are safe, intelligent, cost effective and accessible to patients. It aimed to promote the integration of robotics in medicine and patient care, and provide a regular forum for surgeons, engineers and researchers in basic sciences to exchange ideas and explore new challenges and opportunities in robotic surgery. This year, we attracted 52 papers from 10 countries and after systematic peer review, 37 papers were selected for presentation at the Symposium. The topics covered range from clinical highlights and multi-specialty applications of robotic surgery, new engineering platform designs, intra-operative imaging and navigation, human robot interaction, ergonomics, to economic and general considerations of robotic surgery in routine clinical settings.

In addition to the excellent papers and posters presented by the participants, one highlight of the Symposium was the lively yet insightful panel debate on the social, economic and patient benefit of robotic surgery. The views presented touched upon some of the fundamental issues related to the development and introduction of new technologies to the healthcare systems. It also highlighted the importance of ensuring tangible patient benefit, as well as wider, more equal access of these new technologies to patients. Focusing on technological innovation but with a strong emphasis on clinical translation and direct patient benefit is a key message derived out of this debate. We hope such a forum will become a tradition of the symposium and the unique mixture of the clinical and technical audience will steadily grow in future years.

We would like to thank the entire Programme Committee, the Best Paper Awards Committee and the Local Organising Committee for giving up their precious time ensuring timely review of all the papers submitted and helping to provide an excellent symposium programme. The meeting wouldn't be possible without the commitment and hard work of a dedicated team. In particular, we are grateful to Karen Kerr, Isobel Anderson, Raphaela Raupp, Sejal Jiwan, Robert Merrifield, Daniel Elson, Su-Lin Lee and Adrian Chung for working behind the scenes and for their tireless effort in managing all aspects of the symposium organisation.

It was our pleasure to welcome the Symposium attendees to London. We were fortunate and privileged to have the Royal Society as the venue of the Symposium. Situated in the heart of central London, it is just a short walk away from key landmarks such as Buckingham Palace, Pall Mall and St James Park. We trust that the attendees also took the opportunity to explore the rich culture and history of the city during their stay in London.

May 2010

Guang-Zhong Yang
Ara Darzi

Organisation

General and Programme Co-Chairs

Guang-Zhong Yang
Lord Ara Darzi

Programme Committee

Pietro Cerveri	<i>Politecnico di Milano</i>
Nick Cheshire	<i>Imperial College London</i>
Paolo Dario	<i>Scuola Superiore Sant'Anna, Pisa</i>
Prokar Dasgupta	<i>King's College London</i>
Hubertus Feussner	<i>Technical University Munich</i>
Gabor Fichtinger	<i>Queen's University Canada</i>
Blake Hannaford	<i>University of Washington</i>
Koji Ikuta	<i>Nagoya University, Japan</i>
Branislav Jaramaz	<i>Carnegie Mellon University</i>
Gabor Kosa	<i>ETH Zürich</i>
Jacques Marescaux	<i>University Hospital, Strasbourg</i>
Nassir Navab	<i>Technical University Munich</i>
Bradley Nelson	<i>ETH Zürich</i>
Vipul Patel	<i>Global Robotic Institute, Florida</i>
Geoff Pegman	<i>R U Robots Limited</i>
Domenico Prattichizzo	<i>University of Siena</i>
Ferdinando Rodriguez y Baena	<i>Imperial College London</i>
Lee Swanstrom	<i>University of Oregon</i>
Mark Talamini	<i>University of California</i>
Russ Taylor	<i>Johns Hopkins University</i>
Chris Thompson	<i>Harvard Medical School</i>
Justin Vale	<i>Imperial College London</i>
Steve Wexner	<i>Cleveland Clinic Florida</i>

Best Paper Awards Committee

Leonard Fass (Chair)	<i>GE Healthcare</i>
Justin Cobb	<i>Imperial College London</i>
Brian Davies	<i>Acrobot & Imperial College London</i>
Patrick Finlay	<i>Prosurgics</i>

Local Organising Committee

Karen Kerr	Su-Lin Lee
Isobel Anderson	Daniel Leff
Thanos Athanasiou	Erik Mayer
Colin Bicknell	George Mylonas
Adrian Chung	Daniel Stoyanov
Daniel Elson	Julian Teare

Table of Contents

Platforms and System Development

Robotic Platform for an Interactive Tele-echographic System: The PROSIT ANR-2008 project	1
<i>A. Fonte, T. Essomba, P. Vieyres, J. Canou, P. Fraisse, S. Zeghloul, A. Krupa, P. Arbeille</i>	
Evaluation of Robotic Endovascular Catheters in Arch Vessel Cannulation	3
<i>C.V. Riga, N.J.W. Cheshire, M. Hamady, C.D. Bicknell</i>	
Software & Hardware Integration of a Biomimetic Flexible Probe within the ROBOCAST Neurosurgical Robotic Suite	5
<i>S.Y. Ko, L. Frasson, B. L. Davies, F.M. Rodriguez y Baena</i>	
Clinical Accuracy of Robot-Assisted Prostate Biopsy In Closed MRI Scanner.....	7
<i>H. Xu, A. Lasso, S. Vikal, P. Guion, A. Krieger, A. Kaushal, L.L. Whitcomb, G. Fichtinger</i>	
Haptic Feedback Modelling during Tool-Tissue Interaction with an Arthoscopic Hooked Probe	9
<i>Y. Tenzer, C. Schwingshackl, A. Gondhalekar, B.L. Davies, F.M. Rodriguez y Baena</i>	
Improving System Accuracy in Computer Aided Robotic ORL Surgery.....	11
<i>B. Bell, N. Gerber, J. Salzmann, E. Nielsen, G. Zheng, C. Stieger, L.P. Nolte, M. Caversaccio, S. Weber</i>	

Clinical Experience and Trials

A dual-centre, cohort comparison of open, laparoscopic and robotic-assisted radical cystectomy	13
<i>O. Elhage, B. Challacombe, M.S. Khan, P. Rimington, B. Coker, D. Murphy, A. Grieve, P. Dasgupta</i>	
Robotic Partial Nephrectomy – First UK Series.....	15
<i>A. Alleemudder, T. Dudderidge, A. Rao, D. Hrouda, J. Vale, B. Khoubehi</i>	
First 500 cases of robotic-assisted laparoscopic prostatectomy from a single UK centre: Learning curves of two surgeons	17
<i>N.L. Sharma, D. Lee, A. Papadopolous, S. Vowler, N.C. Shah, D.E. Neal</i>	

Technological and Clinical Developments

EVOLAP, an Active Laparoscope Positioner devoted to Ergonomics.....	19
<i>B. Herman, B. Raucent, J. Donnez, E. Dombre</i>	

A Novel Articulated Robot for Natural Orifice Transluminal Endoscopic Surgery: Overcoming the Technical Challenges	21
<i>J. Clark, M. Sodergren, D. Noonan, J. Shang, C. Payne, D.R.C. James, T. Athanasiou, J. Teare, A. Darzi, G.-Z. Yang</i>	
Single port manipulator for minimally invasive surgery	23
<i>S. Can, A. Fiolka, A. Schneider, A. Knoll, H. Feussner</i>	
Force Sensor Free Bilateral Teleoperation for Robotic Surgery - Feasibility Evaluation through Human Perception Test.....	25
<i>E. Naerum, B. Hannaford and O.J. Elle</i>	
Bimanual Robot for Single-Port Laparoscopic Surgery with on-board actuation	27
<i>U. Scarfogliero, M. Piccigallo, C. Quaglia, G. Petroni, P. Valdastrri, A. Menciassi, and P. Dario</i>	
Poster Presentations	
The oncological outcomes of Robotic-assisted Radical Prostatectomy in a high volume UK institution	29
<i>T. Dudderidge, L. Lavan, J. Beatty, T. Rashid, E. Wan, B. Challacombe and C. Ogden</i>	
Robotic-Assisted Surgery in the Gulf Cooperation Council.....	31
<i>J. Abi-Nahed, J. Nuyens, B. Abulaban</i>	
Randomised controlled trial of Laparoscopic, <u>OP</u> En and <u>Robot</u> Assisted prostatectomy as treatment for organ-confined prostate cancer	33
<i>E.K. Mayer, D. Piercy, D.C. Cohen, K. Kerr, R. Lewis, C. Corbishley, E. Hall, J. Vale, A. Darzi</i>	
Stereo Video Reconstruction for Registration in Augmented Reality Robotic Radical Prostatectomy.....	35
<i>D. Chen, D. Cohen, D. Stoyanov, A. Anstee, E.K. Mayer, G.-Z. Yang, A. Darzi, P. Edwards</i>	
Using ECG in Motion Prediction for Radiosurgery of the Beating Heart	37
<i>F. Ernst, B. Stender, A. Schlaefer, A. Schweikard</i>	
Spatial awareness enhancement in Natural Orifice Translumenal Endoscopic Surgery (NOTES) by means of an additional visualisation	39
<i>V. Karimyan, F. Orihuela-Espina, D.R.C. James, J. Clark, M. Sodergren, A. Darzi, G.-Z. Yang</i>	
Image Guided Robotic Radical Prostatectomy	41
<i>S. Thompson, G. Penney, D. Hawkes, O. Elhage, and P. Dasguta</i>	
A Single Centre Experience of Robot-Assisted Laparoscopic Pyeloplasty	43
<i>C. Slawinski, O. Elhage, B. Challacombe, N. Hegarty, P. Dasgupta</i>	
Swimming Micro Robot for Ventricular Capsule Endoscopy	45
<i>G. Kósa, G. Székely</i>	

Analysis of endorectal probe kinematics during prostate biopsies	47
<i>C. Torterotot, P. Mozer, M. Baumann, M.-A. Vitrani, G. Morel</i>	
Three Dimensional Tracking and Image Registration Using a da Vinci Triple Endoscope System	49
<i>N.T. Clancy, D. Stoyanov, V. Sauvage, D.R.C. James, G.-Z. Yang, D.S. Elson</i>	
Design of A Robotic Accessory for Abdominal Surgery	51
<i>B.R. Reddi, U.Grandhi</i>	
An assessment of the physical impact of a complex surgical task on surgeons: comparison between robotic assisted, laparoscopic and open techniques.....	53
<i>O. Elhage, B. Challacombe, A. Shortland, P. Dasgupta</i>	
First Surgical Procedures under Camera-Augmented Mobile C-arm (CamC) guidance	55
<i>S. Weidert, L. Wang, J. Landes, A. von der Heide, N. Navab, E. Euler</i>	
Realistic simulation of catheters and guidewires in vascular interventional radiology	57
<i>V. Luboz, T. Odetoyinbo, J. Zhai, P. Littler, T. How, D. Gould, F. Bello</i>	
Dynamic Modeling of a Multipart Probe for Soft Tissue Intervention: Simulation Preliminaries	59
<i>E. S. Nobari, F.M. Rodriguez y Baena</i>	
Force vs. Displacement during Tool Insertion: Techniques and Modelling Approaches	61
<i>T. Parittotokkaporn, P. Degenaar, B.L. Davies, F.M. Rodriguez y Baena</i>	
Design of a Magnetically Activated Stereoscopic System for Single Port Laparoscopy	63
<i>M. Silvestri, M. Simi, C. Cavallotti, M. Vatteroni, P. Valdastrri, A. Menciassi, P. Dario</i>	
A Multimodal Silicone Phantom for Robotic Surgical Training and Simulation	65
<i>M. Lerotic and S.-L. Lee</i>	
Health Economics and Robotic Knee Replacement Surgery	67
<i>S.A. Hurst, J.P. Cobb</i>	
Maintaining Constant Tissue Contact Force for an Imaging Probe during Confocal Laser Endomicroscopy	69
<i>D.P. Noonan, C.J. Payne, J. Shang, R. Newton, A. Darzi, G.-Z. Yang</i>	
Design of a Flexural Transmission for a Dexterous Telesurgical Robot for Throat and Upper Airway: A Preliminary Result	71
<i>C.H. Kuo, R.H. Taylor, J.S. Dai, I. Iordachita</i>	
Robotic Assisted Parathyroidectomy	73
<i>N. Tolley, A. Arora, F. Palazzo, G. Garas, E. Edwards, R. Dhawan, J. Cox, A. Darzi</i>	
Author Index	75

Robotic Platform for an Interactive Tele-echographic System: The PROSIT ANR-2008 project

The PROSIT consortium: PRISME institute¹ Orleans University, Robosoft², LIRM Montpellier University II³, PPRIMME⁴ Poitiers University, INRIA Rennes⁵, INSERM 930-UMPS⁶ Tours University,

¹*aicha.fonte@univ-orleans.fr*, ^{4,1}*Terence.Essomba@etu.univ-poitiers.fr*,
¹*pierre.vieyres@bourges.univ-orleans.fr*, ²*joseph.canou@robosoft.fr*, ³*fraise@lirmm.fr*,
⁴*Said.Zegloul@lms.univ-poitiers.fr*, ⁵*Alexandre.krupa@irisa.fr*, ⁶*arbeille@med.univ-tours.fr*

INTRODUCTION

One of telemedicine's major applications is to provide skilled medical care to patients who are in some way isolated from the specialised care they need while maintaining high quality and controlled interactions with the distant experts. This is especially the case for patients living in isolated areas with reduced or substandard medical facilities. As ultrasound imaging is becoming more and more a part of emergency medical or surgical decision-making, there is a greater need for this technique to be accessible in a majority of the isolated areas lacking ultrasound specialists.

However, this specialised image investigation is an "expert-dependant" technique. Hence in the last decade, several robotized telemedicine concepts and scenarios have been investigated [1]. While this first generation of simple tele-echographic systems are now commercially made available by Robosoft (F), the potential market can only be addressed with more sophisticated interactive functionalities. This is the main goal of PROSIT ANR French national project [2], as these new interactive functionalities require scientific and technology breakthroughs.

PROSIT goal is to develop an interactive and complex master-slave robotic platform for a tele-echography diagnosis application. The development of this platform is based on the expertise of six partners: PRISME (Orleans University-coordinator), Robosoft, INRIA Rennes [3], LIRMM [4] (Montpellier II), PPRIMME [5] (Poitiers university) and INSERM930 [6] (UMPS-Tours University). In this paper, we will focus on the bilateral teleoperation issue and more specifically on the input device; its role is to provide the medical expert with a close rendering of the distal environment, that is the contact force between the ultrasound probe held by the robot end-effector and the patient's body.

MATERIALS AND METHODS

The PROSIT tele-echography platform is a teleoperation scheme composed of three main parts (fig. 1):

- The expert station: the medical expert receives the patient ultrasound images and uses a dedicated input device to control the orientations of the end-effector,
- The patient station: a robotic mobile emergency unit combined with an ultrasound device. A paramedical assistant maintains the probe holder robot on a chosen patient's anatomical area according to the expert's needs,
- The communication link that provides a minimum 256kbps bandwidth (terrestrial, satellite...)

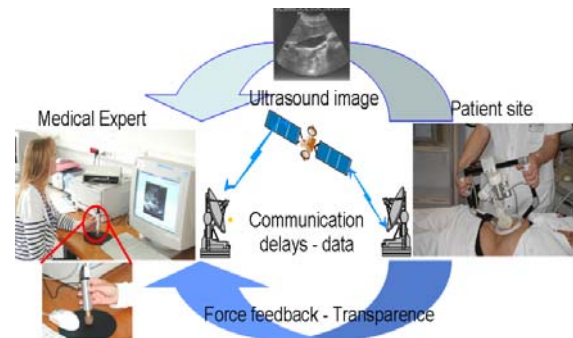


Fig. 1 Platform developed for PROSIT with a dedicated hand-free input device on the expert side, and probe holder maintained by the paramedical assistant on the patient side.

When the robot end-effector is equipped with a force sensor (Fig. 2), it provides the force information of the robot interaction with its environment that can be fed back to the operator via the communication network. The rendering of the distal environment properties (e.g. impedance of the patient's body) to the human operator is performed using a haptic input device. PROSIT challenge is to design a new bilateral teleoperated scheme based on a hand-free haptic device (fig.3). In order to provide the medical expert with the best transparency and robust solutions, one has to take into account the consequences of variable time-delays problems inherent to the Internet communication links. Several approaches are being currently tested within PROSIT Framework; one being developed by Fraise [4] proposing a robust control force strategy by considering the upper boundaries of the environment stiffness and the static gain of the dynamic model. The other scheme under development is based on the network theory approach [7, 8] to maintain transparency and minimum steady state error in force and position

using the passivity of the wave variables properties of [9,10].



Fig. 2: 4 DOF PROSIT-0 prototype, the prismatic z axis carries the ultrasound probe and maintains it in contact with the patient's skin and is based on the PRISME patent [10]

The development of these schemes as well as of the haptic device is based on the users requirements defined by INSEM390 partner using developed robotic mechanical architecture [6].

RESULTS

The first PROSIT prototype has been built. It is a 4-DOF serial type robot with a remote centre of motion. This RCM corresponds to the contact of the ultrasound probe tip with the patient's skin. The prismatic z-axis enables to exert a maximum force of about 20N on the patient's body. One of the main characteristics is that it can hold any type of ultrasound probes used in the medical radiology department; it is under technical and clinical tests with Tours university hospital. This prototype is teleoperated via any communication links and using a passive input device with a flock of bird (FOB) position sensor from ascension technology. However, to satisfy the users requirements and improve the system transparency, a new hand-free haptic device for PROSIT has been designed; it has a similar appearance as of a standard ultrasound probe; it is a light and easily transportable, active haptic system.

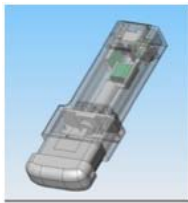


Fig. 3: Haptic probe CAD providing the environment impedance variations to the operator

It integrates inertial sensors and an accelerometer in order to obtain angular and displacement variations in order to register the expert's hand movements; these sensors are an alternative to the FOB system as they are not sensitive to electromagnetic fields. This ergonomic haptic probe integrates a force sensor and an actuator to provide, a good rendering of the environment impedance variations during the tele-echography act. The position accuracies have been assessed using the Vicon Nexus motion capture system. A force sensor at the slave system provides the force applied by the ultrasound sensor on the patient's skin and sends the information in real time to the master site.

DISCUSSION

On the clinical aspect, the tele-echography robotised system performance is evaluated by comparing it to a conventional echography done on the same patient. The medical team evaluates a score expressed as a percentage of the number of patients for whom the organs could be visualised using the robot with respect to the number of patients for whom all organs could be visualised using conventional echography. With this prototype, 87% of abdominal robotic echographies were successful in visualising all the set of organs needed to provide a reliable diagnosis. These preliminary results show the need of such a system in comparable emergency situations. In order to improve these results, visual servoing will be added to the system to track a region of interest of the ultrasound image to compensate for mechanical defaults or data loss in the communication link.

Acknowledgement: this work is supported by the "Agence Nationale de la Recherche" grant number ANR -CONTINT 017-2008-2011

REFERENCES

- [1] P Vieyres, Section editor, "Echography systems and services", in M-health, Emerging Mobile health Systems book, Springer publisher, ISBN : 0-387-26558-9, pp. 441-444, 2006
- [2] PROSIT project web page: <http://www.anr-prosit.fr/PROSITeng/> ;
- [3] R. Mebarki, A. Krupa, F. Chaumette. Image Moments-based Ultrasound Visual Servoing. ICRA'08, Pasadena, CA, May 2008.
- [4] P. Fraisse, P. Dauchez, F. Pierrot, Robust Force Control Strategy based on Virtual Environment, Advanced Robotics Journal, Robotics Society of Japan, vol 21, N°3-4, pp.485-498, 2007.
- [5] JP Gazeau; S. Zeghloul, G Ramirez, Manipulation with a polyarticulated mechanical han: a new efficient real-time method for computing fingertip forces for a global manipulation strategy, Robotica, Vol. 23; 479-490, 2005.
- [6] Arbeille P, Capri A, Ayoub J, Kieffer V, Poisson G. Use of a robotic arm to tele operated abdominal ultrasound. Am J Roentgenology ; AJR; 188: 317-322. 2007.
- [7] A. Fonte, F. Courrèges, G. Poisson, P. Vieyres : Bilateral control based passivity concept : application to Tele-echography. 10th IEEE Inter. Conf. on MMAR2004, Miedzyszdroje, Poland, 30Aug.-2Sept 2004
- [8] A. Aziminejad, M. Tavakoli, R.V. Patel, and M. Moallem, Wave-based time delay compensation in bilateral teleoperation: Two-channel vs four-channel architectures, A. Control Conf., pp.1449-1454, July 2007.
- [9] W.S. Kim, B. Hannaford, and A.K. Fejczy, "Force-reflection and shared compliant control in operating telemanipulators with time delay", IEEE TRA, vol. 8, no. 2, pp. 176-185, April 1992
- [10] N.A. Tanner and G. Niemeyer, "Online tuning of wave impedance in telerobotics", IEEE Conf. on Robotics, Automation and Mechatronics, vol. 1, pp. 7-12, Dec. 2004
- [11] Patent N° n°9903736 « three degree-of-freedom and RCM robot- Université d'Orléans; 25 march 1999

Evaluation of Robotic Endovascular Catheters in Arch Vessel Cannulation

Riga CV^{1,2}, Cheshire NJW^{1,2}, Hamady M³, Bicknell CD^{1,2}

¹Department of BioSurgery & Surgical Technology (SORA)

²Department of Vascular Surgery

³Department of Interventional Radiology

Imperial College London

c.riga@imperial.ac.uk

INTRODUCTION

Conventional catheter instability and the risk of cerebral embolization may limit the uptake of minimally invasive endovascular procedures in patients with challenging aortic arch anatomy. Efficient stable sheath placement in the common carotid artery (CCA) is a crucial determinant of success in carotid artery stenting (CAS) in particular, avoiding embolisation secondary to manipulation in the arch and CCA origin as well as ensuring a stable platform for introduction of endovascular tools into the internal carotid artery (ICA). The purpose of this study was to investigate whether complex endovascular arch vessel intervention can be enhanced by a remotely-steerable robotic catheter system.

MATERIALS AND METHODS

The Sensei™ System (Hansen Medical, Mountain View, Ca) is a remotely steerable catheter system controlled via a “master–slave” electromechanical mechanism. The workstation console is remote and away from the radiation source, and displays imaging and catheter tip force sensing feedback data, for planar orientation and navigation. The robotic catheter consists of a flexible, multidirectional inner guide (11-French (Fr) outer diameter, 8.5-Fr inner diameter) with a 270° bend radius and 7 degrees of freedom, inside a unidirectional outer guide sheath (14-Fr outer diameter, 11-Fr inner diameter); standard endovascular tools can be inserted through its lumen.



Fig 1- The robotic workstation
17 operators (9 vascular surgeons, 7 interventional radiologists, 1 cardiologist) of varying endovascular experience were recruited to participate in the study.

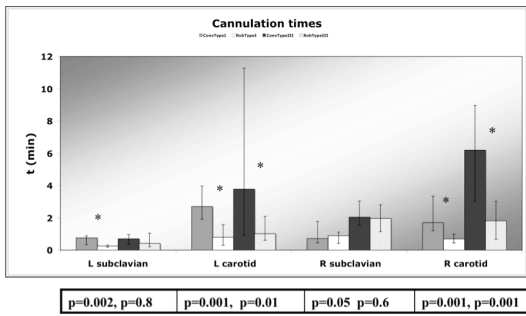
Each operator was asked to cannulate the left subclavian (LSA), left common carotid (LCCA), right subclavian (RSA) and right common carotid (RCCA) arteries within 2 within CT-reconstructed pulsatile flow phantoms representing a Type-I and a Type-III aortic arch configurations, under fluoroscopic guidance, using conventional and robotic techniques. Operators were randomly assigned to conventional or robotic techniques as the first procedure undertaken. The phantoms were filled with a blood-mimicking water-glycerol mixture (60:40 by volume concentration) and circulated using a pulsatile blood pump providing physiologically realistic blood-flow waveforms. All procedures were performed in the angiography suite and recorded for blinded video assessment.

Quantitative (vessel cannulation times, wire/catheter tip movements, and vessel wall hits) and qualitative metrics (using a validated procedure-specific-rating scale (IC3ST)) assessed by two blinded observers (Cronbach's $\alpha=0.94$) were compared.

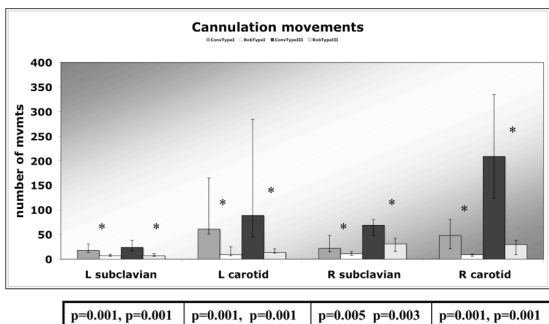
Mere arch vessel cannulation, however, does not necessarily reflect technical success in complex endovascular procedures such as CAS. Equally important is the ability to advance stiff-guidewires and other endovascular tools whilst maintaining stability at target sites. In order to determine the stability of the robotic catheter during stiff-guidewire exchanges, an adjunctive study was carried out: A single experienced operator cannulated the LCCA and RCCA using standard-Terumo wires, which were then exchanged for 0.035-inch stiff-guidewires under fluoroscopy, using robotic and conventional catheters. Exchanges took place at 3 distinct points, with the catheter-tip at: 4cm (Point-A), 2cm (Point-B) and 0cm (Point-C) from the carotid artery ostium. Five commonly used, conventional catheters were tested. 108 stiff-guidewire exchanges in total were recorded for video-assessment. Catheter tip deflection from each point during guidewire exchanges (distance in cm) was measured in a 2-dimensional plane using the recorded digital images.

RESULTS

Times: the median times for cannulation of the carotid arteries were significantly reduced using the robotic catheter system for both type arches:

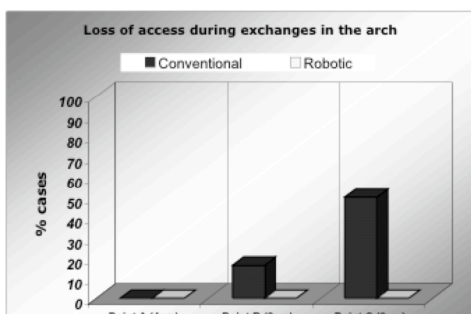


Movements: the median number of movements at the wire/catheter tip was also significantly reduced for all vessels with robotic catheterization techniques for both type arches:



Embolization risk: vessel wall contact with the aortic arch wall was reduced to a median of zero with robotic catheterizations. CCA ostium contact still took place, but was significantly reduced. Median catheter tip vessel wall hits were: Type-I Arch: 2 IQR(1.5 – 13) versus 0(0-0) ; p=0.001 for the aortic arch and 4.5 (3.5 – 11.3) versus 2 (1.5 - 3.5); p=0.001 for the CCA origin, and Type-III Arch: 13.8 (9.5 -19) versus 0.5 (0.3 – 1.5); p=0.001 for the aortic arch and 9 (5 -21.5) versus 5 (4 - 9); p=0.04 for the CCA origin.

Stability: In 36 procedures studied (108 stiff guidewire exchanges), robotic endovascular catheters maintained stability at target sites with zero deflection during stiff guidewire exchanges, independent of the distance the catheter was introduced into the carotid vessels. Median conventional catheter deflection was: point-A (4cm into the carotid artery), 0cm(0-0); point-B (2cm into the carotid artery), 0cm(0-4.5) with complete loss of access in 16.7% of cases; point-C (at the CCA origin), 7cm(1.3-9.8) with complete loss of access in 50% of cases. No statistically significant differences between robotic and conventional catheters were observed for points A and B (p=0.47). Robotic catheters, however, demonstrated increased stability at point C; ie at the CCA origin (p=0.03).

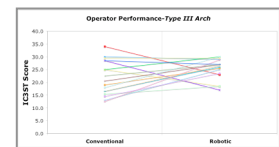
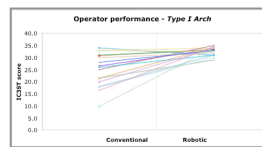


Operator Performance:

Overall performance scores were significantly improved using the robotic system:

Type I Arch: IC3ST score 26/35 IQR (20 -30.8) versus 33/35 (31 -34); p=0.001. 88.2% (15/17) of operators improved their scores using the robotic catheter system. With conventional cannulation, IC3ST scores ranged from 10 to 34, with 76.5% (13/17) of operators demonstrating competence in this model. Robotic cannulation scores ranged from 29 to 34.5, with all 17 operators achieving high-standard performance scores.

Type III Arch: IC3ST score 20.5/35 IQR (16.5-28.5) versus 26.5/35 (23.5 -28.8); p=0.001. 70.6% (12/17) of operators improved their scores using the robotic catheter system. Scores ranged from 12.5 to 34 with conventional techniques, and a mere 47% (8/17) of operators (8/17) demonstrated competence in the angulated aortic arch, whereas with robotic techniques, IC3ST scores ranged from 17 to 30, and 82.4% of the operators attained performance scores at the high-end of the IC3ST scale.



CONCLUSION

For complex endovascular procedures, such as CAS, intuitive robotic endovascular catheters may overcome some of the limitations of standard catheter technology, potentially reduce procedure times, reduce catheter dislodgement, embolization risk and vessel trauma, reduce radiation exposure and improve overall performance scores.

REFERENCES

- [1] Mas JL, Trinquart L, Leys D et al. Endarterectomy versus angioplasty in patients with symptomatic severe carotid stenosis (EVA-3S): a randomised trial. results up to 4 years. Lancet Neurol 2008;7:885e92.
- [2] Ederle J, Featherstone RL, Brown MM. Randomized controlled trials comparing endarterectomy and endovascular treatment for carotid artery stenosis: a Cochrane Review. Stroke 2009;40: 1373e80.
- [3] Riga CV, Cheshire NJW, Hamady M, Bicknell CD. The role of robotic endovascular catheters in fenestrated stent grafting. J Vasc Surg 2010, Apr;51(4):810-9; discussion 819-20.
- [4] Riga CV, Bicknell CD, Cheshire NJW, Hamady M. Initial clinical application of a robotically steerable catheter system in endovascular aneurysm repair. J Endovasc Ther 2009;16:149–53.

Software & Hardware Integration of a Biomimetic Flexible Probe within the ROBOCAST Neurosurgical Robotic Suite

S. Y. Ko¹, L. Frasson^{1,2}, B. L. Davies^{1,3}, F. Rodriguez y Baena^{1,2}

¹Department of Mechanical Engineering, Imperial College London, UK

²Institute of Biomedical Engineering, Imperial College London, UK

³Italian Institute of Technology, Italy
f.rodriguez@imperial.ac.uk

INTRODUCTION

Recent trends in surgical treatment show a preference for minimally invasive surgery (MIS) due to, among others, the benefits of reduced scarring, shorter hospitalization and lower treatment cost. MI neurosurgery is often referred to as ‘keyhole neurosurgery’ [1], since the operation is performed through a small circular opening in the skull (keyhole). Most keyhole neurosurgical procedures are performed through rigid needles, as the tip can be easily localized by detecting the position of the proximal end by means of mechanical or optical tracking systems. Recently however, there have been efforts to introduce a flexible probe to keyhole neurosurgery, which could enable access to deep lesions, which would otherwise be difficult to reach with a rigid probe. In this context, a neurosurgical robotic suite is currently being developed within the context of the ROBOCAST Project (ROBOT and sensors integration for Computer Assisted Surgery and Therapy) [2], where a novel flexible probe, inspired by the ovipositor of parasitic wasps [3], is being

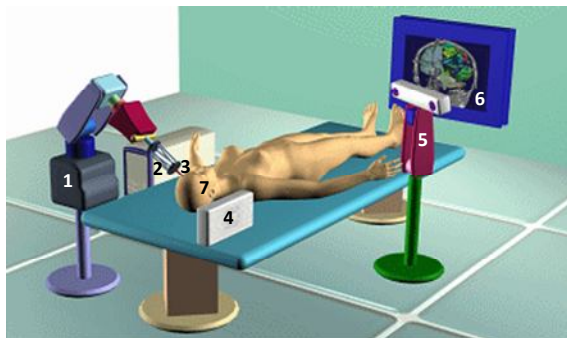
developed by Imperial College (one of the consortium partners) as an end-effector for the system. This paper focuses on aspects of hardware and software integration for the bio-inspired flexible probe, which has enabled modular and seamless integration with other subsystems within the ROBOCAST project.

THE ROBOCAST SYSTEM AT A GLANCE

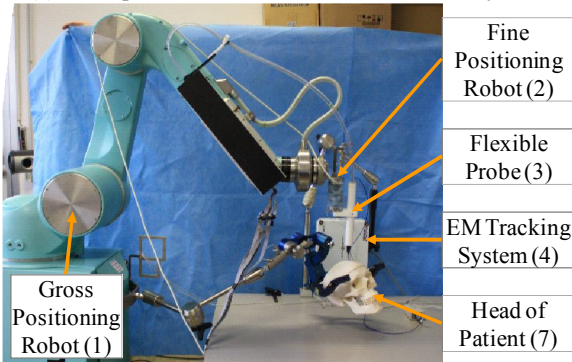
Fig. 1 shows conceptual (a) and real (b) embodiments of the ROBOCAST neurosurgical system. A 6-degree-of-freedom (DOF) serial gross-positioning (GP) robot (1) and a 6-DOF parallel fine-positioning (FP) robot (2) are utilized to support and place a flexible probe (3) near the head of a patient (7). An electromagnetic (EM) tracking system (4) is located in proximity to the patient’s skull to measure the tip position of the flexible probe inside the patient’s brain. An optical tracking system is introduced to monitor robot end effectors and the rigid frame attached to the patient’s head. Pre-operative path planning and intra-operative visualization are performed on the touch screen of a bespoke surgical workstation (6), which is also in charge of maintaining accuracy and patient safety under all operative conditions.

HARDWARE INTEGRATION

The flexible probe capable of two-dimensional trajectory following, currently being developed at Imperial College, takes inspiration from the ovipositor of parasitic wasps. The ovipositor itself does not have any intrinsic musculature; instead, the ovipositor is manipulated remotely by musculature which resides in the metasoma (i.e. the posterior part of the insect’s body). This characteristic also motivates the actuation



(a) Concept Embodiment of the ROBOCAST System



(b) Real Embodiment of the ROBOCAST System

Fig. 1. The ROBOCAST System at a Glance

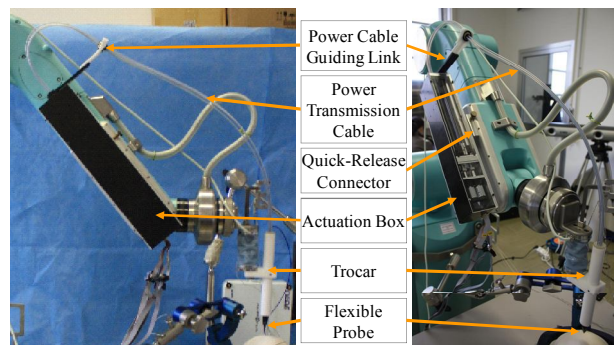


Fig. 2. Actuation System for the Flexible Probe

system of our current prototype, as shown in Fig. 2. The actuation box consists of linear actuators, each of which manipulates the corresponding segment of the probe remotely, through a power transmission cable. The cable itself consists of super-elastic shape memory alloy (SMA) wires, which transmit mechanical power to the probe; a protective PTFE (i.e. Teflon) sleeve is used to minimize friction during motion.

In order to guide the flexible probe to a keyhole in the skull, a custom-made trocar is attached to the FP robot. With a full stroke of approximately 200mm, 1.5mm thick SMA wires are used to prevent buckling. Finally, in order to reduce the force exerted by the power transmission cable on the probe and/or the trocar, a bespoke guiding link is placed on the actuation box, as shown in Fig. 2.

In the operating scenario of ROBOCAST, the GP and the FP robots first move to a pre-operatively determined optimal position and orientation which places the trocar in the correct alignment for probe insertion. The actuation box is then positioned on the GP robot using a quick-release connector, employing a groove and inset combination to ensure a stiff and reliable interlock with little time penalty. At this stage, the flexible probe is inserted into the trocar, which is connected to the FP robot. The flexible probe is then ready to move when a motion command is issued.

SOFTWARE INTEGRATION

In order to facilitate software integration among the consortium partners, the communication between subsystems is implemented through a common object request broker architecture (CORBA) interface [4], as illustrated in Fig. 3. Each subsystem's software has its own CORBA server, through which other subsystems can communicate. Within this context, the flexible probe is controlled by a high-level controller (HLC, responsibility of the University of Karlsruhe, Germany), which is responsible for the correct and safe operation of all subsystems, as well as communication with the surgeon. The HLC delivers a desired trajectory,

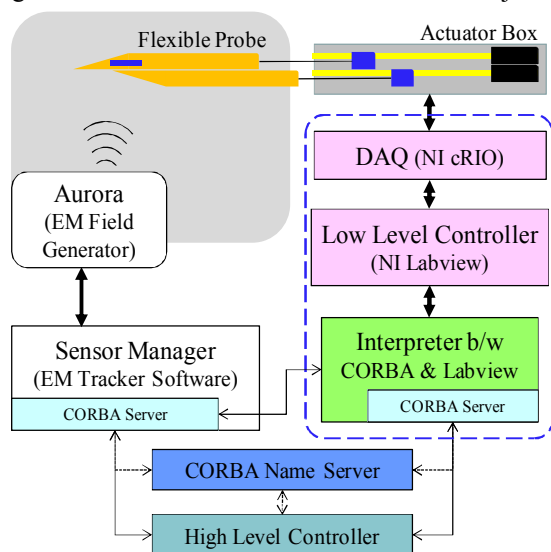


Fig. 3. Software Integration with Flexible Probe

determined by a pre-operative planning application, to the low-level controller (LLC) of the flexible probe. This process also includes the setting up of LLC-specific parameters, such as probe motion speed. The HLC is then responsible for initiating/halting motion and monitoring the probe's status during operation to ensure safety and correct operation at all times.

In order to implement feedback position control of the probe tip, the LLC periodically requests the probe tip position at about 10 Hz from a Sensor Manager (SM, responsibility of Politecnico di Milano, Italy), which also employs CORBA to standardize commands and requests. The SM is responsible for gathering and manipulating information from all of the dynamic reference frames available through the EM and optical tracking systems. On the LLC's request, the sensor manager delivers the latest position/orientation of the tip of the flexible probe, which is then compared to the desired trajectory to produce new control inputs for the probe controller. Here, the position/orientation provided by the SM is already defined in the trocar's coordinate system (i.e. all coordinate transformations are transparently carried out by the SM prior to delivery) to streamline the computational requirements of the position update loop.

CONCLUSION

This article outlines the integration of a novel flexible probe within the ROBOCAST neurosurgical suite. All actuators are separated from the probe and attached to a gross-positioning robot, with actuating force transmitted through a bundle of super-elastic SMA cables. A custom-made trocar, the main function of which is to guide the flexible probe into the skull, is mounted onto the fine-positioning robot. To facilitate software integration, each subsystem is modularized via a CORBA interface. Based on successful hardware and software integration, performance evaluation of the system and its control algorithms is currently underway.

ACKNOWLEDGEMENTS

The support of the EU FP7 programme and the contributions of all ROBOCAST consortium partners are gratefully acknowledged.

REFERENCES

- [1] Perneczky A, Keyhole concept in neurosurgery : with endoscope-assisted microsurgery and case studies. Stuttgart: Thieme, 1999.
- [2] ROBOCAST Project, 2008, Available from: www.robocast.eu
- [3] Frasson L, Ko SY, Turner A, Parittotokkaporn T, Vincent JF, Baena FRY, STING: a soft-tissue intervention and neurosurgical guide to access deep brain lesions through curved trajectories. Proc. IMechE Part H: J. Engineering in Medicine, In press
- [4] Real-time CORBA with TAO™ (the ACE ORB), 2007, Available from: <http://www.cse.wustl.edu/~schmidt/TAO.html>

Clinical Accuracy of Robot-Assisted Prostate Biopsy In Closed MRI Scanner

H. Xu¹, A. Lasso¹, S. Vikal¹, P. Guion², A. Krieger³,
A. Kaushal², L.L. Whitcomb⁴, G. Fichtinger^{1,4}

¹Queen's University, Kingston, Canada; ²National Institutes of Health, Bethesda, USA;
³Sentinelle Medical Inc., Toronto, Canada; ⁴Johns Hopkins University, Baltimore, USA

helen@cs.queensu.ca

INTRODUCTION

Prostate cancer, affecting one in every six men, remains the number one cancer-related death in men [1]. In the pursuit of more accurate biopsy, Krieger and Susil [2,3] developed robotic assistance under MR image guidance. To date, their system has been used in 200+ biopsies at the U.S. National Cancer Institute. A limited validation study was presented earlier [4]. Here we report a more comprehensive retrospective evaluation of the Krieger-Susil biopsy system. We analyze a larger set of patient data in an improved validation workflow and produce a formal statistical analysis and draw strong conclusions.

MATERIALS AND METHODS

Imaging: The patient was placed in the scanner prone, and 2D high-resolution T2 axial volume of the prostate was acquired. The clinician picked biopsy targets in scanner coordinates. The robot was then used to guide a biopsy needle through the rectum into the target sites within the prostate to collect tissue samples. After the needle was in place, 2D axial volume was taken to confirm needle placement. We used these pre and post-needle insertion volumes in our validation.

Registration: Developing a registration algorithm for patient data collected over five years, by many clinicians, with a variety of scanners, imaging protocol, image resolution, field strength, frequency etc. was a challenge. Prostate motion upon needle insertion can be complex as it dislocates differently from surrounding structures, varying from patient to patient. Our goal was to find a method that captures most of the prostate motion for the majority of patients. The pre and post-needle insertions images were examined. We found that while the ensemble of organs moved deformably, each major relevant structures (prostate, rectum, pubic bone) shows little deformation, just recently corroborated by Karnik *et al.* concluded that the results from rigid and non-rigid registration were not statistically significantly different ($p > 0.05$) in transrectal prostate biopsies [5].

We devised a two-step 3D-3D rigid registration scheme using mutual information (MI) to capture this motion. We used the Insight Toolkit to register the pre and post-needle insertion volumes. First, we apply global registration over the rectum, prostate and pubic bone, to capture gross prostate motion in coherence with

robot and patient. Next, we capture residual decoupled prostate motion by further registering the global image with the original fixed image using only the prostate as the region of interest. In doing so, motion in the superior and inferior direction is penalized because the first step should already have corrected for it.

Registration validation: The prostate seldom shows apparent anatomical features in MRI and it can move independently of bony structures, rendering landmark based registration accuracy evaluation inapplicable. Instead, we segmented the prostate, rectum and pubic bone in both the fixed and moving image volumes. Each component organ was registered by aligning surfaces. Finally, the results of surface based prostate registration were compared with the results of MI registration. The transformations of bone and rectum indicated the amount of patient motion during procedure. At least one biopsy for each patient was validated using this method. In addition, all registrations that contained a translation of more than 10 mm were individually validated. Fig. 1 shows the overlay of a segmented model before and after the automatic MI-based registration.

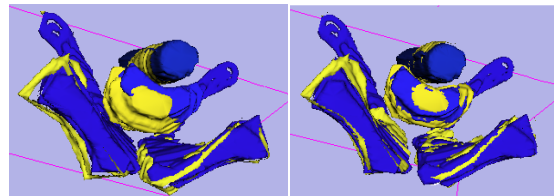


Fig. 1. 3D overlays of segmented rectum, prostate and pubic bone from before (left) and after (right) MI-based registration.

Biopsy Accuracy: We define target displacement as the distance between the original and transformed target (Fig. 2). In order to determine whether this motion is related to the needle insertion direction, the displacement was decomposed into two vectors: one parallel and one orthogonal to the needle. A signed rank test was used to see if prostate motion in the needle direction was significantly larger than the orthogonal one. We define needle placement error as the distance from the original target to the biopsy needle trajectory line (Fig. 2). This is how much the robot missed the intended target in scanner coordinates. The needle trajectory was obtained from rectifying the track in the post-insertion volume. Biopsy error is defined as the distance from the transformed target to the needle line (Fig. 2), which represents the distance between the planned and actual biopsy locations. Since the tissue

biopsy core is over 1.5 cm long, insertion depth is of a lesser issue.

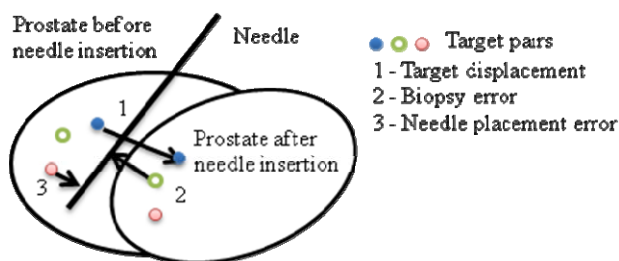


Fig. 2. Illustration of prostate motion during needle insertion and biopsy error calculations.

RESULTS

Registration accuracy: A total of 82 biopsies from 21 patients were evaluated, one half requiring manual validation. Organ segmentation error was about 2 mm. The results from manual registration were used for the ones that were off by 3 mm or more. The inaccuracy was mainly due to poor image quality and patient motion; 11 biopsies contained patient motion greater than 5 mm. After adjustment, all registrations were accurate to 2 mm. **Biopsy accuracy:** Table 1 summarizes the mean, range, and standard deviation for the target displacement, needle placement error, and biopsy error (Fig. 2) of all biopsies and of 11 biopsies which had more than 5 mm patient movement.

Table 1. Data statistics for biopsy accuracy (mm)

	Target disp.		Needle pl.	Biopsy error	
Mean	5.9	7.2*	2.3	4	4.8*
Range	1-13.4	3.7-11.2*	0.1-6.5	0.5-14.1	1.4-8.8*
STD	3.5	2.9*	1.3	2.1	2.3*

* Biopsies for patient motion larger than 5 mm only

Target displacement: Target displacement parallel and orthogonal to the needle direction was also calculated. For the parallel component, 46% of the biopsies moved towards the needle insertion direction (mean distance: 5.7 mm) and 54% went in the opposite direction (mean distance: 2.9 mm). The mean was 4.2 mm in the parallel and 3.4 mm in the orthogonal direction. Results from the Wilcoxon Signed Rank Test showed that parallel motion was not significantly greater than the orthogonal one ($p=0.36$). For the group of patient motion larger than 5 mm, the mean parallel and orthogonal motion was 3.9 mm and 5.3 mm, respectively. To analyze the displacement that was not in the needle direction, the orthogonal component was further decomposed into movements in scanner coordinates. 73% of the biopsies showed a target movement either towards the superior-posterior (SP) or inferior-anterior (IA) direction. However, the correlation coefficient between SI and AP was only 0.56. During MI-based automatic registration validation, the segmented rectum and pubic bone were registered separately. Their motions were different from the motion of the prostate, while bone motion was more similar to prostate motion than to rectum motion.

DISCUSSION

The mean needle placement error (Table 1) is less than clinically significant size of cancer (approx. 4 mm), confirming that the robot is sufficiently accurate if there is no prostate motion. In reality, prostate dislocation cause the target to move, as evident by the 5.9 mm mean average target displacement from the 82 biopsies studied. It results in an average biopsy error of 4 mm, which is on the verge of clinical acceptability.

In the 11 biopsies when patient motion was above 5 mm, we studied the impact of patient motion on biopsy error, revealing that better patient fixation may yield only slight decrease in biopsy error of about 1 mm. The biopsy needle is inserted into the prostate in a mainly superior-anterior direction. It is would be reasonable to assume that the target moves in a direction similar to the needle path. But as statistical tests show no significant difference between target displacement parallel and orthogonal to the needle direction, it means that about half of the displacements were in the needle direction. The other half could be due to patient motion during the procedure, in addition to the impact of needle insertion. Separate registration of the rectum and bone indicates that the prostate can move independently of these two structures. The robot in the rectum limits its ability to move, explaining the observation that prostate moves more with the bone than with the rectum.

In conclusion, even taking into account imperfections of the registration scheme (assuming local rigidity of organs, course out plane resolution, segmentation error), these results clearly and forcefully suggest that motion compensation is necessary before committing the biopsy needle to action. The need for motion tracking is perhaps not surprising, nonetheless this expectation had to be proven and quantified, which is what this paper has achieved.

REFERENCES

- [1] Jemal A, Siegel R, Ward, E, Hao Y, Xu J, Thun M. Cancer statistics. *CA Cancer J Clin.* 2009;59(4):225-49.
- [2] Krieger A, Susil R, Menard C, Coleman J, Fichtinger G, Atalar E, Whitcomb L. Design of novel MRI compatible manipulator for image guided prostate interventions. *IEEE Trans Biomed Eng.* 2008;52(2):295-04.
- [3] Susil R, Menard C, Krieger A, Coleman J, Camphausen K, Choyke P, Fichtinger G, Whitcomb L, Coleman C, Atalar E. Transrectal prostate biopsy and fiducial marker placement in a standard 1.5T magnetic resonance imaging scanner. *J Urol.* 2006;175(1):113-20.
- [4] Xu H, Lasso A, Vikal S, Guion P, Krieger A, Kaushal A, Whitcomb L, Fichtinger G. Accuracy Validation for MRI Guided Robotic Prostate Biopsy. *Proc. SPIE Medical Imaging.* 2010;7625:762517.
- [5] Karnik V, Fenster A, Bax J, Cool D, Gardi L, Gyacskov I, Romagnoli C, Ward A. Assessment of registration accuracy in three-dimensional transrectal ultrasound images of prostates. *Proc. SPIE Medical Imaging.* 2010;7625:762516.

Support: U.S.NIH 5R01CA111288-04, 5R01EB002963-05

Haptic Feedback Modelling during Tool-Tissue Interaction with an Arthoscopic Hooked Probe

Y. Tenzer, C.Schwingshackl, A. Gondhalekar,

B.L. Davies, F.M. Rodriguez y Baena

Mechanical Engineering Department, Imperial College London

ytenzer@ic.ac.uk

INTRODUCTION

Surgical long shape tools, such as the arthroscopic hooked probe, are used during knee-arthroscopy procedures by surgeons to manipulate tissues and diagnose problems. These procedures allow surgeons to assess the physical properties of tissues (such as wear, tear, inflammation, stiffness, etc), which are impossible to evaluate using real-time video observation or MRI and CT mapping. Though manipulating the tissue clearly helps surgeons to diagnose problems, it is not clear which physical properties are significant at the time of interaction between the probe and the tissue.

From previous studies, it is known that when a probe comes into contact with hard tissues, such as bones, vibrations can occur that enhance the tactile feedback.

We first showed that, when a probe comes into contact with a hard surface, such as bone, vibrations occur which potentially enhance the tactile feedback to the surgeon [3]. We then examined the dynamic properties of a hooked probe (probe model 8399.95 by Richard Wolf UK ltd), where it became apparent that tapping on different materials predominantly excites the first vibration mode of the probe and that this frequency does not vary significantly with respect to the properties of the material being tapped. This frequency (which was found to be approximately 500Hz for the probe model used in the experiments) lies within the bandwidth of the human tactile sensory system and will thus be felt by the surgeon during interactions [1,2,4].

This paper reports on a study which was conducted to examine the physical aspects of tool-material interaction by focusing on the dynamic properties of the hooked probe and its ability to deliver tactile information, created at the tip of the hook as the tissue is being manipulated, and perceived at the handle, where the surgeon is grasping the instrument. The dynamic behavior of the probe during an impact is examined. Both probe- and material-dependent parameters are considered, with the aim to formulate a metric able to capture elements of touch perception during the tapping process.

MATERIALS AND METHODS

A tapping experiment was performed and the resulting vibrations, together with the impact forces generated by tapping on different materials, were recorded.

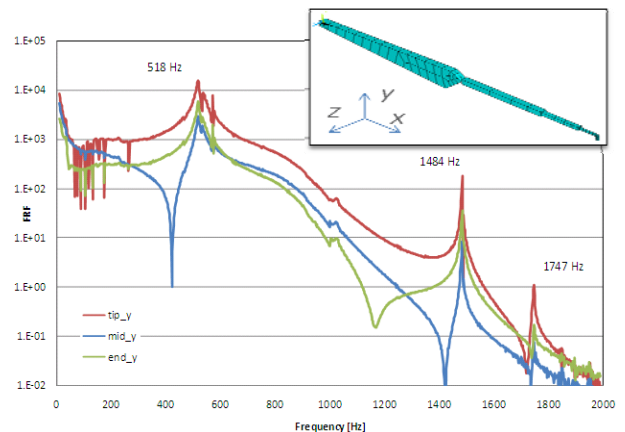


Fig. 1 Vibro-performance of the surgical probe using sine sweep analysis in Y direction, adopted from [4].

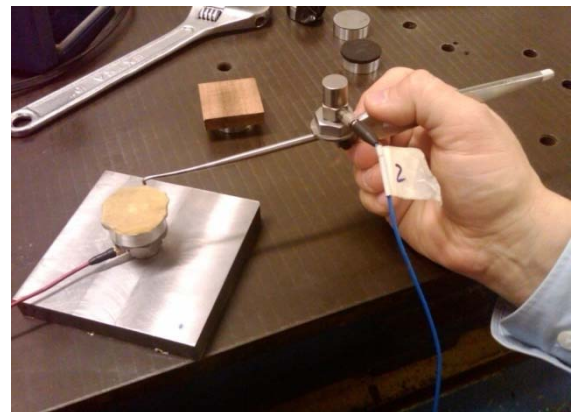


Fig. 2 Experimental setup

Ten subjects were asked to compare the stiffness of five engineering materials (silicon, latex, rubber, wood and steel) by simple tapping (Fig. 2). During the test, each subject was exposed to two materials each time, and pairs of materials were organized to cover all material combinations. The test was repeated two times, leading to 20 comparisons for each subject. Also, every subject was asked to tap three times on every material before making a judgment, which led to a total of 120 recorded taps per subject. During tests, the subjects were blindfolded and white noise was played through headphones to blur the sounds of tapping. The resulting dynamic response of the probe was recorded using an accelerometer (353B03 by PCB Group, Inc.), along with the impact force, measured by a force transducer (B&K 8200) located below the material sample. The data from sensors was acquired using a National Instruments data

acquisition card (NI PXI-4462) and processed using LabView. The response of all subjects about which of any two materials felt stiffer was also recorded.

RESULTS AND DISCUSSION

As previously demonstrated [4], these results show that the vibration response frequency of the probe remains virtually constant throughout all trials, as it is a function of the probe's material, geometry and gripping force/configuration, which did not change significantly in between experiments. With respect to probe-dependent parameters, the ratio between the peak acceleration magnitude (A_{max}) of the probe and the impact force (F_{max}) was computed for all tapping experiments and results show that higher impact force will result in higher acceleration and that this relationship is linear. This implies that user-dependent parameters, such as holding stiffness and position accuracy, have a negligible influence on tapping and confirms that the material properties of the sample do not affect these results. With respect to material-dependent parameters, the duration of the impact (F_{dt}) (measured by the force sensor as the width of the force profile) appears to be inversely proportional to material stiffness, with strong statistical significance (Pearson's correlation coefficient, $r = 0.99$, $p < 0.01$). A box plot illustrating the measured impact duration for all tapping tests arranged by sample is available in Figure 3.

Thus, based on these experimental observations, a new metric is proposed, which is calculated from the force and acceleration data and takes into account the effect of both probe- and material-dependent parameters. The metric, TP, is defined as follows:

$$TP = A_{max}/(F_{max} * F_{dt})$$

A box plot of the proposed metric, arranged by sample material, is shown in Fig. 4. As can be seen, computed TP values for silicon, latex, rubber and wood are significantly different ($p < 0.01$) for each pair, while there is no significant difference ($p = 0.17$) between the TP values of wood and steel; this may explain why, on average, test subjects had difficulty in distinguishing between these two materials. Indeed, while further processing of the results is needed, TP appears to be less correlated to material stiffness ($r = 0.719$, $p = 0.17$) when compared to F_{dt} (Fig. 3), but better correlated to the subjective evaluation of stiffness, as recorded from user trials.

In conclusion, this study provides further confirmation that the frequency of vibrations, as felt by a user's hand during tapping, is not affected by the material properties of the sample being tapped. It also demonstrates that both probe- and material-dependent parameters can be accurately measured and that impact duration correlates strongly with the stiffness of the material being tapped. In an attempt to generalise the touch perception problem, a new metric, TP, is also proposed, which was shown to be repeatable and robust across material samples (Fig. 4). TP also has the potential to be valid across different probes (geometry and material) and a

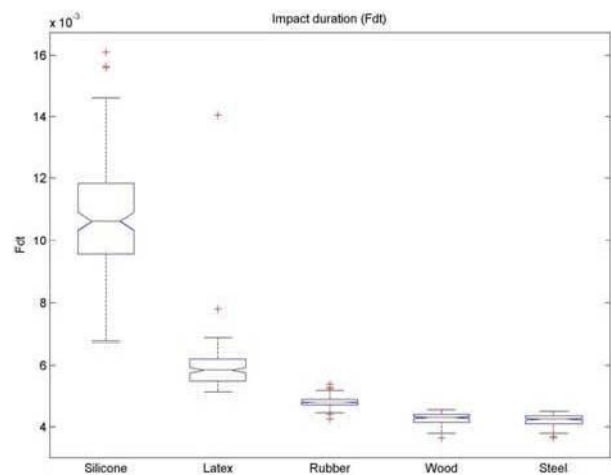


Fig. 3 The measured impact duration for all tapping tests, arranged by material sample.

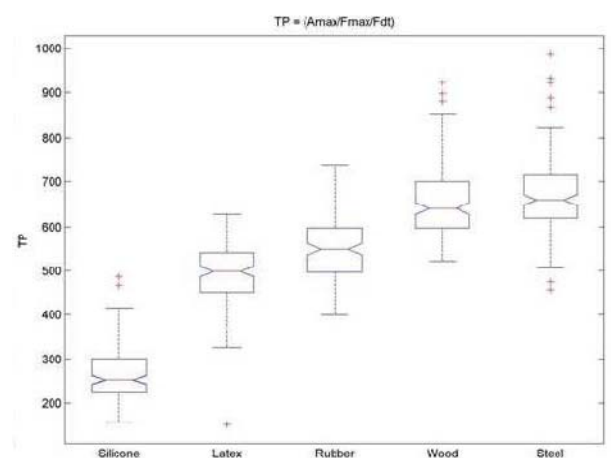


Fig. 4 Novel proposed metric, TP, arranged by sample material.

further set of experiments is currently being run to confirm this hypothesis.

A better understanding of touch perception has significant future potential, as it could lead to smarter instruments, able to recognise material properties automatically, better surgical simulators, where relevant haptic information could help to improve surgical training, and better tools, which could be designed to optimise the transmission of tactile information from the tool point to a user's hand.

REFERENCES

- [1] P. Wellman and R. D. Howe. Towards realistic vibrotactile display in virtual environments. Proceedings of the ASME Dynamic Systems and Control Division, pages 713_718, San Francisco; CA, 1995. Asme.
- [2] A. M. Okamura, et al. Vibration feedback models for virtual environments. In Robotics and automation, pages 674_679, Leuven; Belgium, 1998. Ieee.
- [3] Tenzer Y. et al, Investigation into the effectiveness of vibrotactile feedback to improve the haptic realism of an arthroscopy training simulator, Studies in health technology and informatics 2008;132:517-22.
- [4] Tenzer Y. et al, Recognising material stiffness with an arthroscopic probe, CAOS UK, 2009.

Improving System Accuracy in Computer Aided Robotic ORL Surgery

B Bell¹, N Gerber¹, J Salzmann¹, E Nielsen³, G Zheng¹, C Stieger²,
LP Nolte¹, M Caversaccio², S Weber¹

ARTORG Center for Biomedical Engineering Research, University of Bern

¹*Institute for Surgical Technologies and Biomechanics, University of Bern*

²*Department ENT Surgery, University Hospital Bern*

³*NTB Buchs, University of Applied Sciences Bern*

INTRODUCTION

Reduction of comorbidity and cost has recently extended implementation of minimally invasive surgical techniques into oto-rino-laryngology (ORL) [1]. However, minimally invasive computer aided micro-surgery (CAMS) interventions require an unprecedented level of overall system accuracy. For example, inserting a cochlear implant in a single drill pass requires the definition of a drill trajectory through the facial recess to access the middle ear. This trajectory (approximately 1.0 – 3.5 mm in width) is bounded posteriorly by the facial nerve and anteriorly by the chorda tympani [2-4]. In order to successfully avoid these structures, an overall CAMS system accuracy of 0.2 -0.3 mm is required. Additional benefits of integrating robotic manipulators in ORL surgery include tremor reduction [5], and augmentation of force dependent tissue interaction [6].

Table 1: Accuracy comparison in CAS and CAMS

Error Source	Imaging	Tracking	Regist.	Calib.	Overall
Requirement	Voxel size	RMS	TFE	RMS	TRE
Unit	[mm]	[mm]	[mm]	[mm]	[mm]
CAS	0.50	0.25	1 – 2	0.1	2 – 3
CAMS	0.15	-	0.1 – 0.2	0.01	0.2 – 0.3

In this contribution we discuss ways of achieving this accuracy level, which is an order of magnitude better than current CAS approaches (table 1). Specifically we discuss and present recent findings in:

Imaging: A higher image resolution would decrease the partial volume effect and improve the recognition of small anatomical structures.

Registration: Hand-picked fiducial marker selections are highly variable and dependent on user skill. Additionally, sub-pixel accuracy is required for high precision image registration.

Relative Cranial Tracking: Current tracking systems lack sufficient accuracy for ORL CAMS. Herein we discuss alternative approaches to relate cranial movement relative to the robot base. Through this approach, we bypass navigation errors completely.

Surgical Manipulator / Robot: Because of the small size scale and proximity of critical anatomic structures,

free hand drilling techniques exceed the perception and dexterity of the surgeon to safely circumnavigate these structures. The use of a mechatronic manipulator will greatly enhance surgeon abilities and facilitate precise placement of the implant cavity.

MATERIALS AND METHODS

Imaging study: Investigation of a suitable imaging modality with respect to available image contrast and reproduction quality was performed with cadaver head scans using Computed Tomography (CT) and Digital Volumetric Tomography (DVT) imaging modalities [7].

Automatic landmark detection: A semiautomatic marker detection algorithm was implemented and compared to manual marker detection by quantifying the standard deviation from the results of the two techniques. Manually detected marker centers were chosen by identifying the marker center in appropriate scan planes. In contrast, semiautomatic marker locations were chosen by registering 3D solid CAD model data with voxel intensity gradients. The geometric center of the 3D model was then used as the marker location. Both methods were repeated and their results compared to address repeatability.

Development of surgical manipulator / robot: To achieve the required accuracy [2, 3] and to maintain small positional and rotational deviation throughout the drilling process, a surgical manipulator was developed.

RESULTS

Imaging:

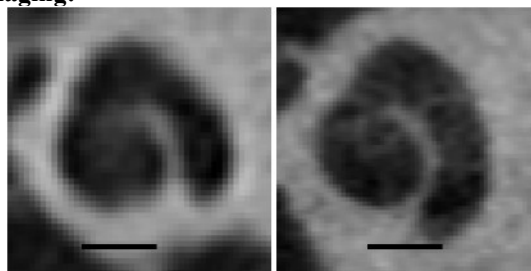


Fig. 1 Comparison of image quality Cochlea in CT (left) and DVT (right). Bar 3mm.

We have identified a Newtom 3G DVT scanner as a suitable imaging means. It allows for scanning of patients with a resolution of (0.15 mm)³ and an effective dose of

0.2 mS (CT: $0.2 \times 0.2 \times 0.63 \text{ mm}^3$, ED 0.6 mS). The suitability of DVT was assessed in a cadaver imaging study and through a neuroradiological expert.

Automatic landmark detection: Using a semiautomatic vs. a manual landmark detection algorithm in DVT images results in a rather small error for repeated detection of the same landmark ($\sigma < 0.1 \text{ mm}$).

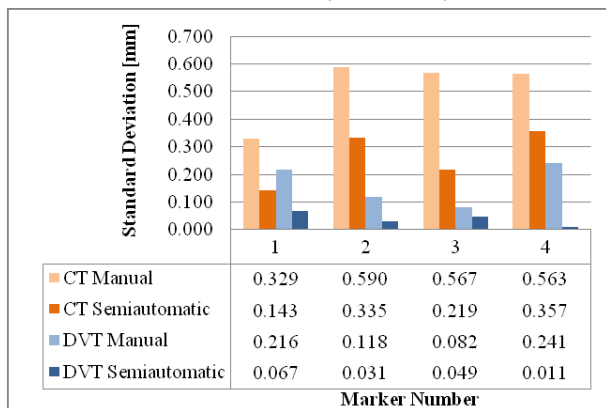


Fig. 2 Comparison of repeatability of landmark detection
Development of a surgical manipulator: A prototype of the robotic manipulator was developed and manufactured. The 5 DoF robot was designed specifically for surgery on the head. The lightweight aluminum chassis was designed to incorporate motor control electronics which interface with higher level control structures using a CAN protocol.

Table 3: Features of the robotic manipulator

Kine-matic	Weight	Payload	Repeatability	Stiffness	F/T Sensor
5 DoF	5Kg	1 Kg	0.01mm	0.01mmN ⁻¹	6 DoF

Due to its minimal weight, the robot can be mounted directly to the surgical table's rail system, resulting in a high base rigidity. The stiffness of the system is then augmented through a direct link to the head fixture device (Mayfield clamp or dental splint). This is in contrast to other approaches using industrial manipulators which are much heavier and require special mounting/fixation [8,9]. Prior to deployment, the robot is draped and the drilling instrument is attached. The robot includes tracking references that allows for spatial measurement of its tool tip in conjunction with encoder measurements. Its operational modalities include pre-planned drilling and milling operations, bounded free-hand milling, and interactive marker registration. Implementation of a 6 DoF force sensor facilitates intelligent force feedback control which enables direct surgeon interaction (bounded milling, marker registration).

DISCUSSION

Computer assistance through instrument guidance and robotic manipulation becomes interesting and feasible in certain high precision surgeries such as cochlear implantation. Successful implementation of robotic cochlear implantation required reassessment of the complete CAS workflow which was optimized towards even higher accuracy. Although the robot's technical accu-

ry is quite high, the integration of this device into a clinical environment is rather challenging since countless non-technical aspects have to be considered. In this paper we have demonstrated our approach to achieve the necessary accuracy by combining state of the art approaches in imaging, registration and robotics.

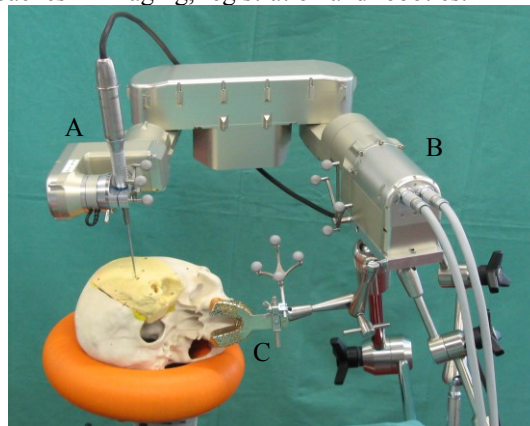


Fig. 3 The lightweight design of the robot allows direct fixation to the surgical table. Marker shields for optional optical tracking shown on end effector with high speed drill (A), manipulator base (B), and dental splint (C).

ACKNOWLEDGMENT

Support for the project comes from the Swiss National Science Foundation (through NCCR CO-ME), the swiss commission for technological innovation and through the companies BienAir S.A. and Phonak Acoustic Implants.

REFERENCES

1. Labadie, R.F., et al., *Minimally invasive, image-guided, facial-recess approach to the middle ear: demonstration of the concept of percutaneous cochlear access in vitro*. Otol Neurotol, 2005. **26**(4): p. 557-62.
2. Noble, J.H., et al., *Automatic segmentation of the facial nerve and chorda tympani in CT images using spatially dependent feature values*. Med Phys, 2008. **35**(12): p. 5375-84.
3. Labadie, R.F., et al., *Clinical validation of percutaneous cochlear implant surgery: initial report*. Laryngoscope, 2008. **118**(6): p. 1031-9.
4. Coulson, C.J., et al., *An autonomous surgical robot for drilling a cochleostomy: preliminary porcine trial*. Clin Otolaryngol, 2008. **33**(4): p. 343-7.
5. Maier, T., et al., *[First clinical use of a new micromanipulator for the middle ear surgery]*. Laryngorhinotologie, 2008. **87**(9): p. 620-2.
6. Brett, P.N., *Moving on from surgical robotics to robotic micro-tools in surgery*. Mechatronics and Machine Vision in Practice, M2VIP 14th International Conference on, 2007: p. 1-5.
7. Dalchow, C.V., et al., *Value of digital volume tomography in patients with conductive hearing loss*. Eur Arch Otorhinolaryngol, 2006. **263**(2): p. 92-9.
8. Rothbaum, D.L., et al., *Robot-assisted stapedotomy: micropick fenestration of the stapes footplate*. Otolaryngol Head Neck Surg, 2002. **127**(5): p. 417-26.
9. Kavanagh, K.T., *Applications of image-directed robotics in otolaryngologic surgery*. Laryngoscope, 1994. **104**(3 Pt 1): p. 283-93.

A dual-centre, cohort comparison of open, laparoscopic and robotic-assisted radical cystectomy

O Elhage^a, B Challacombe^a, M S Khan^a, P Rimington^b, B Coker^c, D Murphy^a, A Grieve^c, P Dasgupta^{a,d}

^a*Urology Centre, Guy's & Thomas' NHS Foundation Trust, London, UK*

^b*Department of Urology, East Sussex Hospitals, Eastbourne, UK*

^c*Division of Health & Social Care Research, Department of Public Health Sciences, School of Medicine, King's College London, UK*

^d*MRC Centre for Transplantation, NIHR Biomedical Research Centre, Guy's Hospital, King's College London, UK*

Corresponding author: oussama.elhage@kcl.ac.uk

INTRODUCTION

Open radical cystectomy (ORC), remains the gold standard treatment for invasive and uncontrolled or high risk superficial bladder cancer [1]. The mortality of ORC has dropped to 1-3% which can be attributed to careful patient selection, improvements in anaesthesia and intensive care medicine. However, morbidity of ORC remains high [1]. Urologists have concentrated their efforts in reducing the morbidity of ORC in this by employing minimally invasive techniques. Laparoscopic radical cystectomy (LRC) was introduced in an attempt to reduce the morbidity of ORC [2-4] and relatively large series have now been reported [5]. More recently robotic assisted radical cystectomy (RARC) has emerged as an attractive alternative to ORC and LRC [6]. While a few comparisons between ORC and RARC have been reported there are none to our knowledge, comparing ORC, LRC and RARC. This is a prospective, non-randomised, cohort comparison of the three techniques. The two participating centres were experienced at ORC and pioneered the introduction of LRC and RARC in UK.

MATERIAL AND METHODS

All patients requiring cystectomy from 2003-8 presenting to Guy's Hospital, London and East Sussex Hospital Eastbourne underwent ORC, LRC or RARC performed by a team of three surgeons (MSK, PR, PDG). Selection was not randomized. Patients with locally advanced disease (T4), previous extensive abdominal and pelvic surgery, previous radio-therapy, uncorrected coagulopathy, those deemed unfit to tolerate prolonged pneumo-peritoneum or steep Trendelenburg position and those declining LRC or RARC were excluded from having minimally invasive

radical cystectomy. All three operative techniques are well described, most recently that of RARC [7]. Post-operative complications were recorded using the Clavien classification system [8] which has been used in urological settings [9, 10] and is regarded as a validated system for these purposes [11]. Demographic and baseline data were summarised using proportions and means where appropriate. Operative time, blood loss and hospital stay were analysed using an analysis of variance model and multiple comparisons between the least square means (LSM) were done with the Tukey-Kramer method. Transfusion and complication rates were analysed using logistic regression with terms fitted allowing a comparison of LRC with ORC and RARC with ORC. Subsequently, adjusted analyses accounting for potential confounding factors ASA grade, gender, age, diversion type and final histology, were conducted to investigate whether any imbalances with respect to these variables due to the non-randomised nature of the study might have influenced the outcomes. Data analysis was conducted using SAS version 9.1 and STATA version 9.2.

RESULTS

A total of 48 patients had RARC, 58 LRC and 52 ORC. The proportions of male to female patients and the diversion types were similar among the 3 groups ($p=0.05$ and $p=0.22$ respectively). The mean ages, ASA grades and final histology staging were however different among the samples ($p=0.04$, $p=0.023$ and $p=0.02$ respectively). Overall positive margin rate in ORC was 10% compared to 4% in LRC and none in RARC. Total number of lymph nodes retrieved, were equivalent in three groups and percentage of positive nodes was not statistically significant. RARC had a statistically longer total operating time ($p<0.0001$), with a mean of 386 minutes, while LRC had the shortest

operating time with a mean of 316 minutes compared with 319 minutes for ORC. The differences in the LSM of operating times between RARC and LRC was about an hour ($p=0.001$) and that between RARC and ORC was just over an hour ($p=0.0002$). The differences in the LSM of operating times between ORC and LRC was 9 minutes and not statistically significant ($p=0.85$). The most striking difference between three groups in operative parameters was estimated blood loss (EBL) and transfusion requirements. EBL was significantly greater in ORC when compared to either LRC or RARC ($p<0.0001$). ORC had a mean EBL of 1352 mls and RARC a mean of 337 mls. The differences in LSM of EBL between ORC and RARC was 1026 mls ($p<0.0001$) and that between ORC and LRC was 904 mls ($p<0.0001$). The differences in the LSM of EBL between LRC and RARC was 121 mls and not statistically significant ($p=0.69$). There were more blood transfusions in ORC ($n=30$; 58%) than in LRC ($n=15$; 26%) or RARC ($n=2$; 4.2%). Patients were about 30 times more likely to have a transfusion if they had ORC than if they had RARC ($p<0.0001$) and about 8 times more likely to have a transfusion if they had LRC compared to RARC ($p<0.006$). Patients were about four times more likely to have a transfusion if they had ORC as compared to LRC ($p<0.007$). Patients having ORC had the longest hospital stay with a mean of 19 days while RARC patients had the shortest hospital stay with a mean of 10 days ($p<0.0005$). The differences in the LSM between ORC and RARC was 9 days ($p<0.0001$). LRC patients had a mean stay of 16 days and the difference in LSM with ORC was 3 days and not statistically significant ($p=0.37$) whereas the difference with RARC was 7 days ($p=0.001$) (table 2). Of the 158 patients in the study 87 had complications during surgery or post-operatively. RARC had the fewest complications ($n=18$; 37.5%) followed by LRC ($n=32$; 55%) and ORC ($n=37$; 71%). Patients were about 4 times more likely to have complications if they had ORC than RARC ($p=0.006$) and about 3 times more likely to have complications if they had LRC than RARC ($p=0.02$). There was no significant difference between complication rates of ORC and LRC ($p=0.65$).

CONCLUSION

ORC remains the gold standard surgical treatment for invasive bladder cancer and uncontrolled or refractory superficial disease. To our knowledge this is the first attempt at comparing ORC, LRC and RARC in a prospective fashion. A selection bias may partly account for certain favourable outcomes of LRC and RARC. Within the limitations of the study, RARC although taking the longest to perform leads to lower blood loss, transfusion and complications when compared to LRC and RARC. That being said, all three techniques have their place in the surgical management of bladder cancer - ORC for difficult cases, LRC where robotics is not available and RARC when technology and expertise are accessible.

REFERENCES

- [1] Herr HW, Faulkner JR, Grossman HB et al. Surgical factors influence bladder cancer outcomes: a cooperative group report. *J Clin Oncol* 2004;22:2781-9.
- [2] Fergany FA Gill IS. Laparoscopic radical cystectomy. *Urol Clin North Am* 2008;35:455-66.
- [3] Parra RO, Andrus CH, Jones JP et al. Laparoscopic cystectomy : initial report on a new treatment for the retained bladder. *J Urol* 1992;148:1140-4.
- [4] Puppo P, Perachino M, Ricciotti G et al. Laparoscopically assisted transvaginal radical cystectomy. *Eur Urol* 1995;27:80-4.
- [5] Cathelineau X, Arroyo C, Rozet F et al. Laparoscopic-assisted radical cystectomy : the Montsouris experience after 84 cases. *Eur Urol* 2005;47:780-4.
- [6] Menon M, Hemal AK, Tewari A et al. Robot assisted radical cysto-prostatectomy and urinary diversion. *BJUI* 2003;92:232-6.
- [7] Murphy DG, Challacombe BJ, Elhage O et al. Robotic-assisted laparoscopic radical cystectomy with extracorporeal urinary diversion: initial experience. *Eur Urol* 2008;54:570-80.
- [8] Dindo D, Demartines N, Clavien PA. Classification of surgical complications: a new proposal with evaluation in a cohort of 6336 patients and results of a survey. *Ann Surg* 2004;240:205-13.
- [9] Shabsigh A, Korets R, Vora KC et al. Defining Early Morbidity of Radical Cystectomy for Patients with Bladder Cancer Using a Standardized Reporting Methodology. *Eur Urol* 2009;55:164-76.
- [10] Tefekli A, Ali Karadag M, Tepeler K et al. Classification of percutaneous nephrolithotomy complications using the modified Clavien grading system: looking for a standard. *Eur Urol* 2008;53:184-90.
- [11] Morgan M, Smith N, Thomas K, Murphy DG. Is Clavien the new standard for reporting urological complications? *BJU Int* 2009;104:434-6.

Robotic Partial Nephrectomy – First UK Series

Adam Alleemudder ¹, Tim Dudderidge, Amrith Rao, David Hrouda, Justin Vale, Bijan Khoubehi †.

Imperial College Healthcare NHS Trust, Urology

† Chelsea and Westminster Hospital NHS Foundation Trust, Urology

¹ adamalleemudder@doctors.org.uk

INTRODUCTION

The incidence of RCC continues to rise in the UK at a rate of 2% per year. In 2006, there were 7840 new cases, making renal cancer the 8th most common malignancy [1]. This is mainly due to the widespread availability of modern imaging detecting smaller and low grade tumours, which account for between 48-66% of all renal tumours. EAU guidelines recommend PN for solitary tumours <4cm as it provides similar oncological outcomes, reduced risk of renal dysfunction and improved survival compared to a radical nephrectomy. It is also an option for tumours 4-7cm when performed in centres with expertise. Although OPN remains the standard of care, there is an increasing trend towards minimally invasive surgery to improve postoperative convalescence. LPN has shown to produce similar intermediate oncological and functional results to OPN while delivering reduced morbidity and quicker postoperative recovery. However, the steep learning curve required has limited its widespread uptake and resulted in underutilisation for the treatment of T1a tumours. Increasingly, surgeons are utilising the Da Vinci robotic system (Intuitive surgical) for PN. Indeed, in 2008, RPN became the fastest growing robotic procedure in the world [2]. Since 2004, several centres have published studies which support the introduction of RPN. Here, we present the first UK series of RPN with 23 consecutive cases.

MATERIALS AND METHODS

Clinical data from 23 patients who underwent RPN between April 2008 and January 2010 were analysed. The procedures were performed by 3 different surgeons with a combined experience of performing more than 150 robotic prostatectomy procedures. The standardized quantitative Nephrometry Scoring System (R.E.N.A.L) was used to determine the complexity of our cases and suitability for RPN [3].

Our technique of RPN uses the 3-arm transperitoneal approach which follows the principle of OPN. A 12mm camera and assistant port and two 8mm ports are placed as

shown (for the right side). Once the lesion is exposed, the margin for resection is marked with diathermy. Pre-prepared sutures and Surgicel bolsters are then placed into the abdominal cavity for use during the reconstruction. These include two 2/0 poliglecaprone and two 1-polyglactin sutures, port length, with a Weck Hem-o-lock clip (TFX Medical, NC) applied at the end with knots either side to stop movement. The Surgicel bolsters (Ethicon, NJ) are prepared by rolling the material into a 5cm cylinder and securing it with 2/0 polyglactin. Once the lesion is fully demarcated and adequately assessed for size and location, bulldog clamps are placed laparoscopically to the artery and then the vein by the assistant. The lesion is resected using the robotic scissors, keeping an adequate margin of healthy tissue around the tumour. The collecting system and base of the renal defect is closed with the poliglecaprone sutures. Floseal (Baxter, Norfolk) is applied to the resection bed and the bolsters are then placed on top. The 1/0 polyglactin sutures are passed from the cortex into the resection bed, over the bolster and out of the resection bed to the cortex where they are secured with a further hem-o-lock clip. This is repeated along the length of the defect. Furthermore the loose ends are then tied over the top of the bolsters. Once completed, the clamps are removed and the time of warm ischaemia is noted. The specimen is placed in an Endocatch bag and removed at the end of the procedure through the camera port site.



Figure 1: Position of patient and placement of ports (right side)

RESULTS

23 patients underwent RPN with a mean age of 54.6 years and tumour size of 2.53cm. The mean operative time was 209.1minutes and median warm ischaemia time of 30 minutes. There were two conversions and four patients required transfusion, with no other major complications. Histology showed RCC in 17 cases.

All surgical margins were negative and to date there have been no local or distant recurrences. The mean R.E.N.A.L Score was 5.56 which suggested all the lesions had a low to moderate complexity and were suitable for partial nephrectomy.

Table 1. Patient demographic, clinical, pathological and operative parameters.

Patient Number (n)	23
Mean Age (years)	54.6 (26-78)
Mean Size of Tumour on CT (cm)	2.53 (1.1-3.87)
Mean Operation Time (min)	209.1 (125-369)
Median Warm Ischaemia Time (min)	30 (15-57)
Mean Estimated Blood Loss (ml)	250 (50-1000)
Conversions (n)	2
Complications (n)	
Intraoperative (n)	1
Postoperative (n)	4
Transfusion (n)	4
Mean Length of Stay (days)	5.0 (2-13)
Pathological Finding (n)	
RCC	17
Oncocytoma	4
Angiomyolipoma	1
Benign Cyst	1
Mean R.E.N.A.L Score	5.56 (4-9)
Positive Margins (n)	0

DISCUSSION

The results of our initial experience are encouraging and similar to other published series. Our mean operative time, blood loss and conversion rates are similar. Importantly, the WIT in this study is around the 30 minutes arbitrary cut-off normally set as the time limit for renal surgery, but this practice is debateable as it is based on anecdotal data and animal studies. The level of complications in our series is acceptably low when compared to other studies and included only Clavien grade 1 and 2 complications. Blood transfusion was required in four cases (19%), which is high in comparison to OPN (1.4% to 7.9%), although we feel this will improve with further experience. The conversion rate during our learning curve of 9.5% compares favourably with 20-25% found in two smaller earlier studies which were describing their early experience. The most important parameter for RPN is the

oncological outcome and to date we have had no positive margins. Intermediate to long-term data has not yet been reported and RPN is only supported by a low margin positive rates and short term imaging follow-up. The oncological effectiveness of RPN is mainly extrapolated from long-term data comparing LPN with OPN. Initial reports comparing RPN with LPN procedures have not demonstrated the advantages of the robotic system and noted few significant differences in the surgical outcome. While some have called for prospective, randomised studies with long term follow-up to accurately compare partial nephrectomy techniques, contemporary studies have begun to show improvements in perioperative outcomes through refinements in technique and experience beyond the initial learning curves. We recognise there are limitations to RPN that include a need for an experienced assistant and a lack of tactile feedback on the instruments when using the console. The preparation time for this approach is also higher and there are financial implications since the initial setup and running costs of the robot system is much higher than laparoscopy.

Our study also incorporated the reproducible R.E.N.A.L Nephrometry Scoring system and our series of 23 cases with low to moderate scores overall proved to be suitable for partial nephrectomy using the robotic approach, except for the second case that was converted. While the score was only 4, the upper pole, posterior location of the tumour proved challenging and reflected our initial inexperience and the limits of using this scoring system. We are satisfied with the results of our initial learning experience and, besides cost and longer operation time, believe RPN is a feasible alternative to and overcomes the challenges surrounding LPN. With experience we anticipate our operative and warm ischaemia times will decrease and larger and more complex tumours will be attempted. For now, OPN will remain the gold standard for partial nephrectomy in most centres. However in view of the rapid pace at which RPN is evolving, together with the ever increasing public demand for minimally invasive surgery, we believe it may eventually supersede OPN and LPN.

REFERENCES

- [1] Cancer Research UK. Kidney cancer Statistics - UK. 15-1-2010. <http://info.cancerresearchuk.org/cancerstats/>
- [2] Gautam G, Benway BM, Bhayani SB, Zorn KC. Robot-assisted partial nephrectomy: current perspectives and future prospects. *Urology* 2009; 74(4):735-740.
- [3] Kutikov A, Uzzo G. The R.E.N.A.L Nephrometry Score: A comprehensive standardized system for quantifying renal tumour size, location and depth. *J Urol* 2009;182:844-853.

First 500 cases of robotic-assisted laparoscopic prostatectomy from a single UK centre: Learning curves of two surgeons

N.L. Sharma¹, D. Lee¹, A. Papadopolous¹, S. Vowler², N.C. Shah¹, D.E Neal¹

¹Department of Urology, Addenbrooke's Hospital, Cambridge UK

²Cambridge Research Institute, Cambridge UK
naomi.sharma@addenbrookes.nhs.uk

INTRODUCTION

Robotic-assisted laparoscopic prostatectomy (RALP) is increasingly used by many centres throughout the world. As with laparoscopic prostatectomy, its introduction is associated with a learning curve. In our centre, a structured mentoring programme has been used to implement RALP and we here report on the outcomes of two surgeons' learning curves, including oncological and functional outcomes, for a total of 500 cases.

MATERIALS AND METHODS

A structured mentoring programme was adopted for the training of two consecutive surgeons (Surgeon 1, with previous open prostatectomy experience and Surgeon 2, with previous laparoscopic experience). The entire surgical team received one week of intensive training at Hackensack Medical Centre, New Jersey. The first 5 cases performed in our centre were mentored by experienced RALP surgeons Dr Peabody and Dr Kaul from the Vatikutti Urology Institute, Detroit, and the subsequent 30 cases were mentored by an experienced laparoscopic radical prostatectomy surgeon, Dr Baumert. After 60 cases Surgeon 2 performed cases with mentoring by Surgeon 1.

Patients eligible for a radical retropubic prostatectomy were offered RALP and absolute contraindications included patient preference for open surgery and previous complex major abdominal surgery. The 3-arm daVinci robot system (Intuitive Surgical) was used for all cases and the technique is based on that described by the Vattkikuti Institute¹ with some modifications, including the use of the Rocco stitch².

Using a prospective, ethically-approved database, we evaluated 500 cases of RALP over a 4-year period using patient demographics, pre-operative PSA, pre- and post-operative Gleason score, clinical and pathological stage, operative time and procedure, positive margins, complications, hospital stay and urinary (ICS SF) and sexual function (IIEF).

Surgeon 1 performed 330 cases and Surgeon 2 performed 170 cases. Statistical analysis was performed using logistic regression, linear regression and chi-square test.

RESULTS

Pre-, peri- and post-operative variables are shown for both surgeons in Figures 1 & 2. The majority of men (70%) underwent bilateral nerve-sparing RALP.

	Surgeon 1	Surgeon 2	Overall
No. of cases	330	170	500
Age, yrs (range)	61.3 (40-73)	62.0 (39-74)	61.5 (39-74)
Preop Clinical Stage (%)			
T1a	2 (0.6)	-	2 (0.4)
T1b	2 (0.6)	2 (1)	4 (0.8)
T1c	211 (64)	99 (60)	310 (62)
T2a	87 (26)	47 (28)	134 (27)
T2b	17 (5.5)	9 (5)	26 (5)
T2c	4 (1.2)	5 (3)	9 (1.8)
T3	7 (2.1)	8 (4.7)	15 (3)
Mean PSA, µg/l (range)	8.1 (0.9-36.8)	8.4 (0.5-25.0)	8.2 (0.5-36.8)
Median Preop Gleason Score (range)	6 (4-9)	6 (6-8)	6 (4-9)
D'Amico Risk Group (%)			
Low	141 (43)	68 (40)	209 (42)
Intermediate	165 (50)	76 (45)	241 (48)
High	24 (7)	26 (15)	50 (10)

Fig. 1 Pre-operative variables for both surgeons.

The overall major complication (Clavien III-V) rate was 1.4%. These included 1 death in recovery (due to a myocardial infarction), 2 post-operative bleeds requiring laparoscopic drainage, 1 thrombosis and compartment syndrome of the lower limbs, 1 small bowel injury requiring laparotomy, 1 small bowel obstruction secondary to a port site hernia requiring laparotomy and 1 recto-urethral fistula.

	Surgeon 1	Surgeon 2	Overall
Mean blood loss, ml (<i>range</i>)	256 (20-3000)	318 (20-1250)	278 (20-3000)
Mean OR time, min (<i>range</i>)	168 (63-420)	205 (112-360)	181 (63-420)
Pathological Stage (%)			
pT2	178 (54)	87 (51)	265 (53)
pT3a	137 (42)	73 (43)	210 (42)
pT3b	11 (3)	9 (5.4)	20 (4)
pT4	3 (0.8)	-	3 (0.6)
pT0	1 (0.2)	1 (0.6)	2 (0.4)
PMR by Stage (%)			
pT2	17	15	16
pT3a	28	33	30
pT3b	45	67	55
pT4	100	-	100
Overall PMR	23	26	24

Fig. 2 Peri- and post-operative variables for both surgeons.

For both surgeons, blood loss significantly reduced with experience ($p=0.029$). The mean robotic operative time was approximately 2 hours after 250 cases and operative time for both surgeons significantly reduced with experience ($p<0.0001$).

The overall positive margin rate (PMR) for both surgeons was 24% and there was a significant association between positive margins and pathological stage ($p<0.001$, chi-square test). Using multivariate logistic regression analysis it was found that the D'Amico risk group had a highly significant effect on outcome, with a patient of high risk being 2.6 times more likely to have a positive margin than a patient of low risk ($p=0.0045$).

Using multivariate logistic regression (adjusting for age, D'Amico risk group and pathological stage), there was a trend towards a reduction in risk of positive margins with increasing number of cases performed by both surgeons, although this was not statistically significant ($p=0.48$). However, analysis of the last 50 cases performed by each surgeon showed that current stage-specific PMRs are 8% and 19% (surgeon 1) and 13% and 24% (surgeon 2), for pT2 and pT3a disease, respectively.

For both surgeons, over 94% of men are continent or wearing only 1 pad and 75% of men who underwent bilateral nerve sparing are potent sufficient for intercourse (with or without assistance), at a minimum of 12 months follow-up. These outcomes were significantly better with greater surgeon experience.

DISCUSSION

The introduction of RALP should be accompanied by a structured mentoring programme in order to minimize the learning curve effects. Our results are comparable to those from other major international centres³. Both oncological and functional outcomes continued to improve during the series, suggesting the learning curve for RALP is higher than previously considered^{4,7}.

REFERENCES

- [1] Menon, M., A. Tewari, and J. Peabody, Vattikuti Institute prostatectomy: technique. *J Urol*, 2003. 169(6):2289-92.
- [2] Rocco, B., et al., Posterior reconstruction of the rhabdosphincter allows a rapid recovery of continence after transperitoneal videolaparoscopic radical prostatectomy. *Eur Urol*, 2007. 51(4):996-1003.
- [3] Badani, K.K., S. Kaul, and M. Menon, Evolution of robotic radical prostatectomy: assessment after 2766 procedures. *Cancer*, 2007. 110(9):1951-8.
- [4] Menon, M., et al., Laparoscopic and robot assisted radical prostatectomy: establishment of a structured program and preliminary analysis of outcomes. *J Urol*, 2002. 168(3):945-9.
- [5] Artibani, W., et al., Learning curve and preliminary experience with da Vinci-assisted laparoscopic radical prostatectomy. *Urol Int*, 2008. 80(3):237-44.
- [6] Ahlering, T.E., et al., Successful transfer of open surgical skills to a laparoscopic environment using a robotic interface: initial experience with laparoscopic radical prostatectomy. *J Urol*, 2003. 170(5):1738-41.
- [7] Mikhail, A.A., et al., Robotic-assisted laparoscopic prostatectomy: first 100 patients with one year of follow-up. *Urology*, 2006. 68(6):1275-9.

EVOLAP, an Active Laparoscope Positioner devoted to Ergonomics

B. Herman^{1,3}, B. Raucent¹, J. Donnez², E. Dombre³

¹Center for Research in Mechatronics, Université catholique de Louvain, Belgium

²Department of Gynecology, Cliniques universitaires Saint-Luc, Belgium

³LIRMM, CNRS – Montpellier University of Science and Technology, France

benoit.herman@uclouvain.be

INTRODUCTION

Ergonomics has a major influence on the acceptance of a robot in the operating room, as space and time are highly valued in today's surgery. Several laparoscope positioners have been developed since the mid-90s, so as to solve problems posed by manual camera handling [1]. All these devices allow the surgeon to control the camera displacements *via* a 'hands-free' interface (e.g. voice recognition, head tracking, miniature joystick), and offer improved image stability at rest [2].

Nevertheless, current systems suffer from several drawbacks. They are generally space-consuming around the table or above the patient's abdomen. Most have mechanical axes of rotation that require accurate alignment with the incision. Consequently, the position of the robot cannot be chosen freely by the surgeon. Set up and break down operations must be performed carefully, and increase total operative time. In addition, the motions of these systems are limited in range and quite basic, mainly due to their electromechanical structure and the control method or device. In most cases the laparoscope moves at a constant angular speed and the available directions are simply 'left-right', 'up-down', and 'in-out', without any possibility to combine them in real-time teleoperation so as to obtain more natural oblique displacements towards the target. Lastly, due to their kinematics, laparoscope motions are not always identical to natural motions obtained by hand manipulation with direct visual feedback from the monitor. This difference between actual image shifts and the ones expected by the surgeon may induce confusion as to the actual laparoscope configuration, and disorder hand-eye motions.

Although active scope holders do have the potential for improving ergonomics of laparoscopy, the numerous weaknesses of existing devices tend to slow down their acceptance and their spread in hospitals.

MATERIALS AND METHODS

From the above analysis, we drew up a list of important requirements in order to design a new robot that would meet surgeons' needs and expectations. The distal tip of the laparoscope (inside the peritoneal cavity) needs to be moved through a large workspace, although the robot should be compact and its motions not too cumbersome. The surgeon should be allowed to place the robot in a convenient position, without being constrained by the

trocar position, so as to allow all the team members to choose their own position freely. Installation and set up should be fast and easy. Finally, the robot should be controlled through an ergonomic and intuitive interface that provides an immediate response and offers more capabilities than only basic motions at constant speed.

With the help of practitioners, these needs were translated into weighted criteria used subsequently during the design process to compare solutions and select the optimal one objectively. The proposed design consists of three main components (Fig. 1):

(1) A main 2 degrees-of-freedom (DOF) remote manipulator is fastened on one of the lateral table rails through a height adjustment mechanism. Table mounting allows a change of table set up during the procedure without requiring any robot adaptation.

(2) A passive arm connects the end-effector of the main manipulator to the laparoscope *via* two orthogonal passive joints. It has also several joints that can be unlocked for adjustment during installation, once the main manipulator has been secured on the table in a convenient position. The main manipulator induces angular motions ('pan' of the video images) from the table side and the rigid arm transfers these swivelling motions to the laparoscope.

(3) A local zoom device located at the distal end of the passive arm translates the laparoscope into the cannula ('zoom') without any displacement of the arm.

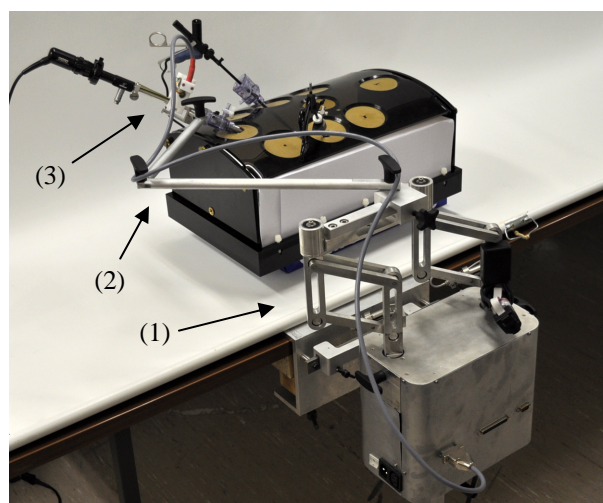


Fig. 1 Overview of the prototype of EVOLAP, an active laparoscope positioner devoted to ergonomics.

This decoupled architecture is capable of producing large intra-abdominal displacements of the lens with limited robot motions above the patient's abdomen.

The main 2-DOF remote manipulator has a particular kinematic structure, consisting of several orthogonal parallelograms, which *translates* the end-effector onto the surface of a half-sphere. This motion can then be reproduced above the patient's abdomen without the need for any alignment between the robot and the incision. Priority can thus be given to the optimal placement of the surgical team around the patient, the robot being positioned conveniently next to them on the suitable side of the patient (e.g. on the right side of operating workspace for a right-handed surgeon with his major hand above the table), regardless of the insertion point of the laparoscope, or the type of procedure. A PCT patent application describing the general decoupled architecture of the robot and the particular kinematics of the main manipulator was filed in 2008 [3].

An omnidirectional and proportional joystick, attached to the minor-hand instrument, allows the surgeon to control the motions of the robot in real-time. Compared to voice or head control, this input interface offers some interesting functionalities. It can combine 'left-right' and 'up-down' motions to pan the video images in any direction, and the speed of the laparoscope can be adjusted by tilting the joystick more or less.

A kinematic modelling of the motions achieved by existing laparoscope positioners highlighted the occurrence of inaccurate image displacements or wrong camera orientation in specific robot configurations. An original definition of operational coordinates was proposed to remedy this important ergonomics issue.

The main manipulator is also equipped with a static balancing spring mechanism, and a high efficiency transmission was designed to ensure back-drivability, affording the possibility to move the laparoscope either with the joystick (tele-operated active mode) or by hand (manual passive mode) with a force equivalent to the one required by classic passive devices. The total weight of the device is less than 10 kilograms, making it easy to carry and to mount on the table. A complete technical description can be found in [4].

Several phantom trials were carried out during the design process to assess the duration of installation, and to tune the controller parameters. Finally, a first clinical trial was performed to evaluate performances in real practice, as ergonomics and usability cannot be assessed by any other means. Details of experimental *in vitro* and *in vivo* validation can be found in [5].

RESULTS

The *in vivo* procedure went off successfully and uneventfully. Compactness of the robot allowed all the team members — the surgeon, two assistants, a nurse and a supervising engineer — to stand next to the table and work normally, without being bothered by its presence. Intra-abdominal workspace (ranging from 0° to 80° in 'up-down' direction and software restricted from -50° to 50° in 'left-right' direction for safety) was

sufficient to reach all desired angles and depths, while arm and robot motions did not restrict the surgeon's freedom of motion with his surgical instruments. Speed control and joystick sensitivity helped the surgeon to drive the laparoscope quickly and with precision, and omnidirectional displacements allowed him to navigate easily. The surgeon reported subjectively that image stability was better than ordinary with an assistant, without any spurious motion of the laparoscope.

DISCUSSION

A novel robotic laparoscope holder has been developed, with special attention devoted to the ergonomics requirements of minimally invasive laparoscopic surgery. A particular robot architecture was proposed to allow large displacements of the laparoscope in the abdominal cavity, although the device is compact and quite lightweight. Its kinematic structure does not require any alignment with the laparoscope swivel point, this allowing the surgeons to choose their own placement without additional constraints.

A first *in vivo* procedure was performed with the prototype and demonstrated the feasibility of the solution. Compactness of the main structure was appreciated. Image stability was very good throughout the whole procedure, regardless of the configuration of the laparoscope and the respiratory motions.

Surgeons found the instrument-mounted joystick very intuitive and more comfortable than other control devices. Whereas voice, head or foot control permits only sequential motions at constant speed, the proposed joystick allows accurate omnidirectional displacements and real-time speed adjustment.

Further *in vitro* experiments should be carried out to quantify the advantages of the robot and its interface, by measuring motion time and path length to reach a target. A series of clinical trials should also be performed by surgeons from various specialities in order to assess usability and measure image stability.

REFERENCES

- [1] Stassen HG, Dankelman J, Grimbergen CA. Open versus minimally invasive surgery: a man-machine system approach. *Trans Inst Meas Contr.* 1999;21(4-5):151–162.
- [2] Jaspers JE, Breedveld P, Herder JL, Grimbergen CA. Camera and instrument holders and their clinical value in minimally invasive surgery. *Surg Lap Endosc Percut Tech.* 2004 June;14(3):145–152.
- [3] Herman B, Raucent B, Tran Duy K, Polet R, Donnez J. A hybrid manual-robotic system for controlling the position of an instrument. PCT patent application filed on June 12, 2008, published online on December 31, 2008 under reference WO2009/000658.
- [4] Herman B, Dehez B, Tran Duy K, Raucent B, Dombre E, Krut S. Design and preliminary *in vivo* validation of a robotic laparoscope holder for minimally invasive surgery. *Int J Med Robot Comput Assist Surg.* 2009 Sep;5(3):319–326.
- [5] Herman B, Tran Duy K, Dehez B, Polet R, Raucent B, Dombre E, Donnez J. Development and first *in vivo* trial of EVOLAP, an active laparoscope positioner. *J Minim Invasive Gynecol.* 2009 May/June;16(3):344–349.

A Novel Articulated Robot for Natural Orifice Transluminal Endoscopic Surgery: Overcoming the Technical Challenges

James Clark¹, Mikael Sodergren¹, David Noonan², Jianzhong Shang², Christopher Payne², David R.C. James¹, Thanos Athanasiou¹, Julian Teare¹, Ara Darzi¹, Guang-Zhong Yang¹.

1. *Division of Surgery; Imperial College London, UK.*
2. *The Institute of Biomedical Engineering; Imperial College London, UK.*

INTRODUCTION

Heralded as the next step in the evolution of minimally invasive surgery, Natural Orifice Transluminal Endoscopic Surgery (NOTES) has attracted significant interest since its introduction^{1, 2}. As the numbers of those that support the continual efforts to explore the approach grows³ so do the number opposing^{4, 5} with particular focus on the safety concerns with regards to the extensive learning curve of the technique, the lack of appropriate instrumentation and indeed even lack of purposefully designed surgical endoscopes for the procedure.

However the potential benefits of the approach in terms of the obviation of any eventration and a lower risk for herniation, wound infection and adhesion formation ensure that there are many groups still focusing on demonstrating that the technique is safe by continuing to perform and publish large prospective clinical series⁶.

The technique is in its infancy with many hurdles yet to be overcome before widespread clinical acceptance is assured⁷. These are mainly centred around two distinct areas; patient safety and clinical usability or technical ergonomics. Both have to be addressed before NOTES can become a serious intervention within mainstream surgical practice.

The inherent instability provided by the endoscope as an operative platform has been the focus of significant research interest, as the greatest challenge to NOTES is being able to overcome this without compromising on the unique flexibility of the access which is central to the approach.

It is fast becoming realised that for the natural orifice technique to be safe and effective a radical shift in surgical technology is required. The adoption of robotics into NOTES, as it did in early laparoscopic surgery, will enable many of the ergonomic challenges to be met and promote a safer and more reliable technique with a shorter operative learning curve. This article describes a novel hyper-redundant flexible robot which has the potential to overcome many of the challenges facing the natural orifice technique.

The system described in this paper is a multifaceted articulated robot with 6 degrees of freedom which can access the body cavity through a standard 12mm trocar and controlled using a novel remote tele-operated joystick. Visualisation is obtained with an onboard camera fixed at the tip of the device. A central working channel enables standard endoscopic instruments to be passed through the device for tissue manipulation.

METHODS

Exploration of the Natural Orifice Approach: In-vivo transvaginal peritoneoscopy and proceed

This protocol followed appropriate UK Ethical approval and multiple simulator trials. A 70Kg live porcine model was used for the trial. Visualisation of the manoeuvrability of the robot within the peritoneum was ascertained using the on board camera and a separate 10mm laparoscope inserted through a transabdominal port also used to insufflate the abdomen with carbon dioxide to a pressure of 14mmHg.

A posterior colpotomy was performed and transvaginal access gained using a 15mm laparoscopic port (Applied Medical, Rancho Santa Margarita, CA. US), adapted in-house to a length of 250mm to enable the pelvic sacral promontory to be cleared before insertion of the device.

Peritoneal exploration was performed using the robot alone with identification of upper and lower abdominal organs. Standard endoscopic biopsy forceps were introduced down the working channel and a liver biopsy was performed. Pelvic organs, although complete retroflexion of the device at present is still elusive the pelvic adnexia remained only partially visualised but future iterations will enable this to be corrected.

As a final assessment a hybrid NOTES cholecystectomy was performed with the robot used as the sole tool to visualise the gallbladder. The cholecystectomy was completed within 25 minutes and no intraoperative complications were confirmed on post-mortem.

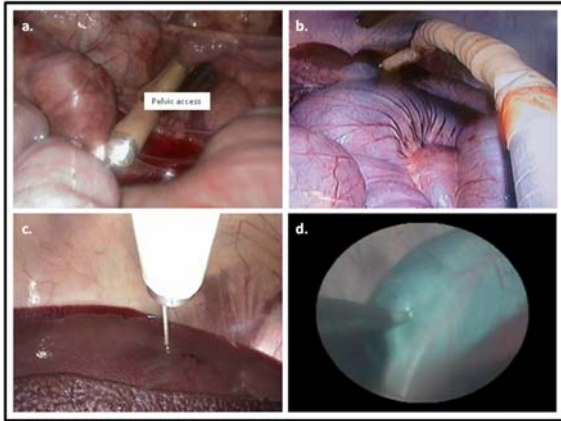


Fig 1. (a) Device exiting the pelvis; (b) device manoeuvring into position in the upper abdomen; (c) performing a liver biopsy; and (d) manipulating the gallbladder with endoscopic instruments (view from the onboard camera).

These results from our early in-vivo work show that even at this prototype stage it is a clinically usable instrument⁸ demonstrating feasibility for a number of clinically relevant procedures. It offers not only the flexibility to optimise the operative view from a remote setting, whether positioned at the operating table to enable the surgeon to perform solo operating reducing external instrument clutter or as a means of reducing the number of surgical assistants around the operating table by enabling the camera assistant to be unscrubbed and adjusting the view remotely. The ability to control such a robotic endoscope as well as manipulate the instruments is unprecedented within the NOTES arena.

The most significant benefit to such a device however is the potential of being able to offer the conventional minimally invasive surgeon all the benefits of a computer enhanced platform without the loss of intimacy between surgeon and patient that current robotic devices incur. Furthermore, the significant size reduction when compared to the current competitors is so dramatic that it has the very real potential of enhancing uptake of robotic equipment into theatre and the exposure of as yet currently unconsidered robotic interventions. With the overall reduction of the footprint of such a device within the operating room often comes the potential for significant cost reductions particularly in comparison to the current robotic devices.

ACKNOWLEDGEMENTS

The project is supported by the Wellcome Trust under a Strategic Translational Award [GR083689].

REFERENCES

- [1] Kalloo AN, Singh VK, Jagannath SB, et al. Flexible transgastric peritoneoscopy: a novel approach to diagnostic and therapeutic interventions in the peritoneal cavity. *Gastrointest Endosc* 2004;60:114-7.
- [2] Marescaux J, Dallemagne B, Perretta S, et al. Surgery without scars: report of transluminal cholecystectomy in a human being. *Arch Surg* 2007;142:823-6; discussion 6-7.
- [3] Kaouk JH, Haber GP, Goel RK, et al. Pure Natural Orifice Transluminal Endoscopic Surgery (NOTES) Transvaginal Nephrectomy. *Eur Urol* 2009.
- [4] Kobiela J ST, Mackowiak M, Lachinski AJ, Sledzinski Z. NOTES-third generation surgery. vain hopes or the reality of tomorrow? . *Langenbecks Arch Surg* 2008;393:405-11.
- [5] Hall. Is natural orifice transluminal endoscopic cholecystectomy as safe as laparoscopic cholecystectomy? *Arch Surg* 2008;143:604.
- [6] Federlein M, Borchert D, Muller V, et al. Transvaginal video-assisted cholecystectomy in clinical practice. *Surg Endosc*.
- [7] Zacharakis E, Purkayastha S, Teare J, Yang G-Z, Darzi A. Natural Orifices Transluminal Endoscopic Surgery (NOTES): who should perform it? *Surgery* 2008;144:1-2.
- [8] Clark J, Sodergren M, Noonan D, et al. A novel articulated robotic laparoscope for single incision and natural orifice surgical applications; preliminary usability trials in a live porcine model; *Surg Endosc Suppl 1 (Abstract SAGES Conf 2010)*

Single port manipulator for minimally invasive surgery

S. Can^{1,3}, A. Fiolka¹, A. Schneider¹, A. Knoll³, H. Feussner^{1,2}

¹ Research Group MITI, Klinikum rechts der Isar der TUM, Germany

² Department of surgery, Klinikum rechts der Isar der TUM, Germany

³ Chair of Robotics and Embedded Systems, Technische Universität München, Germany
salman.can@tum.de

INTRODUCTION

Although minimally invasive surgery has many advantages compared to open surgery, its performance is restricted due to technical limitations. Besides the development of new instruments, the current focus is set on trauma reduction by performing single port operations or transluminal surgery (NOTES) [1]. The development of instruments with enhanced flexibility is a major challenge and therefore intensively investigated by various research institutes [e.g. 2]. Usually, the intra-abdominal flexibility of rigid laparoscopic instruments that is limited due to the entry port is augmented with additional distal articulations. NOTES operations depend to an even greater extent upon a suitable, newly designed single lumen universal tool [3]. The first approach devoted to this problem is the endoscope-based octopus system as developed by Swanstrom et al [4]. Anubis (Karl Storz, D) and Endosamurai (Olympus, J) are other NOTES platforms designed for transluminal surgery. However, these systems have a small operating range, limited flexibility and opposite or retroflexive working is not possible. We developed the “Highly Versatile Single Port System” (HVSPS) to overcome these drawbacks. The idea is, literally spoken, to bring the surgeon’s head, shoulders and arms into the abdominal cavity to regain the flexibility of open surgery. The specific aim of this study is the evaluation of the HVSPS prototype for single-port laparoscopic cholecystectomy.

MATERIALS AND METHODS

A: Hardware of the single port system

The developed semi-rigid single port platform consists of two manipulators and a telescope. Fig. 1 shows a schematic design of the HVSPS. The manipulators and the telescope are inserted together through an insert with three lumens. This ensemble is introduced gas-tightly into the abdominal cavity using a 33 mm trocar. It is guided through a telemanipulator, which is attached to the insert. The guiding manipulator has four degrees of freedom (DOF), what enables pivoting the system at the fulcrum, a linear movement into the body and the rotation of the complete single port system.

The hollow manipulators with 5 DOF have an outer diameter of 12 mm. Flexible instruments are introduced through the central channels and can be controlled or changed manually. The bendable section of the manipulators (2 DOF) has a length of 75 mm followed by a 50 mm long hollow tube and an additional

articulation (1 DOF). Two additional DOF at the distal end of the manipulators provide a rotation of 270 degrees in each direction and a linear movement of 80 mm into the abdominal cavity. Visualization of the situs is realized by a flexible telescope with 10 mm diameter and 5 DOF. This solution was implemented with a commercial 6 mm endoscope, which is inserted through a 10 mm tube that has a distal deflection of 30 degrees. Given this ensemble, the telescope can move in an S-form so that the instruments of both manipulators can be observed in their entire operating range.

The HVSPS is automated and controlled over a real-time Matlab-Simulink application. Currently, both manipulators, motorized and steered using Bowden wires, cope a total of ten degrees of freedom. The operator controls each articulation individually with two joysticks as input device. With two meters distance to the patient, the drive system is placed into the periphery.

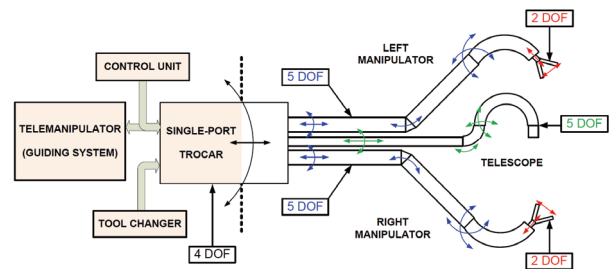


Fig. 1: Schematically design of the “Highly Versatile Single Port System”

B: Simulation environment of the platform

The simulation of elaborate mechanics plays a central role regarding the prediction of developing features, system functionality and teaching facilities. Therefore, a simulation environment of the complete system is programmed. The main reasons for this purpose are listed below:

- Development of new surgical manipulators
- Design optimization of the prototype
- Identification of the appropriate interface
- User training for the physicians

A complete surgical scenario with the HVSPS attached to the SoloAssist (Aktormed, D) telemanipulator, which is mounted on an operating table, is implemented in the Coin3D open source graphics development tool. Equal to the hardware, all the functionalities are controlled using two joysticks as input devices.

Instruments with multiple articulation and high flexibility, e.g. “snakelike” structures, lead to over-determined kinematics. Resulting difficulties in the

handling require new human-machine interface approaches. The simulation provides a platform to evaluate different input devices to determine an adequate interface for a single port system. Finally, the training and teaching with the simulation introduces the system to the physician. The functionalities of the HVSPS are taught to surgeons during repeated training sessions. Based on their performance the indented evaluation of the real system is accomplished.

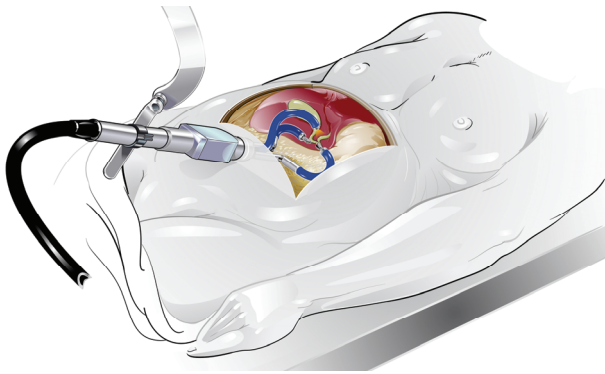


Fig. 2: Schematic drawing of a gallbladder dissection using the HVSPS

C: Evaluation scenario of the single port laparoscopic cholecystectomy

The experiments are performed by a surgeon, who controls both manipulators with the two joysticks, a gastroenterologist, who manually controls the flexible endoscope and two assistants who control the remaining functionalities, as well manually.

After insufflation of the peritoneum with a Verres needle, the HVSPS is introduced into the abdominal cavity through one incision in the middle of the abdomen (Fig. 2). With a retractor, which is inserted through an auxiliary incision, the liver can be retained out of the operating field. As a final step of the cholecystectomy, the gallbladder is recovered through the main incision after a last check up for bleeding.

RESULTS

A laparoscopic gallbladder dissection was accomplished during 2 hours on the ex-vivo ELITE trainer, which provides conditions close to the real in-vivo cholecystectomy. At present, we already performed three cholecystectomies with the HVSPS in survival animal experiments under general anesthesia. The complete surgical intervention, without technical set-up takes between 95 to 130 minutes.

The surgeries were accomplished using flexible instruments (grasper, scissors, etc.) that were introduced through the manipulators. They could be exchanged within seconds for different tasks. After the ligation of the cystic duct and cystic artery with coagulation current, dissection of the gallbladder was achieved by using the conventional grasping and cutting instruments. Fig. 3 shows the gallbladder, held with a grasper through the left manipulator and dissected using a TT knife introduced through the right one. The opposition of the manipulators was essential for intuitive working.

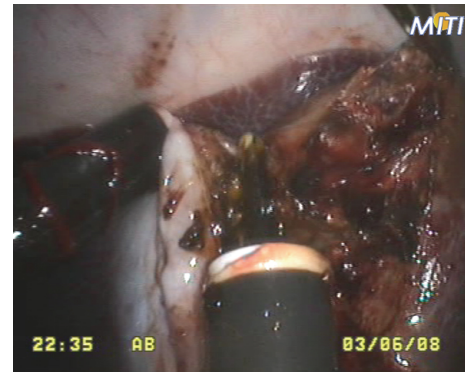


Fig. 3: Cholecystectomy in an animal experiment: Endoscopic view of the situs with the HVSPS manipulators

The complete surgical intervention was guided by commands of the surgeon, who controlled the manipulators. Proper coordination of the physicians was essential for the performance and quality of the intervention. Communication and occasional disaccord of the surgeons was time-consuming. Nevertheless, with increasing experience of the physicians, the operations are performed consistently in less time.

DISCUSSION

Minimally invasive cholecystectomy is feasible using the multifunctional single port platform HVSPS. However, compared to the conventional laparoscopic cholecystectomy, the operation took considerably longer. This is resulting from the difficult handling of the system with various degrees of freedom and the essential coordination of the individual actions of the participating physicians. This extended time can be reduced by optimizing the fully automated HVSPS, introducing an intuitive human-machine interface, an integrated simulation and planning environment. In addition to mechanical optimization and further evaluations, the main focus will be set on the intuitive human-machine interface and the integrated intelligence that is required for such elaborated systems.

REFERENCES

- [1] Feussner H, Can S, Fiolka A, Schneider A. Hybrid surgery-the way towards notes the challenge for computer science. Biomedical Imaging: From Nano to Macro, 2008 ISBI 2008 5th IEEE International Symposium on 2008;1383-6.
- [2] Yamashita H, Iimura A, Aoki E, Suzuki T, Nakazawa T, Kobayashi E, Hashizume M, Sakuma I, Dohi T. Development of endoscopic forceps manipulator using multi-slider linkage mechanisms. Journal of Japan Society of Computer Aided Surgery 2005;7(2):201-4.
- [3] Feussner H, Wilhelm D, Meining A, Schneider A, Fiolka A, Can S, Friess H. NOTES Technical Aspects-Hype or Hope?, Surgical technology international 18 (2009) 26
- [4] Swanstrom LL, Kozarek R, Pasricha PJ, Gross S, Birkett D, Park PO, Saadat V, Ewers R, Swain P. Development of a new access device for transgastric surgery, Journal of Gastrointestinal Surgery 9 (2005) 1129-1137.

Force Sensor Free Bilateral Teleoperation for Robotic Surgery - Feasibility Evaluation through Human Perception Test

Edvard Naerum^{1, 2}, Blake Hannaford³ and Ole Jakob Elle^{1, 2, 4}

¹The Interventional Centre, Oslo University Hospital, Oslo, Norway

²Institute of Clinical Medicine, University of Oslo, Oslo, Norway

³Department of Electrical Engineering, University of Washington, Seattle, WA, USA

⁴Department of Informatics, University of Oslo, Oslo, Norway

edvard.narum@medisin.uio.no

INTRODUCTION

The implementation of force feedback in teleoperated robotic surgery has proven difficult, in part because of the problems associated with mounting force sensors at the tip of the surgical instruments [1]. These problems relate to the small size of the instruments in minimally invasive surgery, and disposability/sterilizability issues. Yet, research does suggest that force feedback in teleoperated robotic surgery is desirable [2, 3]. This motivates the search for teleoperation controllers that do not rely on force sensors, but still manage to deliver adequate force feedback to the surgeon.

Çavuşoğlu et al. [4] presented an optimization scheme that was specifically aimed at controllers for robotic surgery. They showed how to maximize the sensitivity of a teleoperation controller, in terms of its ability to convey changes in tissue compliance to the surgeon. It was found that force information is essential for sensitivity. With the problems associated with force sensors in mind, we developed a framework for the transformation of a general controller for bilateral teleoperation into a *Force Sensor Free* (FSF) controller with the same stability and transparency characteristics [5]. In an FSF controller force information is acquired by estimation rather than by measurement. In this paper the FSF transformation is applied to Çavuşoğlu's controller, and a subjective comparison of the pre- and post-transformation controllers is carried out by asking a number of subjects to participate in a palpation task. The goal of this human perception test was to show that the optimized controller and its FSF counterpart have the same tissue compliance discrimination capability.

MATERIALS AND METHODS

The design of the human perception test followed closely that of Sherman et al. [6]. Our teleoperation setup consisted of two PHANTOM 1.5 haptic devices (SensAble Technologies, USA) serving as master and slave robots. The setup is shown in Fig. 1. The slave was equipped with a Nano17 force sensor (ATI Industrial Automation, USA). Bilateral control was implemented on a PXI-8195 embedded computer (National Instruments, USA) using LabVIEW 2009. Three controllers were implemented, all optimized according to [4]; a position-position controller (PP), a three-channel forward-flow controller (SO), and the

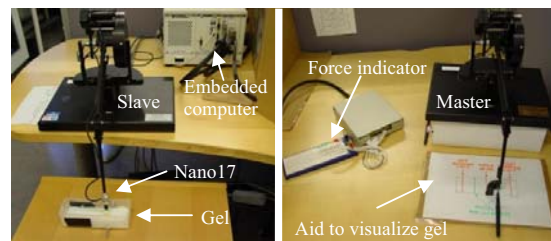


Fig. 1 Teleoperation setup, with master PHANTOM to the right and slave PHANTOM to the left.

FSF equivalent of the SO controller (SOFSF). Human tissue was simulated with a polyvinyl alcohol (PVA) gel with approximate dimensions of 20x50x160mm. Three gels were made, and 5mm metal bolts were submersed in each, at depths of 7mm, 9mm and 11mm from the surface. The bolts ran along the 50mm width of the gels, and were placed at about $\frac{1}{4}$ along the 160mm length.

The perception test was based on Two Alternative Forced Choice (TAFC). 16 subjects aged from 24 to 67 participated in the test, 12 males and 4 females. All subjects had little experience with the use of a teleoperation system. 3 subjects were laparoscopic surgeons. The subjects each completed a series of 60 palpation sessions, 45 of which were done robotically using the teleoperation setup and 15 were done manually using a pen. The slave site, as well as the pen held in the hand, was obstructed from the subjects' view during all sessions. Each session lasted 10 seconds, during which the subject was allowed to palpate the gel along its length in search of the bolt. The subject then said whether the bolt was located to the left or right of the middle of the gel. Ahead of each session a MATLAB routine randomly chose which of the three gels (7mm, 9mm or 11mm) and three controllers (PP, SO or SOFSF) were used, and the left/right location of the bolt. At the end of the 60 palpation sessions the subject was asked to rank the three controllers from 1 to 3 based on the qualitative 'overall feel'. A period of 20 seconds was granted for the qualitative testing of each controller. The subject's response after a palpation session was categorized as correct or incorrect. We expected to see an outcome of the human perception test that listed the manual palpation on top as the golden standard in terms of percentage overall correct responses. Then, next on the list we expected to see the SO and SOFSF controllers side by side, followed by the PP controller at the bottom.

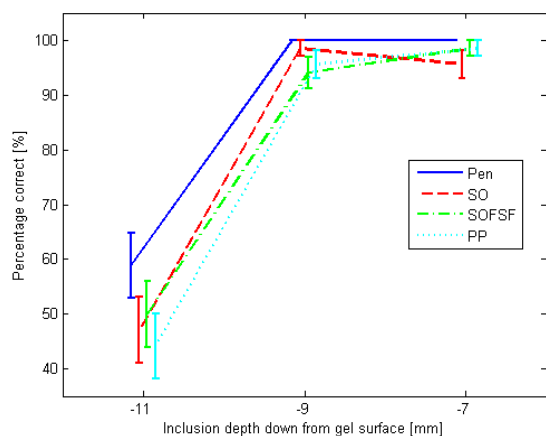


Fig. 2 Percentage correct responses \pm standard error, as a function of bolt inclusion depth.

RESULTS

Fig. 2 shows the overall percentage correct responses for each controller as a function of bolt depth. Not surprisingly, the solid line of the manual palpation lies above all the other lines, indicating the superiority of manual palpation. The other three controllers are much harder to separate. For the 11mm inclusion we do see the tendency of the internal ranking we wanted beforehand. However, a closer look reveals that they all have percentages close to 50%, indicating that the responses were based on guesswork. For the 9mm and 7mm inclusions almost all responses were correct. Strangely, the accuracy of the SO controller decreases from 9mm to 7mm. It is hard to attribute this effect to anything but coincidence. For the pen the percentage is 100% for both 9mm and 7mm.

Table 1 contains the ranking of the SO, SOFSF and PP controllers, as judged by the subjects. The rows show how many subjects ranked a particular controller as the best, the second best, and the third best. Studying the diagonal of the table, there is a strong tendency that the SO controller offered the best feel, followed by the SOFSF controller in second place, and the PP controller in third place. The top ranking of the SO controller is also supported statistically by the fact that none of the confidence intervals along the first row intersect. The same statistical support is not there for the ranking of the SOFSF and PP controllers.

DISCUSSION

An important aspect to consider with this test is whether manual palpation has to be the golden standard. What are the engineering challenges that need to be addressed to create a perception capability in teleoperated surgery beyond that of direct palpation? The obstacle most likely to be encountered is system stability. In particular, the optimization scheme used for the SO/FSF controllers does not limit sensitivity below human capability. However, it is limited by the requirement that system stability must be guaranteed.

Rank	SO	SOFSF	PP
1st	(7.6) 12 (14.8)	(0.2) 2 (6.1)	(0.2) 2 (6.1)
2nd	(0.6) 3 (7.3)	(5.7) 10 (13.6)	(0.6) 3 (7.3)
3rd	(0.0) 1 (4.8)	(1.2) 4 (8.4)	(6.6) 11 (14.2)

Table 1 The number of times a particular controller was ranked first, second, and third based on the 'overall feel'. In parentheses are the lower and upper 95% confidence intervals, computed with the MATLAB routine 'binofit'.

In Fig. 2 we go from guesswork at 11mm to certainty at 9mm and 7mm. Here lay the main problem with the design of the test. Ideally we would have had more gels, with smaller depth intervals. In that way we would be better able to observe when a particular controller moves away from the certainty phase and enters the guesswork phase. For the three controllers this change of phase needs to take place at different depths in order for a difference in sensitivity to be measured. We also had problems with uneven gel surfaces. A robust way of producing gels is necessary, such that bolts can be placed at a certain depth with high accuracy.

The outcome of the palpation sessions in Fig. 2 was intended used as a basis for logistic regression analysis, as in [6]. However, given the lack of results in the transitional phases, we were unable to distinguish the SO, SOFSF and PP controllers from one another. We would most probably have found significant factors through a regression analysis, such as inclusion depth, but the focus was the performance of the controllers. Hence, the main results of this study were a set of design aspects that must be improved to increase the chance of achieving the desired outcome, plus a qualitative ranking (Table 1) that did separate the controllers to some extent.

REFERENCES

- [1] P. Puangmali, K. Althoefer, L.D. Seneviratne, D. Murphy and P. Dasgupta, "State-of-the-art in force and tactile sensing for minimally invasive surgery", *IEEE Sensors J.*, vol. 8, no. 4, pp. 371-381, Apr. 2008.
- [2] O.A.J. van der Meijden and M.P. Schijven, "The value of haptic feedback in conventional and robot-assisted minimal invasive surgery and virtual reality training: a current review", *Surgical Endoscopy*, vol. 23, no. 6, pp. 1180-1190, Jan. 2009.
- [3] G. Tholey, J.P. Desai and A.E. Castellanos, "Force feedback plays a significant role in minimally invasive surgery: results and analysis", *Annals of Surgery*, vol. 241, no. 1, pp. 102-109, Jan. 2005.
- [4] M.C. Çavuşoğlu, A. Sherman and F. Tendick, "Design of bilateral teleoperation controllers for haptic exploration and telemanipulation of soft environments", *IEEE Trans. Robot. Automat.*, vol. 18, no. 4, pp. 641-647, Aug. 2002.
- [5] E. Naerum, O.J. Elle and B. Hannaford, "Force Sensor Free Bilateral Teleoperation", *to be published*.
- [6] A. Sherman, M.C. Çavuşoğlu and F. Tendick, "Comparison of teleoperator control architectures for palpation task", in *Proc. ASME Symposium on Haptic Interfaces for Virtual Environment and Teleoperator Systems*, Orlando, USA, pp. 1261-1268, Nov. 2000.

Bimanual Robot for Single-Port Laparoscopic Surgery with on-board actuation

U. Scarfogliero, M. Piccigallo, C. Quaglia, G. Petroni,

P.Valdastri, A. Menciassi, and P. Dario

CRIM Lab, Scuola Superiore Sant'Anna, Pisa, Italy

u.scarfogliero@sssup.it

INTRODUCTION

Laparoscopic surgical techniques constitute a standard in today's medicine. Although the patient benefits from the reduced invasiveness, the surgeon's sensory and motor capabilities are limited [1]. The insertion points limit the freedom of movements of a rigid laparoscopic instrument to only four degrees of freedom (DOF): this means that each reachable point inside the abdomen can only be approached with a fixed orientation of the instrument.

In the last years, novel surgical techniques are arising from research to clinical practice with the aim of further reducing invasiveness and access trauma. Natural orifices transluminal endoscopic surgery (NOTES) [2] is a totally scarless technique by which it is possible to reach the peritoneal cavity through a transluminal incision performed with flexible instruments inserted either from the mouth, the anus, or the vagina [3], [4]. At the moment NOTES is performed with traditional endoscopic instrumentation that is not specifically designed for this kind of surgery, thus making even more difficult many typical surgical tasks requiring triangulation, large workspace and a large number of degrees of freedom.

A novel technique between traditional laparoscopic surgery and NOTES is single-port laparoscopy (SPL), that consists in a single incision at the umbilicus through which multiple instruments can be placed [5]. This seems to have more possibilities to be accepted as a standard practice in a short period since it allows a direct access to the abdominal cavity by exploiting a preexisting scar, and avoiding additional incisions on the patient's body. However SPL has more limitations than the laparoscopic approach, because it does not allow triangulation from two different points, thus severely limiting the dexterity of the surgeon, although several *ad hoc* instruments have been developed and are already on the market [5].

The da Vinci Surgical System (Intuitive Surgical Inc., Sunnyvale CA, USA) solved the dexterity problems of traditional laparoscopic surgery. Recently the da Vinci Surgical System has been applied also to NOTES [6] and to SPL [7] demonstrating that both these procedures are feasible using current robotic system, though with considerable limitations.

Robotic systems designed specifically for NOTES and SPL approaches have the potential of making scar-less surgery effective and reliable, thus paving the way to

the next generation of scar-less surgical robots. Several robotic solutions have already been specifically designed for NOTES [8]. However, the lack of a stable anchoring and the size constraint imposed by the endoluminal access prevent them to reach the same performance in terms of force and speed as the da Vinci Surgical System. On the other hand, a robotic system designed for SPL may benefit from both a direct and rigid link with an external support and a considerably large diameter of the access port. This approach has been pursued by the authors in designing a novel bimanual and modular robotic system to be used in single-port surgery. This paper presents the design and preliminary tests of SPRINT, Single-Port lapaRoscOpy bImaNual robotT.



Fig. 1 3D concept of the bimanual robot for Single Port Laparoscopy.

MATERIALS AND METHODS

SPRINT is a multi-arms robot aimed at enabling bimanual interventions with a single access port (Fig.1). The robotic arms are introduced in the abdomen through a cylindrical access port. According to medical constraints, the maximum diameter achievable of the orifice is 30-35 mm [5]. The umbilical access port has been specifically designed to allow the insertion of each arm separately, and each arm could be removed in order to clean or replace the tool. The surgeon controls the robotic arms in a master-slave configuration through a dedicated console, and the robotic arms reproduce the movements of the surgeon's hands.

Up to 4 arms can be inserted: in addition to the two main arms, a stereoscopic-camera holder and, for example, a retractor could be introduced. A central lumen of 12 mm is left open after the insertion of the arms, and assistive tools could be inserted for additional tasks (e.g. hemostatic sponge, suturing needle and wire).

As regards the desirable robotic arm diameter, keeping it in the range of 15-20 mm would allow to extend the impact of the presented design from SPL to NOTES, following a similar approach to the one proposed in [8], where a 17 mm diameter bimanual robot is introduced endoscopically through the esophagus to perform a NOTES cholecystectomy. For the same reason, the total length of each robotic arm has been targeted to 120 mm. Each arm is a 6-DOFs manipulator with an anthropomorphic serial configuration. The arrangement of DOFs in the kinematic chain has been selected to match the workspace and dexterity required by surgeons.

The proximal DOFs used for positioning the tool inside the workspace need to generate higher torque respect to distal DOFs used for orienting the tool in the desired direction. Thus, the first two proximal joints (i.e. corresponding to the shoulder in a human arm) are actuated by motors placed outside the arm, and mechanical-power transmission is performed by a rigid (as in the current prototype) or flexible coupling. In this way bigger motors can be used, providing the power needed for actuating the arm at a speed comparable to the surgeon hand, with a force on the tip of 5N. The other 4 DOFs are actuated by on-board actuation, thus avoiding the use of cables for transmitting mechanical power.

RESULTS

In order to verify the feasibility of this design and to assess the validity of system's dimensioning, a robotic arm was fabricated and a master-slave console was set-up. The total length of the robotic-arm in this first prototype is 142 mm, from the first joint (i.e. the shoulder) to the base of the tool: 64 mm for the arm, 70 mm for the forearm, and 8 mm for the distal link. The maximum diameter of the arm is 23 mm. Tests have been carried out in which the prototype has been used by an experienced surgeon for a pick-and-place exercise. A set-up was prepared with some rings and holders in order to verify the dexterity of the arm in a master-slave tele-operated configuration and the overall usability. The aim of the exercise was to use the robotic-arm with a hook-shaped tool to pick a ring from one ring-holder and place it on another one. The surgeon was asked to perform the exercise watching the testbed scene on a video display as captured by an endoscopic camera (Fig.2), positioned in the same configuration as in a real surgical intervention.

DISCUSSION

In this paper a novel robotic platform named SPRINT for SPL in a master-slave configuration has been presented. As far as the authors know, this is the first reported bimanual teleoperated robot purposely designed for an umbilical SPL access.

The system allows high dexterity, thanks to 6 DOFs for each arm and can generate 5 N force on the tip while moving at a speed comparable to surgeon's hand. Each arm can be introduced and removed separately, thus

allowing changing the surgical instrument on the fly. Two additional smaller arms could be inserted in the same access port. A first single-arm prototype of the design described in the paper has been fabricated, assembled and tested in a pick-and-place task. Future works will address a reduction in robot size and diameter, and further tests for control improvements.

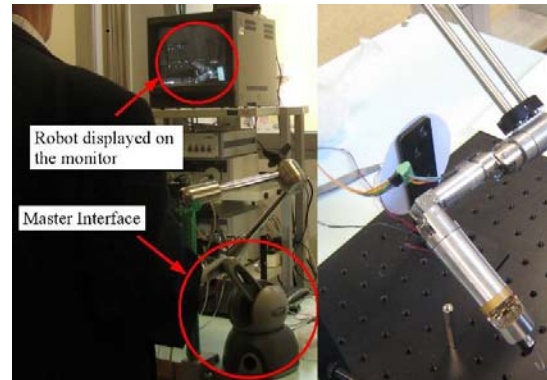


Fig. 2 Picture of the testbed for the pick-and-place exercise (left) and close-up picture of the SPRINT arm prototype (right).

REFERENCES

- [1] H. G. Stassen, C. A. Grimbergen, and J. Dankelman. *Engineering for Patient Safety: Issues in Minimally Invasive Procedures*. CRC, 2004, ch. Introduction to Minimally Invasive Surgery, pp. 2–18.
- [2] A. N. Kalloo, V. K. Singh, S. B. Jagannath, H. Niiyama, S. L. Hill, C. A. Vaughn, C. A. Magee, and S. V. Kantsevov. Flexible transgastric peritoneoscopy: a novel approach to diagnostic and therapeutic interventions in the peritoneal cavity. *Gastrointest Endosc*, vol. 60, no. 1, pp. 114–117, Jul 2004.
- [3] G. Buess and A. Cuschieri. Raising our heads above the parapet: Es not notes. *Surg Endosc*, vol. 21, no. 6, pp. 835–837, Jun 2007.
- [4] S. Horgan, J. P. Cullen, M. A. Talamini, Y. Mintz, A. Ferreres, G. R. Jacobsen, B. Sandler, J. Bosia, T. Savides, D. W. Easter, M. K. Savu, S. L. Ramamoorthy, E. Whitcomb, S. Agarwal, E. Lukacz, G. Dominguez, and P. Ferraina. Natural orifice surgery: initial clinical experience. *Surg Endosc*, vol. 23, no. 7, pp. 1512–1518, Jul 2009.
- [5] M. Neto, A. Ramos, and J. Campos. Single port laparoscopic access surgery. *Techniques in Gastrointestinal Endoscopy*, vol. 11, pp. 84–93, 2009.
- [6] G.-P. Haber, S. Crouzet, K. Kamoi, A. Berger, M. Aron, R. Goel, D. Canes, M. Desai, I. S. Gill, and J. H. Kaouk. Robotic notes (natural orifice transluminal endoscopic surgery) in reconstructive urology: Initial laboratory experience, *Urology*, vol. 71, no. 6, pp. 996–1000, 2008.
- [7] W. M. White, G.-P. Haber, R. K. Goel, S. Crouzet, R. J. Stein, and J. H. Kaouk. Single-port urological surgery: Single-center experience with the first 100 cases, *Urology*, vol. 74, no. 4, pp. 801–804, 2009.
- [8] A. Lehman, J. Dumpert, N. Wood, L. Redden, A. Visty, S. Farritor, B. Varnell, and D. Oleynikov. Natural orifice cholecystectomy using a miniature robot, *Surgical Endoscopy*, vol. 23, no. 2, pp. 260–266, 2009.

The oncological outcomes of Robotic-assisted Radical Prostatectomy in a high volume UK institution

Tim Dudderidge, Lisa Lavan, John Beatty, Tina Rashid, Elaine Wan,
Ben Challacombe and Chris Ogden

Royal Marsden Hospital, London
timdudderidge@doctors.org.uk

INTRODUCTION

Robotic-assisted laparoscopic prostatectomy (RALP) is now the preferred technique of surgery for localised prostate cancer in the USA and the growth in numbers of *daVinci* Surgical Systems in the UK suggests a similar trend. Furthermore with increasing awareness of PSA testing, greater numbers of younger men are being diagnosed with prostate cancer. There are a growing number of competing technologies in this field with patients regularly offered multiple treatment options including surgery (open, laparoscopic & robotic-assisted), active surveillance, radiotherapy (conformal, intensity modulated, brachytherapy) and also high intensity focussed ultrasound and cryotherapy in the context of clinical trials. All treatments are focussed on reduced toxicity with equal efficacy to open radical prostatectomy (ORP). The patients' expectations have altered such that incontinence and erectile dysfunction are less acceptable costs when attempting to cure prostate cancer.

The standard against which these treatments are compared is inevitably to ORP despite the declining use of this technique. ORP oncologic outcomes may initially be assessed by positive margin rates (PMR) and early biochemical outcomes. The largest UK series of ORP (n=1001) delivered a PMR of 52% [1]. A meta-analysis in the USA (n=22,164) showed a better PMR of 24% (reviewed in [1]) and may be judged as a reasonable standard against which to compare RALP outcomes.

The published oncologic RALP data from the UK is limited and represents the learning curve of the first group in the UK to undertake RALP [2]. Here we present our experience of 309 consecutive cases of RALP using the *daVinci S* Surgical System performed by a single primary surgeon in the UK. We focus on reporting the oncological results pending formal analysis of functional assessments.

PATIENTS AND METHODS

The RALP patient care pathway

Patients with localised prostate cancer are discussed at our multi-institutional multi-disciplinary meeting. Those patients suitable for surgery are seen in the outpatient clinic by the surgeon, where all suitable management options are discussed. The specific risks

and benefits of robotic surgery are discussed. Patients are pre-assessed and relevant co-morbidities identified and any necessary pre-operative investigations organised. Body mass index (BMI) is an important consideration and where appropriate patients are asked to reduce weight to a BMI <35 in order to improve their outcome.

Patients are admitted on the morning of surgery and are given a phosphate enema. Patients have a general anaesthetic and a transversus abdominis regional anaesthetic. Patients are placed on a non-slip mat in lithotomy position with 25° trendelenberg incline. Using a Hassan technique to place the primary port, three robotic 7mm ports are placed as well as two laparoscopic ports for the assistant (5mm and 12mm). Patients undergo a standard antegrade nerve sparing prostatectomy in suitable cases. Athermal dissection of the nerve bundles is performed using Weck hem-o-lock clips to secure the vessels and additional haemostatic agents are used where appropriate. In high risk cases wider margins are taken at the discretion of the surgeon and after discussion with the patient.

Typically, patients return directly to the ward and are encouraged to eat and drink normally and mobilise early. The pelvic drain is removed the following morning unless drainage is excessive. Patient's expectations are geared towards discharge around 24 hours after surgery with a urethral catheter in situ. Patients return 7 to 10 days later for removal of their catheter and wound clips, and are taught pelvic floor exercises. They are reviewed 4 weeks after their surgery. PSA measurements are taken at 3-monthly intervals after their surgery during the first year six-monthly for the next year and then yearly thereafter.

We have maintained a clinical database since the beginning of the robotic prostatectomy programme. Using the excellent electronic medical records at our institution we are able to continuously update all demographic, peri-operative, clinical and pathological data. A cohort with a minimum of 6 months since surgery were identified for this report and data optimised by individual case review. Missing data were completed by direct contact with the patient, GP or other specialist if the follow-up was delegated to another doctor.

RESULTS

Study cohort

309 Patients who underwent RALP from January 2007 to September 2010 were identified. The cohort has a minimum of 6 months and mean of 14 months follow up.

Patient Demographics

The subjects' ages ranged from 40-74, with a median of 61 years. BMI ranged from 17 to 38 (mean 27.2). Co-morbidity was recorded in 60.8% of patients.

Pre-operative disease factors

Presenting PSA ranged from 1.4ng/ml to 49ng/ml, with a mean of 8.6ng/ml. PSA \geq 10ng/ml was present in 89/309 patients. The diagnostic prostate biopsy Gleason score was 3+3=6 (n=143), 3+4=7 (n=122), 4+3=7 (n=25), 4+4=8 (n=6), 3+3=6 (n=2), 4+5=9 (n=6), 5+4=9 (n=1), unknown = 4. Clinical stage was recorded as T1 in 234, T2 in 58. Sixteen patients could not be assigned a clinical stage and this relates to the nature of the referral base with many patients' cases prepared outside our institution and monitored elsewhere. In these cases records of initial findings were not always available on our electronic patient record nor local paper notes. MRI staging was available in 215 patients and gave the following staging T0=10, T1=23, T2=163, T3=22.

Peri-operative data

Although not the focus of this study, we have previously described our median operative time (255 mins), console time (145 mins), fluid loss (200ml) and inpatient stay (2 days) in earlier descriptions of the cohort here described [5].

Complications

The complications seen in the cohort are detailed below.

Need for endoscopic removal of Hem-o-lock clips	12
Bladder neck stricture	6
Prolonged troublesome incontinence	3
Implant of artificial urinary sphincter	1
Patients transfused	7
Conversion to open	1
Rectal injury and diversion	1
Laparotomy for bleeding	1
Port site hernia	1
Pulmonary embolism	1
Prolonged drain output	2

Histopathology

Specimens were examined by a Consultant Histopathologist with expertise in urological malignancy. Specimens were analysed in a standardised fashion. Prostate weight ranged 12g to 142g (mean 52g). Gleason scores in the final specimens ranged from 6 to 9 (Gleason sum 6=75 patients, 7=212 patients, 8=7

patients and 9=11 patients). Organ-confined disease was identified in 249 patients. 55 patients had extra-prostatic disease. Any evidence of carcinoma at the inked surgical margin was classified as a positive surgical margin. In patients with organ-confined disease, there were 73 (24%) patients with a positive margin. Patients with extracapsular disease had positive margins in 31/55 (56.4%) cases compared to 42/254 (16.5%) patients with organ confined disease.

Cancer outcomes

Of those with organ confined disease and a positive margin, 3/42 (7%) have developed biochemical recurrence to date compared to 5/31 (16.1%) patients with extracapsular disease. In total there have been 15/309 patients with biochemical recurrence including only 1 patient with organ confined disease and negative margins (Gleason 7 tumour). Furthermore 2 patients developed metastatic disease bringing the total number of treatment failures to 19/309 (5.5%). Biochemical recurrence unsurprisingly appears to be associated with high grade disease with 12 patients having Gleason 7 disease, 2 with Gleason 8 and 3 with Gleason 9 disease.

Of those with disease recurrence there has been one death (pT3a, Gleason 9, positive margins, early recurrence with bone and brain metastases managed with hormones unsuccessfully). The remaining patients included one other with metastatic disease, currently on hormones, 12 patients treated with salvage prostate bed radiotherapy and 3 patients on hormones pending radiotherapy. Two patients have biochemical recurrence after radiotherapy.

DISCUSSION

Here we have described the oncologic outcomes from RALP at our institution. The margin rates and need for salvage radiotherapy are at very acceptable levels despite having a relatively high risk patient cohort. The assessment of functional outcomes is the next focus of our study in this patient group.

REFERENCES

1. Bott, S.R., et al., Radical prostatectomy: pathology findings in 1001 cases compared with other major series and over time. *BJU Int*, 2005. **95**(1): p. 34-9.
2. Mayer, E.K., et al., Robotic prostatectomy: the first UK experience. *Int J Med Robot*, 2006. **2**(4): p. 321-8.
3. Experience of Radical Robotic Prostatectomy using the DaVinci S Robot in Localised Prostate Cancer. Rashid TG, Dudderidge T, Zahur S, Kini M, Jameson C, Ogden CW BAUS annual meeting, Manchester, June 2008.

Robotic-Assisted Surgery in the Gulf Cooperation Council

J. Abi-Nahed¹, J. Nuyens¹, B. Abulaban¹

¹*Qatar Robotic Surgery Centre, Qatar Science & Technology Park, Doha, Qatar*

{jabinahed, jnuyens, babulaban}@qstp.org.qa

INTRODUCTION

Robotic-Assisted Surgery (RAS) is gaining rapid ground in almost every corner of the world and the Gulf Cooperation Council (GCC*) countries are no exception [1, 2]. Thus far, the total number of robotic-assisted surgical procedures has been limited despite increased numbers of installed surgical robots in GCC. There are currently no published statistics on the total number of RAS performed within GCC, yet stating that RAS in GCC is at early adoption stage is hardly debatable. In general, there is a common misconception that RAS technology is easily adopted in GCC compared to the western world due to affluent local populations and substantial investments in healthcare infrastructure in the region. However, as we will see in this paper, GCC countries are faced with region-specific challenges making the widespread adoption of such technology a truly challenging task.

In this paper, we examine key factors underlying the relatively low-level of RAS activity in the GCC region. These region-specific factors may explain the particularity of the GCC region and provide indications as to the future directions of RAS in the GCC area.

MATERIALS AND METHODS

In the past few years, GCC countries have heavily invested in their healthcare sectors [3] to accommodate rapid population growth mainly due to high population growth-rate and increased immigration. The traditional trend of sending patients overseas to receive adequate treatment is now limited due to its prohibitive cost as populations grow steadily [3, 4]. Therefore GCC states are aiming at establishing local world-class hospitals offering advanced care for their patients. A prominent example of such endeavour is the Sidra Medical and Research Centre due to open in 2012 in Qatar.

Amongst attractive novel technology sought by GCC hospitals is RAS with daVinci[®] platform from Intuitive Surgical; it is by far the most popular commercial system used for RAS on soft tissue and is considered the state-of-the-art in surgical technology. There are currently 11-installed daVinci[®] Platforms in GCC, from which 9 are currently used for clinical practice. Nevertheless, the challenges associated with setting up successful robotic programmes are significant, and in the GCC countries, these challenges are exacerbated by

several region-specific factors namely (1) limited availability of local training, (2) an asymmetric population *i.e.* high ratio of expatriates to local population, and (3) high competitiveness over qualified workforce.

(1) *Limited Local Training:*

A major challenge facing adoption of RAS is training; training surgeons in RAS technology has allegedly been reported as a major limiting factor, which is preventing fast adoption of RAS. Until recently, there were no training centres in the GCC able to cater for the need of local surgeons to extensively train on RAS platforms and get the necessary skills and confidence to adopt RAS in their routine practice. Training programmes need to be comprehensive and capable of adapting to different audiences. In addition, the language of the training is clearly a vital element of achieving successful RAS programmes and GCC need to have a centre capable of delivering high-level training in different languages including Arabic. Hopefully, the newly established Qatar Robotic Surgery Centre in Doha will alleviate this element and contribute to successful RAS programmes in GCC.

(2) *Asymmetric Populations:*

The ratio of expatriates to local population is higher in GCC compared to European or American standards [3]. In GCC context, one may safely assume that expatriate populations especially coming from Asian countries have lower income compared to local affluent populations. Therefore this asymmetric distribution of population-types limits the widespread adoption of RAS because the patient is evidently paying for the procedure; even if this is currently not the case in some hospitals, it will be so in the near future as it is the only sustainable solution. Furthermore, the high traffic of inflow/outflow of expatriates from and to GCC as witnessed by the latest economic downturn makes it even more difficult to estimate the influence of such factors on RAS adoption.

Asymmetric population also applies to the surgical teams involved in RAS. Performance of trained teams would be hindered when replacing any of its members. Having to replace team members is unfortunately a highly probable situation due to the current excessive asymmetric populations. In [4] the authors report on average as much as 75% of expatriate physicians practicing in GCC.

(3) Competitiveness over Workforce

Most GCC countries suffer similar problems related to the lack of adequate workforce. They must resort to expatriates to fulfil their needs [3, 5]. However, in today's general economic climate, there is a dual challenge; financial resources are becoming less generous, and competition in the region is becoming fierce. Different members of GCC are making several large-scale investments simultaneously. For instance, Sidra Medical and Research Centre in Qatar, Cleveland Clinic is partnering with key institutions in UAE, and Kuwait is committing substantial amounts into building new hospitals. Therefore, finding adequate staff to employ and be part of RAS teams is currently a challenging task highly prevalent in GCC and will only be exacerbated in the near future as more competing hospitals will try to attract highly qualified staff.

RESULTS

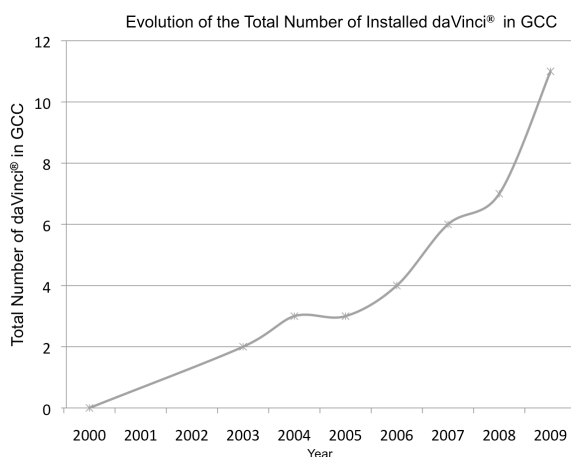


Fig. 1 Total number of installed daVinci® within GCC during the past decade showing continuous increase of robots [1].

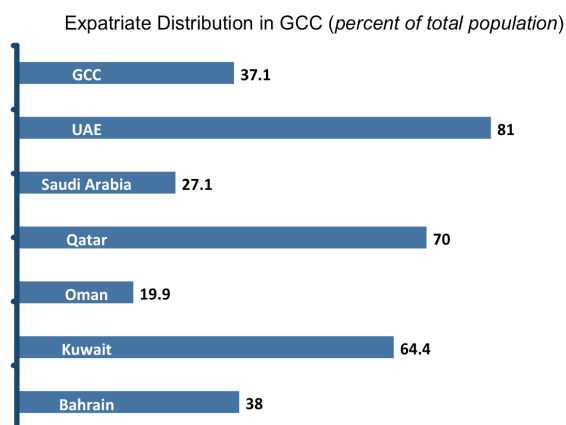


Fig. 2 Percentage of expatriates for each country in GCC[†]

Fig 1 shows the total number of daVinci® installed in GCC; it can be seen that the number of robots increased

from 2 in 2003 to 11 systems in 2009. More systems are on the way to be installed indicating that this trend will continue in the near future. Fig. 2 shows the percentage of expatriates within GCC. It can be seen that on average, GCC countries host about 37% of expatriates compared to the total population. This is a visibly a high number affecting inevitably the global economy and in particular the RAS adoption. One should note that statistics in GCC are rare and not easy to find, and these number are only rough estimates as mentioned in [3-5].

DISCUSSION

Few people dispute the role of new surgical technologies in today's operating theatres. The daVinci® robot is being increasingly adopted in most advanced economies, and in GCC countries. Rumours run about more GCC and middle-eastern countries planning to adopt daVinci® for their clinical practice. There are currently two GCC countries employing such robots in their clinical practice, namely Qatar and Saudi Arabia. As we have discussed in this preliminary study, GCC countries have region-specific elements, which need to be accounted for when analysing RAS in GCC. For instance, we have seen that training, population asymmetry, and competitiveness over workforce are key elements that may hamper the success of robotic programmes. Fortunately, the newly established Qatar Robotic Surgery Centre - a venture of Qatar Science & Technology Park (QSTP) - will mitigate these constraints. The centre offers comprehensive programmes for different levels providing the needed training and confidence to sustain successful robotic programmes particularly for GCC countries. Yet, one may wonder if all countries will enjoy visionary leadership inspiring excellence and progress, as is the case for instance in the state of Qatar.

ACKNOWLEDGMENTS

We wish to thank our innovation team at QSTP, Rachida Riad and Nadiya Farah for their help in gathering data.

REFERENCES

- [1] www.intuitivesurgical.com, 2009.
- [2] Khairy GA, et al. A new era in laparoscopic surgery. Saudi Medical Journal, 2005; (26): 777-780.
- [3] The Economist Intelligence Unit, The GCC in 2020, Outlook for the Gulf and the Global Economy. The Economist. 2009
- [4] Mourshed M, Hediger V, Lambert T, Gulf Cooperation Council Health Care: Challenges and Opportunities. World Economic Forum, Global Competitiveness Reports, McKinsey & Company, 2009; p 55-64
- [5] Kapiszewski A, Arab versus Asian migrant workers in the GCC countries. United Nations Expert Group Meeting on International Migration and Development in the Arab Region. 2006; p. 15-17.

* GCC countries are: Bahrain, Kuwait, Oman, Qatar, Saudi Arabia, and the United Arab Emirates.

[†] This graph is adapted from [5], numbers are estimates

Randomised controlled trial of Laparoscopic, OPEn and Robot Assisted prostatectomy as treatment for organ-confined prostate cancer

EK Mayer¹, D Piercy², DC Cohen¹, K Kerr¹, R Lewis², C Corbishley³, E Hall², JA Vale¹, AW Darzi¹

On behalf of the Trial Management Group

¹ *Department of Surgery and Cancer, Imperial College London*

² *Clinical Trials and Statistics Unit, The Institute of Cancer Research, Sutton*

³ *Department of Cellular Pathology, St George's Healthcare NHS Trust, London*

e.mayer@imperial.ac.uk

BACKGROUND TO THE PROPOSAL

Radical prostatectomy is an established treatment for organ-confined prostate cancer and has traditionally been performed as an open procedure. The requirement for precise surgery within the confines of the pelvis means that radical prostatectomy is ideally suited to exploiting the potential advantages of minimally invasive techniques, with or without the assistance of robotic technology. Currently, choice of surgical approach for radical prostatectomy is determined by a combination of local availability and surgeon's personal bias and experience, rather than by evidence-based practice

DESIGN

Multi-centre Randomised Controlled Trial (RCT), Phase III Feasibility Study

Patients are randomised to laparoscopic versus open versus robot-assisted radical prostatectomy.

AIMS

To demonstrate feasibility of patient recruitment. Ultimately, results of a phase III study will provide evidence as to whether the proposed advantages of minimally invasive techniques translate into improved oncological, clinical and quality of life outcomes. In addition, results will provide evidence to support the cost effectiveness of each approach.

OUTCOME MEASURES

Primary endpoint: Success of recruitment and randomisation. The aim is to recruit 75 patients in a 12 month period (e.g. between 12 and 24 months after all centres have been open to recruitment). The number of patients offered entry to the trial will be recorded in screening logs, and reasons sought (if available) from those patients who decline to take part.

Secondary endpoints:

Clinical and patient-orientated outcomes: Operation duration, blood loss, transfusion rates, peri-operative haemoglobin change, peri-operative complications, length of hospital stay, pathological specimen positive margin rates and biochemical progression-free rates, sexual function, urinary continence and quality of life measures.

Compliance: A compliant patient will be defined as one who receives their allocated treatment and the standardised peri-operative care. We aim to show that more than 80% are compliant.

POPULATION

Patients with organ-confined prostate cancer

ELIGIBILITY

Patients become eligible once they have decided on surgical treatment for their prostate cancer. As is standard practice, all cases will be discussed in an MDT forum. Suitability of trial entry will be guided by the following criteria:

Inclusion criteria:

- Prostate cancer patient who has chosen radical prostatectomy as treatment (with or without lymphadenectomy)
- Clinical stage T1/T2a/T2b/T2c, Gleason score ≤ 7 & PSA ≤ 20
- Aged ≥ 18 years
- Written informed consent

Exclusion criteria:

- Patient medically unfit for surgery
- Prior pelvic radiotherapy or rectal excisional surgery
- Positive bone scan or evidence of nodal metastases on MRI or CT
- Neoadjuvant hormone therapy

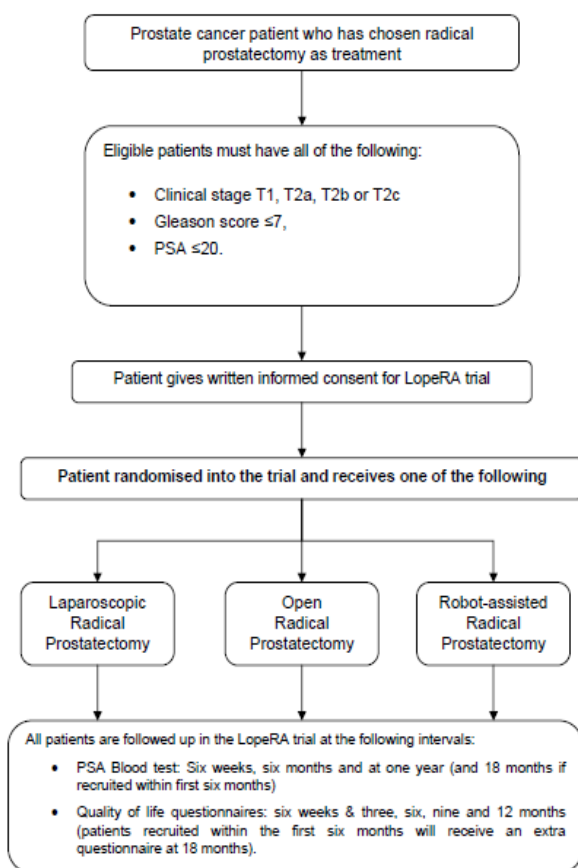
Central randomisation will be performed by the ICR Clinical Trials and Statistics Unit (ICR-CTSU), Institute of Cancer Research, Sutton.

CONCLUSION

This feasibility study aims to show that sufficient recruitment of patients can take place to conduct a phase III randomised controlled trial of open versus laparoscopic versus robotic prostatectomy. Should the results be favourable, the trial group would then be in a position to obtain further funding and ethical approval to conduct the further research.

This trial is funded by Cancer Research UK, trial number CRUK/09/008

STUDY SCHEMA



Patients who consent to take part in the quality of life study will complete quality of life questionnaires as baseline evaluation.

Patients recruited within the first six months of the trial will be asked to fill out an extra questionnaire and have an extra PSA blood test at 18 months.

The following centres and surgeons are participating:

Guy's and St Thomas' NHS Trust

- Prokar Dasgupta (Centre PI), Declan Cahill, Rick Popert

Imperial College NHS Trust

- Justin Vale (Centre PI), Matt Winkler, Bijan Khoubehi

Royal Marsden Hospital NHS Trust

- Tim Christmas (Centre PI), Chris Ogden

Heatherwood and Wexham Park Hospitals NHS Trust

- Omer Karim (Centre PI)

Trial Management Group (TMG)

In addition to PIs and research nurses at participating sites, TMG members are:

Institute of Cancer Research

- Emma Hall (Co-Investigator)

- Deborah Piercy (Trial Manager)

- Rebecca Lewis (Trial Manager)

- Clare Cruickshank (Urology Trial Manager)

Imperial College London

- Ara Darzi (Chief Investigator)

- Justin Vale (Co-Investigator)

- Erik Mayer (Clinical Co-ordinator)

- Karen Kerr (Research Manager)

- Daniel Cohen (Clinical Research Fellow)

St George's Hospital Healthcare NHS Trust

- Cathy Corbishley (Consultant Histopathologist)

Stereo Video Reconstruction for Registration in Augmented Reality Robotic Radical Prostatectomy

Dongbin Chen, Daniel Cohen, Danail Stoyanov, Ann Anstee, Erik Mayer,
Guang-Zhong Yang, Ara Darzi, Philip 'Eddie' Edwards

*Department of Cancer and Surgery, Imperial College London
dongbin.chen@imperial.ac.uk*

INTRODUCTION

Prostate cancer is the most common form of cancer amongst men. It is essential for surgeons to know the spatial location of the prostate and its relation to the surrounding anatomy to achieve full resection without loss of erectile or urinary function. In this paper, we present a method to establish 3D correspondence between a preoperative imaging model of the prostate and local neurovasculature and the stereo intraoperative video from the da Vinci robot. The resulting alignment between 3D video reconstructions and the 3D models built from preoperative MR images can be used to provide augmented reality visualisation on the stereoendoscopic view. The stereo visual environment of the system should provide good 3D perception and enable structures beneath the surface to be seen as though the real tissue were transparent.

METHODS

A stereo image matching algorithm is developed for the proposed method of 3D reconstruction. This stereo image matching algorithm selects the ratio of the directional variance [1] as the image feature for the pixel of the matching image, and searches for the point on the target image with maximum correlation coefficient as the matching point. We use the epipolar line constraint and the limited search area as the boundary condition in the matching algorithm. The epipolar line constraint uses stereo calibration parameters to relate a point in one stereo image to line in the corresponding image. We also reduce the search space further by looking only within a limited depth which corresponds to a limited horizontal disparity. These constraints can improve the robustness of the matching results and save computing time.

The stereo triangulation measurement is applied to reconstruct the 3D location from a pair of matching points and the stereo camera calibration parameters. Finally the 3D model surface produced from MRI scans can be registered to the reconstructed 3D data.

From visual inspection we find the matching algorithm provides correct corresponding points in 92% of cases on the selected stereo images. The selected stereo images include a pair of phantom images and several pairs of stereo images that were captured from real operations.

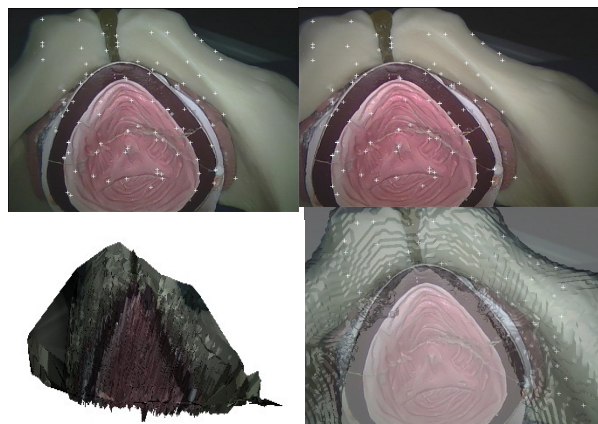


Fig. 1 The stereo images of phantom with the marked matching points produced by the proposed stereo image matching algorithm, a snap of its 3D reconstruction result and an image of overlay 3D pelvis model.

We found that the 3D data reconstructed by the method, though robust in most cases, can produce significantly noisy reconstructions. The main reason is that ratio between the focal length (~ 20 mm) and the based line of the stereo cameras which is around 5 mm is too large. If the 3D shape is to be reconstructed more precisely, we must obtain more accurate results of camera calibration, baseline and each pair of matching point. The significant distortion in the stereoendoscopic view, though calibrated for, may also be a source of error.

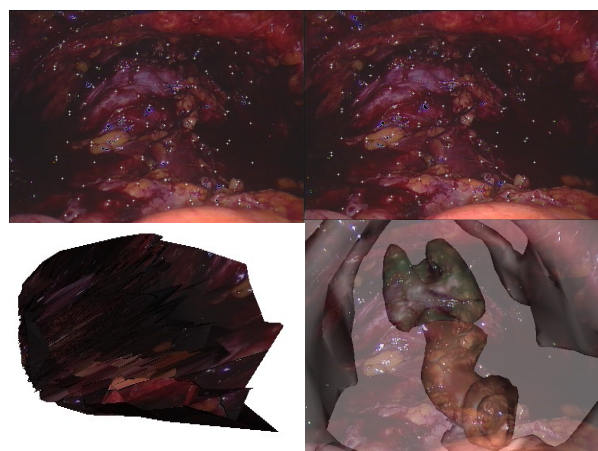


Fig. 2 The stereo images of a patient with the marked matching points produced by the proposed stereo image matching algorithm, a snap of its 3D reconstruction result and an image of overlay 3D pelvis model.

matching algorithm, a snap of its 3D reconstruction result and an image of overlay 3D pelvis model.

Surface registration is the process of alignment of the image to the physical space of the patient. This can be achieved using algorithms such as iterative closest point.

RESULTS

We are currently analysing images from m 10 patients using our methods and the results will be presented at the workshop. The bottom right image of Fig. 1 and 2 present a registration result from stereoendoscope images on the phantom and a patient. Initial results suggest that improvements in accuracy may be required.

We hope to improve calibration using a live GPU-based implementation. We are investigating whether the method of Stoyanov et al [2] may produce more robust surfaces. Photo-consistency may provide good alignment without the need to reconstruct the surface as proposed for robotic coronary artery bypass [3]. There is also the possibility to use intraoperative imaging, particularly ultrasound to provide internal anatomy and give some measure of tissue distortion.

DISCUSSION

In this paper we have addressed the problem of 3D reconstruction from stereo images. In particular, we have focused on the how to reconstruct robust 3D locations from stereo images. Our approach is simple and fast. The robustness of 92% is an encouraging figure. We have analysed the sources of noise and proposed solutions to reduce 3D reconstruction and registration errors.

Augmented reality guidance aims to provide improved navigation for the surgeon. This should achieve a better rate of full lesion extraction and minimise damage to surrounding tissue resulting in reduced recurrence and improved continence and potency for patients with prostate cancer. In the next stage of the research the system will be evaluated live during surgery.

ACKNOWLEDGMENT

We would like to thank Cancer Research UK funding for the research under the project number C24520/A8087.

REFERENCES

- [1] Kass, M., Witkin, A. Analyzing oriented patterns. *Computer Vision, Graphics, and Image Processing* 37 1987: 362-385.
- [2] D. Stoyanov, A. Darzi, and G.-Z. Yang, Dense 3D Depth Recovery for Soft Tissue Deformation During Robotically Assisted Laparoscopic Surgery, in *MICCAI*, 2004: 41-48.
- [3] M. Figl, D. Rueckert, D. Hawkes, R. Casula, M. Hu, O. Pedro, D. Zhang, G. Penney, F. Bello, P. Edwards, Image guidance for robotic minimally invasive coronary artery bypass, *Comp. Med. Imag. & Grap.* 34(1) 2010: 61-68.

Using ECG in Motion Prediction for Radiosurgery of the Beating Heart

F. Ernst, B. Stender, A. Schlaefer, A. Schweikard

Institute for Robotics and Cognitive Systems, University of Lübeck

{ernst, stender, schlaefer, schweikard}@rob.uni-luebeck.de

INTRODUCTION

A new, emerging application for robotic radiosurgery is treating atrial fibrillation by irradiating the beating heart [1, 2]. For this method, the CyberKnife's motion compensation system [3] is used to deliver highly focused radiation to the beating heart to create ablation lines around the pulmonary veins. To improve the system's targeting accuracy, motion prediction is needed to compensate for inevitable latencies. The current generation of the CyberKnife sports a latency of approximately 120 ms. It has been shown that live tracking of the ablation site using 3D ultrasound is indeed possible [4, 5]. We have recently studied the applicability of motion prediction algorithms used in tracking respiratory motion [6]. A new idea to improve prediction quality is to make use of an additional surrogate signal: the ECG. Using a custom-built synchronisation board, a biosignal amplifier and a high-speed IR tracking camera, we have synchronously recorded the ECG and cardiac apex beat motion trace of a healthy male volunteer.

MATERIALS AND METHODS

Data Acquisition: Pulsatory motion was recorded using the accuTrack 250 tracking system (atracsys LLC, Switzerland). This device can record the position of infrared LEDs with extremely high temporal and spatial resolution. Four LEDs were placed in the fifth intercostal space of a male test person. Using this approach, the heart's apex beat could be recorded with very high precision. Measurement noise was reduced by averaging

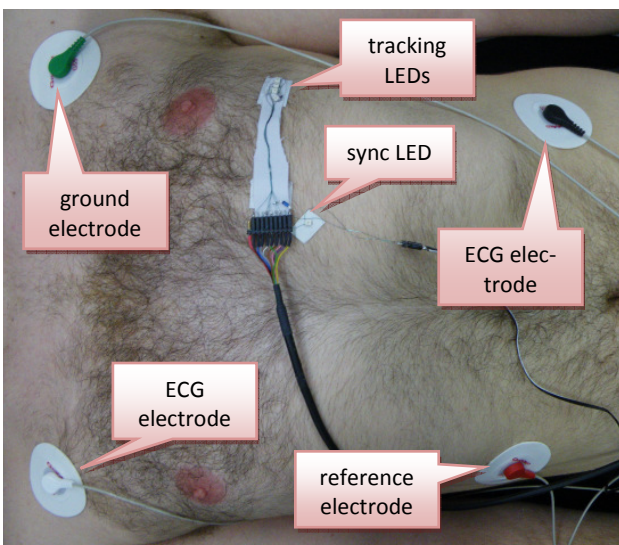


Fig. 1 Setup used for data acquisition. The photograph shows the four tracking LEDs (top), the ECG electrodes and the LED used to synchronise the ECG to the position tracking.

the measured position of the four LEDs. A fifth LED was recorded to synchronise to ECG acquisition. The sampling rate was set to 1166.04 Hz, i.e., each LED was sampled at 233.21 Hz.

The ECG data was acquired with a g.USBamp 24 bit biosignal amplifier (g.tec Guger Technologies, Austria). The resulting sampling frequency was set to 1200 Hz, a 50 Hz notch filter was applied on the internal measurement signals in order to suppress supply frequency components.

Two signals, both of approximately 30 s, were recorded using the setup shown in Fig. 1. During recording, the proband was asked to hold his breath. Fig. 2 shows four

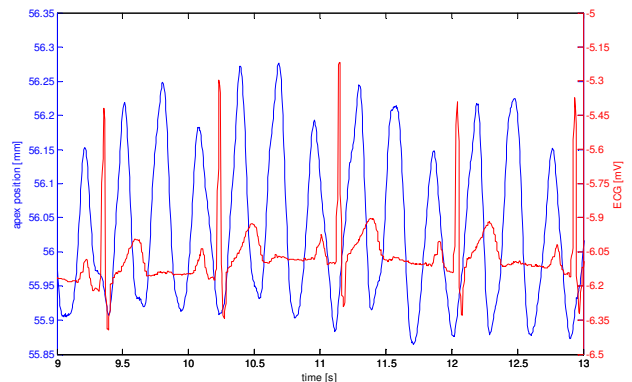


Fig. 2 The graph shows the recorded position of the apex beat (blue) and the ECG (red).

seconds of one of the data sets recorded.

Synchronisation: Synchronisation of the ECG signal with the tracking data was achieved by short-circuiting the ground and reference potentials while switching the Sync electrode simultaneously. A fast PhotoMOSFET relay with four channels (Panasonic AQS225S) was used as switching element. The input voltages for the MOSFETs were generated by a small microcontroller board (Atmel AVR ATmega8). Test Measurements have shown a maximum delay of 5 μ s between the output channels. The delay between a state change of a tracked LED and the detection of this change by the tracking camera's software is approximately 5 ms.

Data Processing: Prior to performing prediction, the recorded data was processed: both the ECG and the pulsatory motion trace were de-trended by removing a running average over 500 samples (two seconds). This was done to eliminate unwanted motion and DC drift in the ECG. The ECG was also smoothed using the method proposed in [7].

Prediction: We evaluated the performance of the SVRpred algorithm. It was introduced in [8] and, in [6],

was found to be most effective when predicting cardiac motion. The algorithm is based on support vector regression and was enhanced such as to include the surrogate signal for prediction. A new parameter, called *surrogate scale*, was introduced. To analyse the performance of the prediction algorithm, we used a graphical prediction tool kit developed at our laboratory [9]. The quality of prediction was determined by looking at the RMS error, i.e., the RMS of the difference between the predicted signal and the real signal.

RESULTS

In the following, the numbers refer to signal one, those in parentheses to signal two.

Temporal correlation: We found the time between the occurrence of the ECG's R-peak and the next peak of the apex beat to be very stable: a mean value of 160 ± 19 (168 ± 18) ms with a standard deviation of 10 (13) ms. Additionally, we have computed the correlation coefficient r between the apex beat motion and the ECG while shifting the ECG in time. We found that the highest correlation can be found for shifting the ECG to the right by 179.4 ms, resulting in a correlation coefficient of $r = 0.28$ (0.38), see Fig. 3.

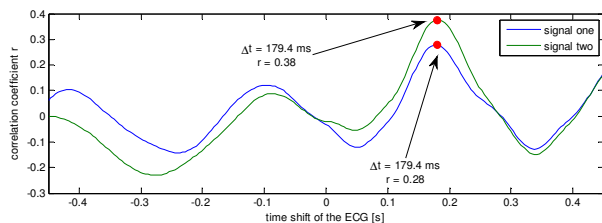


Fig. 3 Correlation coefficients of different shifts in time of the ECG and the apex beat motion. Positive time values correspond to right-shifting, i.e., delaying, the ECG. Maximal correlation is marked with a red dot.

Prediction results: We have evaluated the prediction output of the SVRpred algorithm for multiple combinations of possible parameters. Using a simple grid search, the signal history length, the error insensitivity level and the surrogate scale factor were evaluated. We found that using the surrogate will improve prediction results by approximately 15% (18%). The numbers are given in Tab. 1.

Tab. 1 Prediction results of the SVRpred algorithm on the two signals recorded. The result is in mm RMS compared to the true signal.

	no prediction	w/o surrogate	with surrogate
Signal 1	0.198 mm	0.073 mm	0.062 mm
Signal 2	0.192 mm	0.069 mm	0.057 mm

DISCUSSION

The motion of the cardiac apex as recorded in this work exhibits a surprising three-fold periodicity. We believe that this might be due to contraction and rotation of the heart [10]. From the data recorded we can see that the apex' motion has spectral components at approximately three times the actual heart rate. This makes validation

using ultrasound very hard, since the ultrasound tracking approach can only track at about 20 Hz. Given typical heart rates of 60 to 120 bpm, the signal will be severely undersampled.

The improved prediction quality (15 to 18%) is promising. We plan to further study this using multi-channel ECG and more probands. The fact that the correlation coefficient between the ECG and the apex' motion is highest at a shift of about 180 ms shows that we can expect improvements in prediction for all horizons up to 180 ms. This is well above the current latency of the CyberKnife system of 120 ms.

REFERENCES

- [1] A. Sharma, P. Maguire, L. Fajardo, D. Wong, T. Sumanaweera, and T. Fogarty, "Non-invasive approach to myocardial ablation: Pathology of stereotactic robot targeted high energy x-ray lesions at potential arrhythmia sites," 2008 Heart Rhythm Symposium, *Heart Rhythm* 5(5 supp.):S67, 2008.
- [2] A. Sharma, P. Maguire, D. Wong, T. Sumanaweera, J. Steele, P. Peterson, L. Fajardo, P. Takeda, and T. Fogarty, "New non-invasive therapy for cardiac arrhythmias using stereotactic radiosurgery: Initial feasibility testing," 2007 Heart Rhythm Symposium, *Heart Rhythm* 4(5 supp.):S68, 2007.
- [3] A. Schweikard, H. Shiomi, and J. R. Adler, Jr., "Respiration tracking in radiosurgery," *Medical Physics* 31(10):2738–2741, 2004.
- [4] R. Bruder, T. Cai, F. Ernst, and A. Schweikard, "3D ultrasound-guided motion compensation for intravascular radiation therapy," 23rd International Conference and Exhibition on Computer Assisted Radiology and Surgery (CARS'09, Berlin, Germany), *International Journal of Computer Assisted Radiology and Surgery* 4(supp. 1):25–26, 2009.
- [5] R. Bruder, F. Ernst, A. Schlaefler, and A. Schweikard, "Real-time tracking of the pulmonary veins in 3D ultrasound of the beating heart," 51st Annual Meeting of the AAPM (Anaheim, CA, USA), *Medical Physics* 36(6):2804, 2009.
- [6] F. Ernst, R. Bruder, A. Schlaefler, and A. Schweikard, "Forecasting Pulsatory Motion for Non-invasive Cardiac Radiosurgery," *International Journal of Computer Assisted Radiology and Surgery*, accepted for publication.
- [7] F. Ernst, A. Schlaefler, and A. Schweikard, "Processing of respiratory motion traces for motion-compensated radiotherapy," *Medical Physics* 37(1):282–294, 2010.
- [8] F. Ernst and A. Schweikard, "Forecasting respiratory motion with accurate online support vector regression (SVRpred)," *International Journal of Computer Assisted Radiology and Surgery*, 4(5):439–447, 2009.
- [9] N. Rzezowski and F. Ernst, "Graphical tool for the prediction of respiratory motion signals," *7. Jahrestagung der Deutschen Gesellschaft für Computer- und Roboterassistierte Chirurgie*, Leipzig, Germany, September 24–26 2008, 179–180.
- [10] L. Xia, M. Huo, Q. Wei, F. Liu, and S. Crozier, "Analysis of cardiac ventricular wall motion based on a three-dimensional electromechanical biventricular model," *Physics in Medicine and Biology*, 50(8):1901–1917, 2005.

Spatial awareness enhancement in Natural Orifice Transluminal Endoscopic Surgery (NOTES) by means of an additional visualisation

Vahe Karimyan¹, Felipe Orihuela-Espina^{1,2}, David R. C. James¹, James Clark¹, Mikael Sodergren¹, Ara W. Darzi¹, Guang-Zhong Yang²

¹Department of Biosurgery and Surgical Technology, Imperial College London, UK

²Institute of Biomedical Engineering, Imperial College London, UK

{v.karimyan07, f.orihuela-espina, d.james, j.clark, m.sodergren, a.darzi, g.z.yang}@imperial.ac.uk

INTRODUCTION

New endoscopes specifically designed for Natural Orifice Transluminal Endoscopic Surgery (NOTES) are under development and rapidly entering the market¹. Flexible endoscopes with the ability to be made rigid on demand have been adapted with triangulating instruments to allow for retraction and dissection at the operative site. In the absence of luminal constraints, the endoscope operator is likely to lose his bearings and get disorientated with the consequent potential risk for the patient. Thus, awareness of the endoscope position and orientation in extraluminal spaces is essential both for surgical navigation and patient safety. In the current practice, the endoscope is often retroflexed to determine its position by means of the forward facing camera. This is to ensure that it is not in the vicinity of a visceral organ a potential cause of significant injury and also to determine appropriate positioning of the endoscope for navigation purposes.

We investigate if an additional viewpoint of the scene acquired using a laparoscopic camera through an additional port may enhance the operator's spatial awareness in NOTES, thus resulting in improved navigational skills.

METHODS

A total of 10 surgical naïve subjects were recruited, and asked to perform a navigation task in the simulated NOTES environment (NOSSETM)². (Fig. 1)

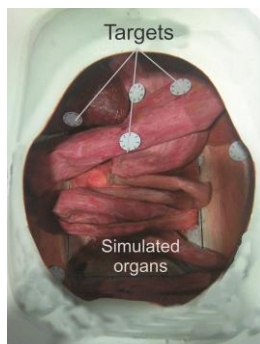


Fig. 1 Open top of the Imperial College Natural Orifice Simulated surgical Environment (NOSSETM) illustrating the simulated organs and the target points.

The navigation course consisted of a 10 target sequence simulating a path likely to occur during a NOTES cholecystectomy. For supplementary visualisation a laparoscopic camera system (Dyonics Digital video camera system, USA), attached to the top left upper distal part of the phantom was used. (Fig. 2) A single coil from an electromagnetic tracking system (EMTS) was attached to the endoscope to track the position of the tip of the tool with the magnetic field generator of the EMTS located under the phantom.

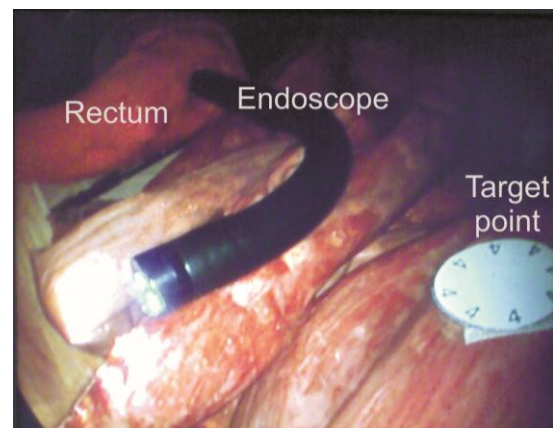


Fig. 2 View from the additional camera visualising the abdominal cavity. The endoscope and one of the course targets in the phantom can be appreciated.

The task was carried out 3 times (1-3 sessions) initially without the auxiliary laparoscopic camera and a final time with it (4th session) by each subject. Navigation between any two targets were not permitted to exceed 1 minute,

Performance outcome measures were number of targets successfully reached during each task, time taken between targets and therefore time taken to complete the whole task. Statistical significance was established at $\alpha=5\%$.

Two dimensional planar histograms of the navigation representing the endoscopic tracked tip positional data were generated by applying a Gaussian filter to the recorded data collected with the EMTS. These histograms were mapped to the scene coordinates following rigid registration.

RESULTS

Mean time required to complete the course was reduced from 365 sec to 275 sec, when the additional camera was available ($p < 0.05$). (**Fig. 3**) Although all subjects visualised more targets correctly during the 4th session (median 5.5 vs 5.0), however this did not reach statistical significance ($p = 0.084$).

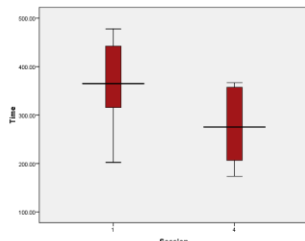


Fig. 3 Total time to complete the path differences between sessions 1 and 4.

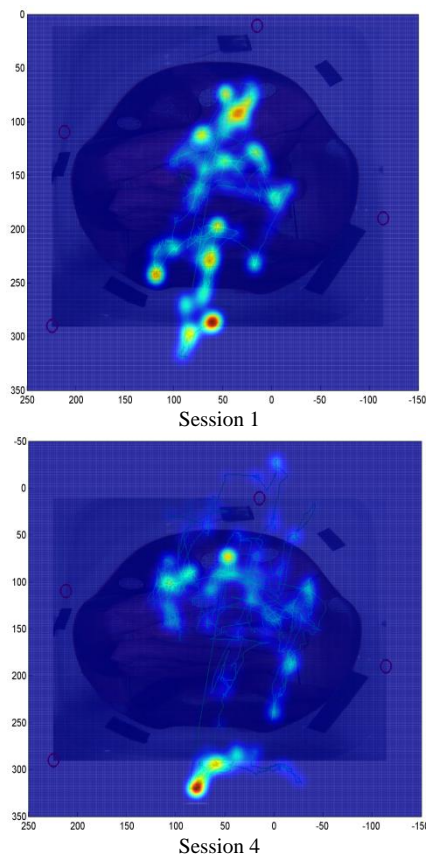


Fig. 4 Endoscope tip dwelling maps of the whole navigation task for subject 1. Redder hues represent longer dwelling times.

Examples of the dwelling maps are illustrated in Fig. 4. These maps allow qualitative assessment of the endoscopic navigation skills. It can be appreciated for instance that the entrance to the abdominal cavity represent a challenging manoeuvre in both examples. It is also apparent that in the first attempt the subject

encounters more taxing hotspots, likely to represent points at which the operator was finding difficulties to navigate. This is in clear contrast with its smoother navigation of the course at his fourth attempt. A plausible explanation is that the additional viewpoint providing supplementary information about the position of the endoscope as well as the surroundings is helping the operator to deliver a smoother manoeuvre.

DISCUSSION

This study was designed to explore the spatial awareness of operators during NOTES navigation and the possible enhancement in this spatial awareness by means of an additional viewpoint of the scene.

Subjects improved their performance at navigating in a NOTES environment as judged by time taken to complete a set course and number of targets visualised. Auxiliary viewpoint in NOTES could ease the navigation of the endoscope in extraluminal environments, by augmenting the operator's spatial awareness and reducing the operation time coupled with an increment in accuracy, thus increasing the patient safety. However since the session order was not randomised, it is acknowledged that this improvement might be a part of the learning curve. Further work is necessary to dissociate the effect of the adjuvant camera and the inherent learning process. Quantitative assessment of the spatial awareness remains a challenge.

REFERENCES

1. Karimyan V, Sodergren M, Clark J, Yang G-Z, Darzi A. Navigation systems and platforms in natural orifice transluminal endoscopic surgery (NOTES). *International Journal of Surgery* 2009;7(4): 297-304.
2. Clark J, Sodergren M, Noonan D, Darzi A, Yang GZ. The Natural Orifice Simulated Surgical Environment (NOSSE): Exploring the Challenges of NOTES without the Animal Model. *J Laparoendosc Adv Surg Tech A* 2009;19(2): 211-214.

Image Guided Robotic Radical Prostatectomy

S Thompson¹, G Penney², D Hawkes¹, O Elhage³, and P Dasgupta⁴

¹Center for Medical Image Computing, UCL, London

²Interdisciplinary Medical Imaging Group, Kings College London

⁴MRC Centre for Transplantation, NIHR Biomedical Research Centre, King's Health Partners, Guy's Hospital, London

³Department of Urology, Guys and St Thomas Hospital, London
s.thompson@ucl.ac.uk

INTRODUCTION

We present results of early trials of a system to overlay preoperative MRI onto endoscope video taken from a daVinci endoscope system during robotic radical prostatectomy. The endoscope is calibrated and tracked so that the MRI can be overlaid in the same coordinate system as the video data and projected onto the screen with the correct camera parameters. The system has two potential applications. The first is that it enables the surgeon to easily refer to the preoperative MRI during surgery. Secondly, it may serve as an initialisation for a model to video registration method to enable the preoperative data to be updated during the procedure. The system has been trialled in five patients, with overlay images provided to the surgeon during surgery in two cases. Further trials are ongoing.

MATERIALS AND METHODS

In order to overlay the MRI onto the endoscope screen it is necessary to register the preoperative MRI data to the video data. There are two approaches to doing this. The first of these is to register the endoscope image to the preoperative model directly using visible landmarks or surfaces. This has the advantage that it is not necessary to track the endoscope or the patient. This method has been used by a number of authors, a recent example of this method applied to robot assisted surgery is presented by Su et al. [1]. We do not wish to use this approach for two reasons. Firstly, it limits the period of time that image guidance is available. Secondly it requires surfaces or landmarks to be segmented from the preoperative image, a process that may be time consuming and/or inaccurate.

In preference to direct registration we attempt to first register the preoperative data to the patient in theatre to locate the data in the coordinate system of an optical tracking system. We then track the endoscope with the optical tracking system. Thus we know where the endoscope is relative to the preoperative image. This approach is common in image guided surgery. Typically fiducial markers are used to register the preoperative data in theatre, an example using magnetically tracked fiducial markers is given by Ukimara and Gill [2]. Our method avoids the need for implanted fiducial markers.

For robot assisted procedures the most common approach to endoscope tracking is to use the daVinci's own kinematic data, see Mourgues and Coste-Manière [3]. We track the endoscope with an optical tracker to try and improve tracking accuracy.

We use the pelvic bone to match the MRI data to the patient in theatre. As the prostate is closely coupled to the pelvic bone, motion of the prostate between the MRI scan and the start of the surgery is minimised. To enable this we have developed a novel shape model fitting method, see figure 1, to find the pelvic bone in the MRI.

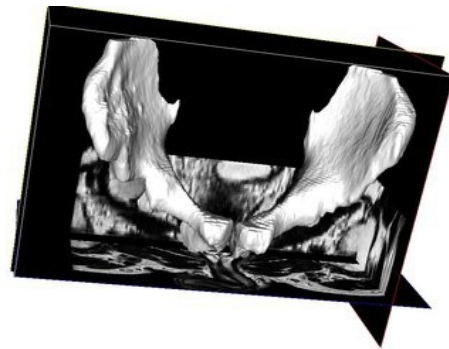


Figure 1. A statistical shape model based on the shape of the pelvis in 21 adult males is used to extract the shape of the pelvis from the preoperative MRI data.

The pelvic bone is found in theatre using a B-mode ultrasound probe tracked using an Optotrak Certus optical tracking system, see figure 2. Approximately 400 ultrasound slices of the patient's pelvis are then matched to the pelvic bone extracted from the MRI data using a point to volume registration algorithm. The algorithm has been shown to work on data collected in theatre. At present, however, the execution time is too long to be used in real time in theatre, though it should be straightforward to correct this with a parallel implementation. Real time clinical implementation to date has used a computer aided direct registration of the MRI to the video data. This uses points predefined on the inner surface of the pubic arch and custom software to align the video and MRI in less than a minute.

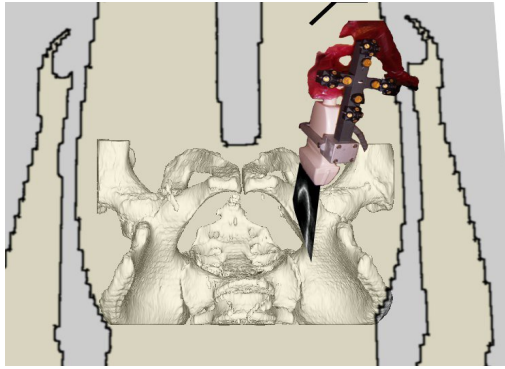


Figure 2. A series of ultrasound images of the patient's pelvic bone are collected in theatre. The position of these in the theatre are determined using an optical tracking system to track a group of infrared emitting diodes attached to the probe.

A custom built collar was fitted to the endoscope to allow it to be tracked with the same optical tracking system as was used for the ultrasound. Results indicate that this gives similar accuracy to using the daVinci's own kinematics. The endoscope is calibrated to determine the projection parameters (focal lengths and distortion) of the endoscope lens.

A slice of the preoperative MRI can now be projected onto endoscopic video. To date this projection has been done on a laptop computer adjacent to the surgeon's console, with plans to integrate it into the console in the future. Figure 3 shows an example overlay.

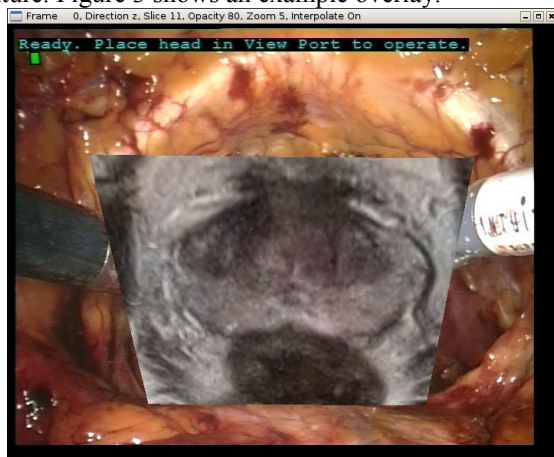


Figure 3. A transverse MRI slice projected onto endoscopic video. The surgeon can move through the MRI volume, change the slice direction and opacity.

RESULTS

The accuracy of the system components has been analysed using phantom, cadaver and real data. The system can project a MRI point onto the screen with an accuracy of approximately 20 pixels. This is visualised in figure 4. The chief source of projection error is the endoscope tracking accuracy.

The system has been tested on five patients to date with more pending. In the last two cases real time overlay

was achieved enabling the surgeon to refer to the overlaid MRI during the procedure.

DISCUSSION

Image guidance during endoscopic procedures is an expanding area of research. The daVinci robot provides a good platform on which to build an image guidance system, though the method presented here is compatible with any endoscopic system. Extension of our method to utilise the 3D projection of the daVinci should, in theory, be straight forward.

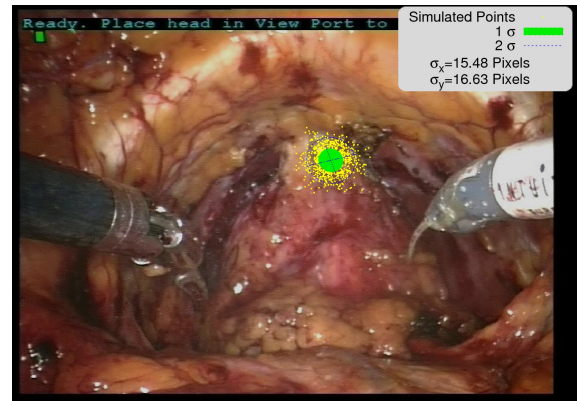


Figure 4. Projection accuracy is around 20 pixels. Here a single point (near the apex of the prostate) has been projected onto the screen 1000 times under the influence of our system errors, giving a visualisation of the size of the system error.

Our system does not correct for movement of the prostate. However, our results indicate that it still provides the surgeon with a useful reference that can be used to aid intra-operative decision making. The ability to refer rapidly to the MRI to visualise tumour locations is useful even though the alignment is not exact.

Work is ongoing to improve the accuracy of the various components, to better integrate them into the theatre environment, and to reduce the time taken for the automatic registration. We are also looking at ways to measure any improvement in surgical outcome.

REFERENCES

- [1] L. Su, B. P. Vagvolgyi, R. Agarwal, C. E. Reiley, R. H. Taylor, and G. D. Hager, "Augmented Reality During Robot-assisted Laparoscopic Partial Nephrectomy: Toward Real-Time 3D-CT to Stereoscopic Video Registration," *Urology*, vol. 73, pp. 896-900, 2009
- [2] Ukimura, O. and Gill, I. S., "Image-Fusion, Augmented Reality, and Predictive Surgical Navigation", *Urologic Clinics of North America* Volume 36, Issue 2, Pages 115-123 (May 2009), 115-123
- [3] Mourgues, F. and Coste-Manière, E., "Flexible Calibration of Actuated Stereoscopic Endoscope for Overlay in Robot Assisted Surgery", in *MICCAI*, Vol. 2488 of LNCS, Springer, pp.25-34

A Single Centre Experience of Robot-Assisted Laparoscopic Pyeloplasty

C. Slawinski, O. Elhage, B. Challacombe, N. Hegarty, P. Dasgupta

Urology Centre and MRC Centre for Transplantation, Guy's Hospital and King's College London

corinna.slawinski@kcl.ac.uk

INTRODUCTION:

Dismembered pyeloplasty is the standard management of pelvi-ureteric junction (PUJ) obstruction, with the aims of symptom relief and preservation of renal function. Traditionally, open techniques have been employed, with excellent success rates of over 90% [1], but are associated high morbidity rates and long periods of convalescence. However, with the advantages and increasing popularity of minimal access surgery, robotic techniques are playing an increasingly important role in the treatment of PUJ obstruction. Here we present the largest UK experience of robot assisted laparoscopic pyeloplasty (RALP) to our knowledge.

MATERIALS AND METHODS:

All transperitoneal Anderson-Haynes dismembered RALPs performed between 2004-2009 were prospectively assessed. Preoperative investigations included full blood count, serum urea and electrolytes, mid-stream urine, MAG3 renogram and a 3D reconstructed CT. A retrograde pyelogram was performed followed by JJ stent insertion. We have previously described our surgical technique, using the three-arm DaVinci® Surgical System (Intuitive Surgical®, Ca), used to perform all procedures [2]. Following surgical repair of the PUJ, JJ stent removal and follow-up MAG3 renograms were performed in all patients at 6 and 12 weeks respectively. All mean values are presented \pm standard deviation (SD).

RESULTS:

32 RALP, 15 left and 17 right, were performed for symptomatic PUJ obstruction, including 2 patients with horseshoe kidneys, one with a duplex kidney, and one re-do balloon dilatation. Mean age at operation was 36.7 ± 11 years. Mean operative and anastomosis times were 165 ± 39.2 mins and 41.2 ± 12.2 mins respectively, with an average robot docking time of 7.5 ± 7.3 mins. Mean blood loss was 59.1 ± 73.3 mls. Complications were seen in 4 patients (12.5%) (1 anastomotic leak required nephrostomy; 1 diathermy injury to the serosa of small bowel required no further intervention; 1 delayed wound healing; 1 post-operative urinary retention in a female required a catheter for 24 hours) and all were treated appropriately with no subsequent problems. Post-operative hospital stay was 2.4 ± 0.9 days. Mean follow up was 30 ± 14.4 months. One patient needed conversion to open due to difficult anatomy, and has consequently not been included in the overall success rate. One patient had worsening renal function and needed a nephrectomy and two were lost to follow up. The other 28 patients (90.3%) had symptomatic

relief and satisfactory drainage on post-operative renograms.

DISCUSSION:

The introduction of robotic surgery has addressed some of the limitations relating to both open and laparoscopic pyeloplasty. We have found a success rate of 90.3% with an average follow-up of 30 months. This is comparable with the current literature, where success rates of over 90% have been seen with follow up ranging 11.7 to 39.1 months [3-6]. Our mean operative time was 165 minutes, falling within the reported range (108-217 minutes) [3-6]. Mean operative blood loss was 59.1 ml and mean hospital stay 2.4 days (with one patient remaining for only 18 hours). These are equivalent to the current data available (ranging 40-60 ml blood loss and 1.1-4.6 days post-operative hospitalisation [3-6]). Currently reported complication rates range between 3.3 - 10.0% [3-6]. Similarly, we experienced complications in 4 patients, resulting in an average of 12.5%. These were all treated appropriately, with no sequelae and no patient requiring re-do operation or surgical intervention. Other previously reported notable complications have included stent migration, gluteal compartment syndrome, a renal pelvis clot, pyelonephritis, febrile urinary tract infection and splenic laceration [3].

Early in our series, the use of methylene blue injection pigmented the skin of one patient, and despite no subsequent lasting problems, its use was consequently abandoned. We experienced one conversion to open during our series, due to difficulty of the anatomy, however the outcome was successful, with no complications and a short period of hospitalisation (3 days). Furthermore, we have seen successful outcomes in the more complicated cases, including duplex and horseshoe kidneys.

We have previously reported our surgical technique [2] which has included completing the anterior wall of the anastomosis first. We have found this to create a more technically straightforward procedure, with no difficulty in subsequently suturing the posterior wall, and consequently a more watertight anastomosis.

A recent systematic review by Braga *et al.* [7] comparing laparoscopic pyeloplasty and RALP found a 10 minute reduction in operating time and a significantly shorter hospital stay associated with RALP. No differences were seen in success or complication rates, making RALP comparable to laparoscopic pyeloplasty. However, the main limitation not only to

this study, but the comparative assessment of these two techniques, is the relative paucity in the number of published studies, and the complete lack of randomised controlled trials.

The major disadvantage to robotic surgery is the associated cost. Link *et al.* [8] found a 2.7 times increase in the cost of RALP in comparison to laparoscopic pyeloplasty. Given these findings, and the equivalence of outcomes with laparoscopic surgery, one might ask how we can justify the introduction or continuing use of RALP?

The laparoscopic approach is technically challenging calling for intracorporeal suturing and a highly proficient laparoscopic surgeon, and is thus limited to experienced centres [5]. The robotic approach offers the advantages associated with minimally invasive surgery, but does not require extensive prior laparoscopic training, facilitating intracorporeal suturing through the EndoWrist® instruments, magnified 3D-vision, motion scaling and tremor filtering [9]. These well recognised advantages may increase the availability and reproducibility of the procedure and allow completion of more challenging procedures [10-12]. Furthermore, surgical training using the robot is faster and may therefore be particularly useful in centres with less laparoscopic experience and for use by surgical trainees [13].

In conclusion our experience with RALP has demonstrated the safety of the procedure and its efficacy, particularly in institutions where robotic surgery is available. We have demonstrated short operative times and duration of hospitalisation, with excellent success rates at long-term follow up. These results are comparable with the current literature. Despite the relatively small number of published studies, the use of robotics in PUJ obstruction appears to have an increasingly solid evidence base. However larger multi-centre studies are needed to directly compare the robotic and laparoscopic techniques. With the increasing availability of robotic systems we anticipate that RALP may become the standard management of PUJ obstruction, with benefits for both surgeon and patient.

REFERENCES:

- [1] Göğüş C, Karamürsel T, Tokatli Z, Yaman O, Ozdiler E, Göğüş O. Long-Term results of anderson-hynes pyeloplasty in 180 adults in the era of endourologic procedures. *Urol Int* 2004;73(1):11-4.
- [2] Murphy D, Challacombe B, Elhage O, Khan MS, Dasgupta P. Robotically assisted laparoscopic pyeloplasty. *BJU Int* 2008, Jul;102(1):136-51.
- [3] Mufarrij PW, Woods M, Shah OD, Palese MA, Berger AD, Thomas R, Stifelman MD. Robotic dismembered pyeloplasty: A 6-year, multi-institutional experience. *J Urol* 2008, Oct;180(4):1391-6.
- [4] Gupta NP, Nayyar R, Hemal AK, Mukherjee S, Kumar R, Dogra PN. Outcome analysis of robotic pyeloplasty: A

large single-centre experience. *BJU Int* 2009, Oct 28. [Epub ahead of print]

- [5] Schwentner C, Pelzer A, Neururer R, Springer B, Horninger W, Bartsch G, Peschel R. Robotic anderson-hynes pyeloplasty: 5-Year experience of one centre. *BJU Int* 2007, Oct;100(4):880-5.
- [6] Patel V. Robotic-Assisted laparoscopic dismembered pyeloplasty. *Urology* 2005, Jul;66(1):45-9.
- [7] Braga LH, Pace K, Demaria J, Lorenzo AJ. Systematic review and meta-analysis of robotic-assisted versus conventional laparoscopic pyeloplasty for patients with ureteropelvic junction obstruction: Effect on operative time, length of hospital stay, postoperative complications, and success rate. *Eur Urol* 2009; 56:848-858.
- [8] Link RE, Bhayani SB, Kavoussi LR. A prospective comparison of robotic and laparoscopic pyeloplasty. *Ann Surg* 2006, Apr;243(4):486-91.
- [9] Eden CG. Minimally invasive treatment of ureteropelvic junction obstruction: A critical analysis of results. *Eur Urol* 2007, Oct;52(4):983-9.
- [10] Sundaram CP, Grubb RL, Rehman J, Yan Y, Chen C, Landman J, et al. Laparoscopic pyeloplasty for secondary ureteropelvic junction obstruction. *J Urol* 2003, Jun; 169(6):2037-40.
- [11] Spencer CD, Sairam K, Challacombe B, Murphy D, Dasgupta P. Robot-Assisted laparoscopic pyeloplasty for the management of pelvi-ureteric junction obstruction in horseshoe kidneys: Initial experience. *Journal of Robotic Surgery* 2009;3(2):99-102.
- [12] Chammas M, Feuillu B, Coissard A, Hubert J. Laparoscopic robotic-assisted management of pelvi-ureteric junction obstruction in patients with horseshoe kidneys: Technique and 1-year follow-up. *BJU Int* 2006, Mar;97(3):579-83.
- [13] Passerotti CC, Passerotti AM, Dall'Oglio MF, Leite KR, Nunes RL, Srougi M, et al. Comparing the quality of the suture anastomosis and the learning curves associated with performing open, freehand, and robotic-assisted laparoscopic pyeloplasty in a swine animal model. *J Am Coll Surg* 2009, Apr;208(4):576-86.

Swimming Micro Robot for Ventricular Capsule Endoscopy

G. Kósa¹, G. Székely¹

¹ Computer Vision Laboratory, D-ITET, ETH Zurich,

INTRODUCTION

Capsule endoscopy is a promising technology enabling getting to destinations in the body that were out of reach of 'traditional' rigid or flexible endoscopes. The potential of such devices is well demonstrated by the M2A capsule manufactured by Given Imaging for the inspection of the small intestines [1]. However, this system's motion is limited to the natural peristaltic movement of the gastrointestinal tract. Other drawbacks are that it can not perform any intervention and its self localization is not accurate (1-3 cm accuracy), therefore a separate open surgery is necessary for treatment if a pathology is discovered by the device. We are interested in developing a capsule endoscope that has the ability to maneuver in 5 DoF (Degrees of Freedom) and it has tools for sensing and interventions. Our clinical target is to perform untethered endoscopic neurosurgery in the lateral ventricles. For further details on the intended medical scenario see [2].

Several groups are working on active capsule endoscopy and swimming micro-robots for medical applications. Menciassi et al. [3] develops a gastric capsule driven by four miniature propellers, powered by batteries and demonstrated a swimming velocity of 21.3 cm/s for an operating period of 7-8 minutes. The capsule's diameter is Ø15 mm and its length is 40 mm. Nelson et al. [4, 5] are working on magnetically driven micro robots for ophthalmic surgery. The micro-robots' overall size is in the order of 100 µm and their velocity is a few mm/s.

In this paper we discuss the overall design of a swimming capsule endoscope (See Fig. 1). We analyze its power consumption and maneuverability. This application was introduced in [2] and its initial design and power consumption breakdown is presented in [6].

MATERIALS AND METHODS

A mobile robot's sub-systems can be divided into several parts according to their function. Such a division was initially suggested by Dario et al. [7] and further developed by Ebefors and Stemme [8]. In [6] we suggested a slightly different component division as follows: Control Unit (CU), Actuation for Positioning (AP), Power Source (PS), Actuation for Manipulation (AM), Sensor Unit (SU) and Communication Transceiver (CT) (arguably one may also include this sub system into the command unit). We are separating the AP and SU in order to distinguish between active and passive capsules.

In our robot the division above is utilized as follows:

- CU (2 in Fig. 1) – Our control unit should convert the SU input into a signal, ready for the CT. In addition, the CU has to interpret the commands from the CT,

consequently generate the AP driving signals. In view of severe power limitations, such tasks can be best solved by specifically designed ICs (Integrated Circuits) [9]. Another option is to use a commercially available CU+CT such as a Texas Instruments CC2430. We assume a power consumption of $S_{PC} + S_{CT} = 5[mW]$.

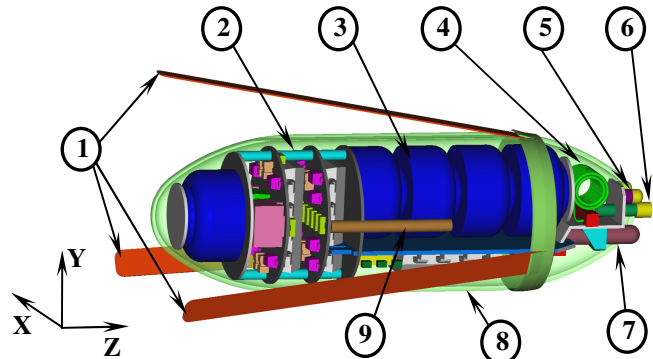


Fig. 1 Schematic view of the swimming capsule: 1)AP-Piezoelectric swimming tails, 2)CU+CT-Integrated circuits, 3)PS-5xZA10 Batteries, 4)CT-Antenna, 5)SU-LED, 6)AM-Biopsy 7)SU- Ø1.2 Medigus, 8)Housing, 9)SU-Tracking coil.

- AP (1 in Fig. 1) – The capsule is propelled by three piezoelectric bimorph actuators with the size of $23 \times 1.7 \times 0.1 \text{ mm}^3$. The tails generate a traveling wave with an amplitude of a few $10 \text{ }\mu\text{m}$ that propels the robot (see [10] for further details on their operation method).

- PS (3 in Fig. 1) – The greatest difficulty in building a miniature mobile robot is the power source. For this capsule endoscope we use 5 commercial zinc-air hearing aid batteries (Renata ZA-10), which we found the best solution available. The power supply of the batteries is $S_{PS} = 5 \cdot 14[mW] = 70[mW]$.

- AM (6 in Fig. 1) – We will develop for this application a tool for biopsy and a holder to place seeds for brachytherapy. Both tools are based on CU triggered quick release of mechanical or chemical energy.

- SU (5 and 7 in Fig. 1) – The sensor unit of the capsule is a new micro camera developed by Medigus using CMOS technology. The camera has a diameter of $\text{Ø}1.2 \text{ mm}$ and length of 4 mm. For illumination we use a commercial LED TLWH1100(T11) by Toshiba. The other sensor is a magnetic tracker coil based on the 6 DoF device Aurora (NDI), providing about 1 mm accuracy. The power needed by SU is $S_{SU} = S_{CAM} + S_{LED} = 26.2[mW]$.

Fig. 1 presents the integration of the different components into a capsule endoscope. The body of the device is based on a 32 mm long and $\text{Ø}12 \text{ mm}$ wide spheroid, which is flattened in order to fit in three swimming tails. In their closed state, the tails are parallel to the body and the capsule fits into a cannula with an inner diameter of $\text{Ø}10.4 \text{ mm}$. When opened, the

swimming tails rotate about their attaching point at front of the body and lock-down at an angle of 10° relative to the capsule's axis of symmetry. At their end they span a diameter of $\varnothing 18.3$ mm.

In order to calculate the maneuverability, we compared propulsive forces to the drag matrices of the capsule's components. Based on low Reynolds number hydrodynamics [11, 12] we assumed that the robot is built of four units: one spheroid representing the body and three cylindrical tails. The achievable linear and angular velocities of the robot can be derived from

$$\mathbf{PF}[\gamma_1 \ \gamma_2 \ \gamma_3]^T = \mathbf{D} \begin{bmatrix} \mathbf{v} \\ \boldsymbol{\omega} \end{bmatrix} = \begin{bmatrix} \mathbf{K} & \mathbf{C}^T \\ \mathbf{C} & \boldsymbol{\Omega} \end{bmatrix} \begin{bmatrix} \mathbf{v} \\ \boldsymbol{\omega} \end{bmatrix}, \quad (1)$$

where \mathbf{P} is a [6x3] matrix depending on geometrical parameters converting the propulsive forces into torques and forces applied on the center of gravity, F is the magnitude of the propulsive force created by a swimming tail, $\gamma_i \in [-1..1]$ are parameters setting the propulsive force's activation and \mathbf{D} is a [6x6] drag coefficient matrix converting the linear velocity vector, \mathbf{v} , and the angular velocity vector, $\boldsymbol{\omega}$, of the center of gravity into force and torque.

RESULTS

Two aspects of the overall design are analyzed in this paper. First, depending on the power budget, we set the AP maximal propulsive force, F . Second, based on (1) we determine γ_i to propel the swimming capsule along its axis of symmetry and turn it around the \mathbf{X} and the \mathbf{Y} axes.

The power budget of the robot is shown in Table 1.

Table 1	PS	AP	CU+CT	SU	Total
mW	70	-33.3	-5	-26.2	5.5

The component with the largest power consumption is the LED which consumes 25 mW at the operating frequency of 10 Hz. The CU+CT part is the smallest although it requires a large volume that can not be used for additional batteries.

Based on the AP power allotment we derived that each swimming tail provides a propelling force of 12.3 μN .

In order to make the capsule swim in the \mathbf{Z} direction, $\gamma_i = 1$ is necessary. The AP can provide a propulsive velocity of 15.1 mm/s in water (1 cP) and the velocities due the cross coupling in the drag matrix \mathbf{D} are negligible. At viscosity of 400 cP the propulsive velocity is 1.1 mm/s.

In order to turn the propulsion's direction around the \mathbf{X} axis, the settings $\gamma_1 = -1; \gamma_2 = .5; \gamma_3 = -.5$ have to be used. As a result, an angular velocity of $\Omega_x = 28.5$ %s is created. In addition, there are residual linear velocities $V_y = 0.42$ mm/s and $V_z = 0.037$ mm/s. Thus, the robot can make a U-turn in 6.3 s meanwhile it moves 2.6 mm in the \mathbf{Y} direction. The minimal volume in which the robot can turn is $1.9 \times 3.4 \times 3.2$ cm³.

Turning around the \mathbf{Y} axis is more difficult ($\gamma_1 = 0; \gamma_2 = 1; \gamma_3 = -1$). The angular velocity is $\Omega_y = 32.5$ %s but the residual linear velocity is large, $V_x = 1.8$ mm/s.

DISCUSSION

Building a swimming capsule endoscope is a challenging task and the greatest difficulty to be faced is to provide sufficient power. We solved this problem in the presented device by using 80% of the robot's volume for zinc-air batteries, choosing low power electronics and efficient piezoelectric actuators.

The robot can maneuver efficiently in the target area of the lateral ventricles and may be used for other tasks, too, such as the inspection of the stomach.

We intend to build this robot and experimentally investigate the accuracy of the theoretical estimates presented in this paper.

REFERENCES

- [1] Iddan G., Meron G., Glukhovsky A., and Swain P., Wireless capsule endoscopy, *NATURE*, 2000 MAY 25;405(6785):417-417.
- [2] Kosa G., Jakab P., Hata N., Jolesz F., Neubach Z., Shoham M., Zaaroor M., and Szekely G., Flagellar swimming for medical micro robots: Theory, experiments and application, in International Conference on Biomedical Robotics and Biomechanics, 2008. BioRob 2008. 2nd IEEE RAS & EMBS, 2008 Oct.:258-263.
- [3] Menciassi A., Valdastrì P., Harada K., and Dario P., Single and multiple robotic capsules for endoluminal diagnosis and surgery, in Biomedical Robotics and Biomechanics, 2008. BioRob 2008. 2nd IEEE RAS & EMBS International Conference on, 2008:238-243.
- [4] Yesin K.B., Vollmers K., and Nelson B.J., Modeling and Control of Untethered Biomicrobots in a Fluidic Environment Using Electromagnetic Fields, *Int. J. Rob. Res.*, 2006;25(5-6):527-536.
- [5] Zhang L., Abbott J.J., Dong L., Peyer K.E., Kratochvil B.E., Zhang H., Bergeles C., and Nelson B.J., Characterizing the Swimming Properties of Artificial Bacterial Flagella, *Nano Letters*, 2009
- [6] Kosa G., "Micro Robots for Medical Applications," in Surgical Robotics - Systems, Applications, and Visions, Hannaford B., Satava R., and Rosen J., Eds., 2010.
- [7] Dario P., Valleggi R., Carrozza M.C., Montesi M.C., and Cocco M., Microactuators for microrobots: a critical survey, *Journal of Micromechanics and Microengineering*, 1992 (3):141.
- [8] Ebefors T. and Stemme G., "Micro-Robotics," in The MEMS Handbook, Gad-El-Hak M., Ed. University of Notre Dame: CRC Press, 2002, pp. 281-2842.
- [9] Casanova R., Saiz A., Lacort J., Brufau J., Arbat A., Dieguez A., Miribel P., Puig-Vidal M., and Samitier J., Towards co-operative autonomous 1cm/sup 3/ robots for micro and nanomanipulation applications: MICRON, 2005 IEEE/RSJ International Conference on Intelligent Robots and Systems, 2005:789-94/CD-ROM.
- [10] Kosa G., Shoham M., and Zaaroor M., Propulsion method for swimming microrobots, *IEEE T ROBOT*, 2007 Feb.;23(1):137-150.
- [11] Cox R.G., The motion of long slender bodies in a viscous fluid Part 1. General theory, *Journal of Fluid Mechanics*, 1970;44(04):791-810.
- [12] Liron N. and Barta E., Motion of a rigid particle in Stokes flow: a new second-kind boundary-integral equation formulation, *Journal of Fluid Mechanics*, 1992;238:579-598.

Analysis of endorectal probe kinematics during prostate biopsies

C. Torterotot¹, P. Mozer^{1,2}, M. Baumann³, M.-A. Vitrani¹, G. Morel¹

¹ ISIR laboratory, University Pierre and Marie Curie, CNRS-UMR7222, Paris, France

² La Pitié-Salpêtrière hospital, urology dpt, Paris, France

³ TIMC laboratory, University Joseph Fournier, Grenoble, France

vitrani@isir.upmc.fr

INTRODUCTION

Prostate cancer is the most common non-skin cancer in men and the second leading cause of cancer death among them. Suspicion of prostate cancer resulting in a recommendation for prostatic biopsy is most often raised by abnormalities found on digital rectal examination (DRE) or by serum prostate-specific antigen (PSA) elevations.

Today, prostate biopsies are carried out using 2D Trans-Rectal Ultrasound (TRUS) probes equipped with a rigidly attached guide for spring needle guns. The procedure is challenging and the punctures locations are not well known:

- the gland moves and gets deformed under the pressure of the TRUS probe;
- the patient is neither immobilized nor under total anesthesia, most patients move significantly during the biopsy procedure.

It is therefore rather complex for the urologist to reconstruct the 3D geometry of the complete procedure, which justifies the worldwide effort in developing assistance navigation and robotic tools [1][2][3]. In this context, the present paper focuses in extracting two crucial geometrical characteristics, from data recorded on 78 patients subject to navigation-assisted prostate biopsies:

- the range of motion of the probe, which is of primary importance in robot design;
- the surface of the prostate sampled, which was never studied in the past to our knowledge. We think this data could be related to post-examination complications or to the efficiency of the cancer detection.

The presented study is thus a preliminary study that is part of the process leading to a robot aimed at improving patients' quality of life by enhancing the prostatic biopsy process.

MATERIALS AND METHODS

In order to increase prostate biopsy accuracy a device called UroStationTM has been developed (Koelis, Grenoble, France [4]). The device is based on a 3D TRUS system (Sonoace X8 scanner, Medison, Korea) linked to a computer with a network cable.

The clinical workflow is unchanged, except that after

each biopsy and before removing the needle, the surgeon acquires a 3D ultrasound image of the prostate. Using image-based registration algorithm [5] the UroStationTM is able to determine the transformation matrix between the current position and orientation of the prostate and a reference position and orientation (3D acquisition made at the very beginning of the examination). Thereby, the UroStationTM gives geometric information in a fixed reference space with respect to the prostate.

As described on [Fig. 1], one can get the coordinates of the transducer, the coordinates of the needle tip and the orientation of the probe. All these coordinates are given in the reference prostate frame which can move with respect to the body for more than one centimeter [6]. Furthermore the patient can move on the examination table. As a result, the analysis of the probe kinematics will be performed in the reference frame.

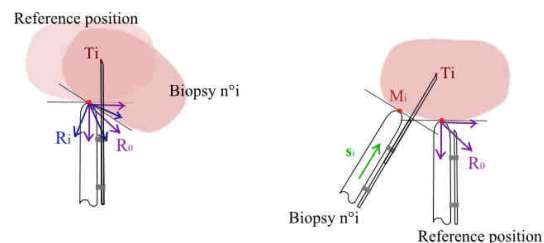


Fig. 1 Representation of the important frames and landmarks

The coordinates of the radial origin of the transducer, which is located at the tip of the probe, and the probe direction can be used to determine the space in which the physician moves the probe. For each examination, we compute an average position and orientation. Then for each biopsy we compute the difference between the current position and the average position. The biggest distance will give us the minimal work space that a robot requires to perform prostate biopsies.

The biopsy needle is brought in contact with the prostate capsule by the surgeon. Then a biopsy gun pushes the needle in the prostate on 22 millimeters. As the needle guide is connected to the probe, its orientation is the same. Using the needle tip coordinates and the ultrasonic probe orientation, one can so derive the coordinates of the needle entry point in the prostatic capsule.

The first twelve biopsies are always achieved in the same order, following a “sextant scheme” [Fig. 2] [7]. It appeared that, with time and frequent use of the

UroStation™, the surgeon performs the biopsies on the same locations but in a different order (for example the surgeon was thinking of doing the biopsy aimed to be the third, but realized afterward that it is placed on the fourth location, so he performs the fourth biopsy on the third location). We developed an algorithm able to calculate the pierced area in each prostate lobe independently from the order of the biopsies.

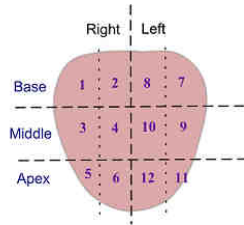


Fig. 2 Sextant biopsy scheme

RESULTS

We used data coming from the examination of 78 patients. The examinations have been performed by three different urologists between January and November 2009.

The robot should be able to work for all the patients. But it appeared that the probe workspace varies a lot between individuals, as it is summed up in the table #1.

	Transducer position difference (mm)	Probe direction difference (deg)
Minimum	5,0	12,2
First decile	7,1	16,7
Median	9,0	21,7
Ninth decile	12,2	26,1
Maximum	20,6	30,2
Average	9,2	21,4

Table #1 Statistic treatment of the maximum differences of each subject

The same variability in results can be observed about the pierced surface. It has a tendency to be correlated with the prostate volume, as it is shown in [Fig. 3.]. The averaged pierced area for one lobe is about 1 cm² only. It also appeared that the left lobe pierced surface is in average bigger than the right lobe one.

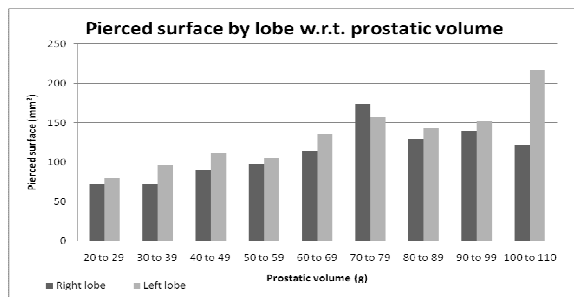


Fig. 3 Value of the pierced area in each lobe, depending on prostatic volume.

DISCUSSION

The results are quite in accordance with the intuitions of the surgeons, concerning the size of the probe

workspace. But we have to keep in mind that this workspace is defined relatively to the prostate, and not relatively to a robot base fixed in the examination room. To be known relatively to the robot base, the robot workspace we found shall so be augmented by the displacement of the prostate relatively to the room. The study of the pierced area brings really new information. The surgeons thought the pierced area was more important for the right lobe than for the left one, arguing it corresponds to a position that is more comfortable for them. But it appeared to be the contrary. This could be due to a weaker precision during the biopsy of the left lobe, which results in an underestimation of the probe displacement by the surgeon.

The results we get also indicate that patients undergo very different examinations one from the other, that probably don't have the same accuracy in cancer detection. A new study, crossing these results with medical data such as cancer detection is currently performed.

This preliminary study shows the interest of adding a robot endowed with comanipulation skills: it could standardize the procedure but also help the surgeon to enlarge the pierced areas. Indeed, the surgeon is limited in his gesture to the displacements that allow him to have a mental representation of the prostate and to locate the needle in it. Thus not all motion combinations are exploited, like the probe rotation around its axis for example. The use of a robot could increase the accuracy of the gesture and thus of the cancer detection, allow local treatment which exposes the patient to less side-effect risks and hence potentially offers a better quality of life to the patient after treatment.

REFERENCES

- [1] Feimo Shen, Ramkrishnan Narayanan, and Jasjit S. Suri, Rapid Motion Compensation for Prostate Biopsy using GPU, 30th Annual International IEEE EMBS Conference, Vancouver, Canada, 2008
- [2] Di Xiao, Louis Phee, John Yuen, Chee Fatt Chan, Feng Liu, Wan Sing Ng, Henry Ho, Choon Hua, Thng, Puay Hoon Tan and Christopher Cheng, Software Design of Transperineal Prostate Needle Biopsy Robot, 2005 IEEE Conference on Control Applications, Toronto, Canada
- [3] G.S. Fischer, J. Iordachita, S.P. DiMaio and G. Fichtinger, Design of a Robot for Transperineal Prostate Needle Placement in MRI Scanner, IEEE 2006
- [4] <http://www.koelis.com>
- [5] M. Baumann, P. Mozer, V. Daanen, and J. Troccaz, Towards 3D Ultrasound Image Based Soft Tissue Tracking: A Transrectal Ultrasound Prostate Image Alignment System, MICCAI 2007
- [6] Maud Marchal, Modélisation des tissus mous dans leur environnement pour l'aide aux gestes médico-chirurgicaux, PhD Thesis, Grenoble, Dec 2006
- [7] A. Villiers, D. Mouton, X. Rébillard, D. Chautard, A. Rufion, F. Staerman and F. Cornud, Conditions de réalisation et schéma de ponctions lors d'une première série de biopsies prostatiques, Recommandations du comité de Cancérologie de l'AFU, Progrès en urologie

Three Dimensional Tracking and Image Registration Using a da Vinci Triple Endoscope System

N.T. Clancy^{1,2}, D. Stoyanov¹, V. Sauvage^{1,2}, D.R.C. James^{1,2}, G.Z. Yang^{1,3},
D.S. Elson^{1,2}

¹*Institute of Biomedical Engineering, Imperial College London,*

²*Department of Surgery and Cancer, Imperial College London,*

³*Department of Computing, Imperial College London*

n.clancy@imperial.ac.uk

INTRODUCTION

Multispectral imaging is used in biomedical applications to detect chromophores such as haemoglobin [1], or for narrowband imaging in flexible endoscopy [2]. The technique works acquiring images of tissue at several wavelengths and combining them, so that a spectrum is obtained at each pixel.

Wavelength scanning is achieved using tuneable filters [1] or mechanical filter wheels [3]. However, the time difference between acquisition of the first and last images may be several hundred milliseconds or longer. In an endoscopic surgical environment, camera movement, motion blur and lack of surface features make registration of the multispectral images challenging and time-consuming.

In this paper, a new system is proposed based on a da Vinci trinocular (three channel) endoscope that simultaneously acquires colour stereo and multispectral images. The aim of the device is to accurately align images of a moving object by tracking its position in 3D after calibrating its three cameras. This paper presents results demonstrating the 3D reconstruction, alignment and multispectral analysis using a standard colour checker card as the moving object.

Although multispectral imaging is discussed here, the same approach may be applied to any imaging technique using sequential acquisition, including fluorescence or polarisation imaging. The device itself may also be readily used in robotic-assisted minimally-invasive surgery [for example, in the da Vinci Surgical Console (Intuitive Surgical, Inc.)], overlaying information on the functional state of the tissue on the 3D shape of the area of interest to provide valuable feedback to the surgeon.

MATERIALS AND METHODS

A da Vinci trinocular endoscope was adapted as shown in Fig 1, by adding imaging and multispectral optics to the stereo and central wide-angle channels. Colour CCD cameras (IDS Imaging GmbH) were used for the stereo pair along with 12.7 mm diameter, 50 mm focal length achromatic focusing lenses. A 45° plane mirror was used to deflect light to the multispectral camera system. A xenon lamp (Karl Storz GmbH) supplied broadband

visible light via a fibre-optic light cable and internal fibre-optic bundle.

A 25.4 mm diameter, 75 mm focal length lens was used to match the field of view of the central channel to that of the stereo pair. The multispectral system then consisted of a liquid crystal tuneable filter [LCTF (range: 400-720 nm, resolution: 10 nm); CRI, Inc] and monochrome camera (Thorlabs, Inc), mounted after the focusing lens.

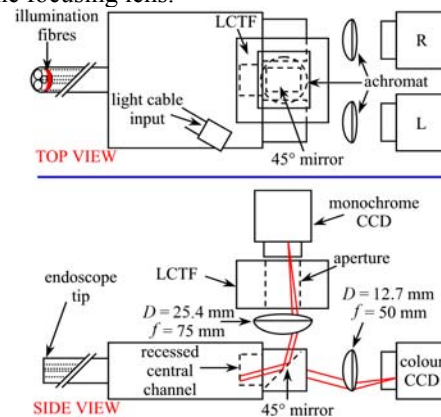


Fig. 1 Optical arrangement of the system showing the positions of lenses for the stereo and multispectral cameras.

The standard pinhole camera model [4] was used to map points in 3D space onto each camera plane using a matrix multiplication factor. This was derived using a calibration routine involving the acquisition of several images of a calibration card (checkerboard) in different orientations and positions [5].

The calibration allowed the positions of each camera relative to each other and a reference coordinate system to be determined. Using this information along with the intrinsic camera parameters obtained in the calibration, the 3D position of a point on an object could be calculated by finding features across the three different views of the scene, projecting light rays through them and recording the point of intersection [6].

A standard colour chart was placed in front of the endoscope and images recorded from the three cameras as its position was changed and the LCTF scanned through a range of wavelengths (420-700 nm in 20 nm steps). The 3D reconstruction method described above was then used along with knowledge of the

object's geometry to 'dewarp' and align each of the images, allowing the multispectral data to be recovered.

RESULTS

Figure 2 shows a set of sample images of the colour chart during acquisition of multispectral data.



Fig. 2 Sample images acquired by the left stereo camera and multispectral camera showing the colour chart in different positions at 500, 640 and 680 nm before (raw) and after alignment.

The 3D position of the card at each wavelength step was calculated, and surface points tracked to determine a transformation to 'dewarp' and align each image with respect to a reference [first image (420 nm)] The aligned images were then analysed by extracting regions of interest to obtain spectroscopic information on the individual colour panels of the checker card. Figure 2 shows the images before and after alignment.

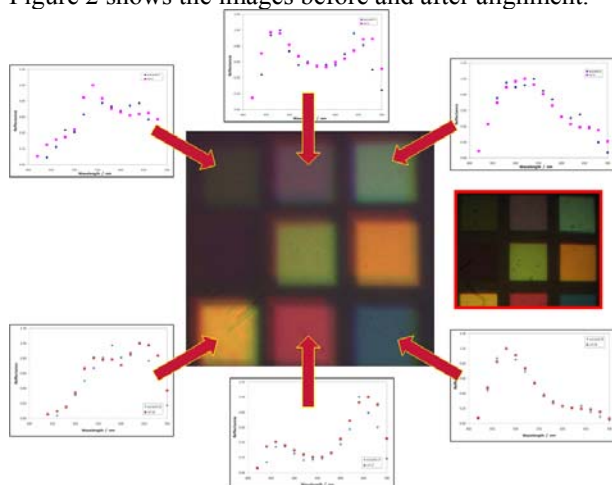


Fig. 3 Panels of the colour card reconstructed using the aligned multispectral images. Agreement was found between reflectance spectra of panels obtained from aligned images (blue) and those from a stationary equivalent (red; inset right).

Reflectance spectra were calculated by dividing the reflected intensity from each colour panel, at each LCTF wavelength, by the corresponding intensity reflected from a white reflectance standard. These were compared to a set of spectra obtained using a set of images of the card while it remained stationary. Additionally, for qualitative testing of the quality of the alignment procedure, the colours in each panel were reconstructed by summing the contributions of each multispectral image, weighted by the measured red, green and blue filter response of the colour cameras. Despite significant movement of the card (in comparison with typical tissue movement *in vivo*; translation range ≈ 3 cm perpendicular to camera axis, 5 cm parallel to axis; rotation $\approx 10^\circ$), the reflectance spectra and reconstructed colours proved a good match

to those of the stationary equivalent. This was quantified using Bland-Altman analysis [7], where it was found that there was negligible bias in the spectra measured by the trinocular system (average difference in reflectance = 0.03), and 95% of the differences were found, on average, in the range ± 0.20 .

The apparent blur on the edges of the colour panels is due to slight misalignment of the 'dewarped' images. However, this error is small (≈ 0.05 cm) in comparison with the gross displacement of the target, and does not prevent recovery of the spectral data.

DISCUSSION

Simultaneous stereoscopic and multispectral imaging has been demonstrated using a trinocular endoscope. The system allows sharp full colour pictures to remain available to the operator throughout navigation and acquisition of data with a reduction in misregistration colouration artefacts near sharp colour borders.

Accurate alignment of the multispectral images has been achieved by tracking points on the target in 3D, eliminating the need for traditional image registration. The technique is currently being adapted for *in vivo* work, where surgeon/tissue movement during acquisition of the multispectral image stack may be compensated for. Further system evaluation experiments will also quantify the relationship between the range of motion of the target and alignment accuracy. The system may also be easily integrated directly onto the da Vinci platform to provide multimodal optical information about the tissue state.

ACKNOWLEDGEMENTS

We gratefully acknowledge the loan of the laparoscope by Intuitive Surgical, Inc. Funding for this project was provided by the UK EPSRC and Technology Strategy Board grants EP/E06342X/1 and DT/E011101/1.

REFERENCES

- [1] Ilias MA, Häggblad E, Anderson C, and Salerud EG. Visible, hyperspectral imaging evaluating the cutaneous response to ultraviolet radiation. Proc SPIE - Imaging, Manipulation and Analysis. 2007;6441:644103.
- [2] Takano JH, Yakushiji T, Kamiyama I, Nomura T, Katakura A, Takano N, and Shibahara T. Detecting early oral cancer: narrowband imaging system observation of the oral mucosa microvasculature. Int J Oral Maxillofac Surg. 2010;39(3):208-213.
- [3] Roblyer D, Richards-Kortum R, Sokolov K, El-Naggar A, Williams MD, Kurachi C and Gillenwater AM. Multispectral optical imaging device for *in vivo* detection of oral neoplasia. J Biomed Opt. 2008;13(2):024019.
- [4] Hartley R and Zisserman A. Multiple view geometry in computer vision. 2000;Cambridge University Press.
- [5] Zhang Z. A flexible new technique for camera calibration. IEEE T Pattern Anal. 2000;22(11):1330-4.
- [6] Scharstein D and Szeliski R. A taxonomy and evaluation of dense two-frame stereo correspondence algorithms. Int J Comput Vision. 2002;47(1/2/3):7-42.
- [7] Bland JM and Altman DG. Statistical methods for assessing agreement between two methods of clinical measurement. The Lancet, 1986;327(8476):307-310.

Design of A Robotic Accessory for Abdominal Surgery

¹Dr. Bhavani Rao Reddi, ²Uttam Grandhi

¹Associate professor of Surgery, Rangaraya Medical college, Kakinada, INDIA

² Mechanical Engineering Group, Birla Institute of Technology and Science , Pilani, INDIA

¹rbhavanirao@gmail.com, ²uttam.grandhi@gmail.com

- **Length:** 7 cm & **Diameter:** 10mm (Standard Laparoscopic Port)

INTRODUCTION

Though advances in Laparoscopy have emerged as instruments like In Vivo Laparoscopes and Articulating Laparoscopes [1]-[4] and Flexible Endoscopes [5], fully capable devices have not yet arrived. The research has led to reducing the number of ports and their sizes, but major part of the instruments are rigid. The long instruments and lack of 3D visual feedback becomes an inherent limitation of the devices used till date. A flexible Robotic accessory that can reach every crevice of abdominal cavity greatly increases the maneuverability. In this paper, we propose a novel design of a robotic accessory controlled by a gloved hand or a set of actuators for performing abdominal surgeries. Recent trend in human-robot interaction [6] has motivated us to implement effective interactivity in the model. Our ultimate aim is to reach a state of unsupervised robotic surgeries with little or no intervention. Also, in the paper we have proposed a novel concept of “Camera Pillar” to give 3D visual information onto the screen of surgeon’s goggles. Additional advantages and other challenges are also discussed.

MATERIALS AND METHODS

The string controlled instrument Fig 1. is made using stainless steel considering the issues of sterility and strength. A flexible rubber sheath which can reach the inside of abdominal cavity either through mouth or laparoscopic port transmits required cables and strings. It also transmits data cables for image transmission and power cable for diathermy and light source. The metallic tips of the device eliminate the need of an additional diathermy tip. The tips can be controlled by a glove like structure from outside the abdominal cavity, Fig 1(a). The device in relaxed mode opens up the instrument as shown Fig 1(b). The instrument can be modified so as to be controlled with actuators that are interfaced to a computer. Different programs can be written for a wide variety of surgeries. Images transmitted through data cables attached to the camera pillars Fig 2(a) and computer onto screens worn by surgeon like goggles gives him 3D view of interior of abdominal cavity.

FINER DETAILS

Considering current challenges and requirements of a surgeon in performing Laparoscopic surgeries, a robotic accessory with a 2-DOF wrist, three 5-DOF fingers with a scissors, a grasper and a forceps as an end effector is proposed.

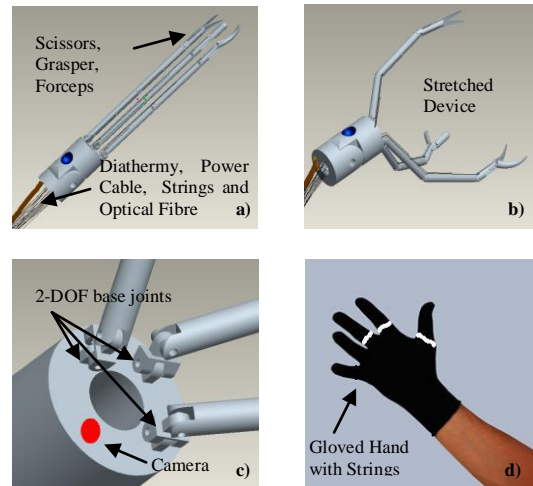


Fig 1. a) Collapsed Device b) Stretched Device c) Base Joints of Fingers and Camera d) Gloved Hand with Strings

- **Tendons:** Each finger joint is loaded with a spring and in default position is in flexed position. 5 tendons control each finger including the end-effectors (Scissors/ Grasper/ Forceps). Therefore, a total of 15 strings (tendons) for 3 fingers . Additional 2 tendons are required for wrist. The entire gadget needs a total of 17 tendons, one diathermy cable, one camera cable and an optical fibre .Steel Wires with sufficient strength and diameters 0.2mm-0.6mm are readily available [8]. The sheath of the device hosting the cables can be accommodated in a diameter of 9mm.
- **Actuation:** The aim is to replicate precise and smooth moments of each finger joint individually and in a well coordinated combined activity either by a Gloved Hand or with the help of a series of Actuators. The actuators are attached to a computer and are programmable to do different and complex surgeries.
- **Image Acquisition:** Image acquisition is done with the help of a, *Camera Pillar*. It is initially dropped into gas inflated abdominal cavity through the 10mm port made for inserting the robotic accessory. A Camera Pillar is a co-axial structure which houses light sources and cameras with inbuilt powerup the equipment. It has a diameter of 9 mm and length of 7.5 cm (in buckled up state). The inner shaft which slides on outer sheath can reach any length up to 14 cms in unbuckled state. The inner shaft has a core that transmits light vertically and cameras with dedicated light sources on its periphery near the

apex. Once placed vertically in the gas filled abdomen, the light pillar is unbuckled to desired length by pressing a lever close to its apex. Reduction in height can be done by simply pressing on its apex. Each pillar acts as tent support for anterior abdominal wall. Any number of Camera Pillars can be used. However, the use of two pillars is minimum requirement to obtain 3-D images.

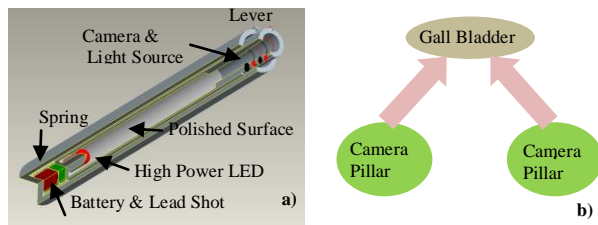


Fig 2. a) Camera Pillar b) Gall Bladder Visualization

Imagine the above scenario. The pillars are placed about 10cms away from point of interest e.g. Gallbladder . Each pillar is placed at a distance of about 7.5 cms (Normal eye position)

- **Data Transfer:** A needle containing data and power cables is punctured through the abdominal cavity into the core of the light pillar. It makes the camera and the light bulbs live. Once, the needle is inserted, it totally illuminates the abdominal cavity and image acquisition starts transmitting to the surgeon's goggles [7] as well as onto the computer monitor.

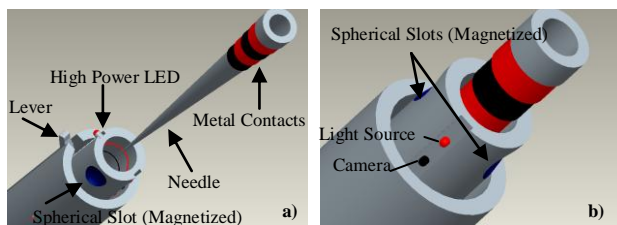


Fig 3. a) Camera Pillar b) Camera Pillar with Needle Inserted

- **Stabilizing the Device:** A uni-polar magnetized pit is provided on the wrist which immediately grasps the stabilizing rod when inserted. The rod is also made hollow (3mm pipe) to suck the secretions and blood that might hinder the operation. After the surgery, it is removed by applying opposite polarity to the rod tip. In the current scenario, of gloved hand model an assistant would be holding the stabilizing rod.

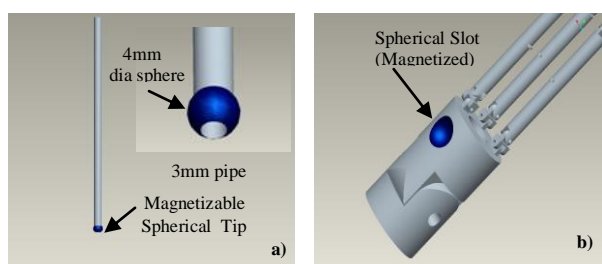


Fig 4. a) Stabilizing Rod (10 cm) b) Slot on device wrist

DISCUSSION

Since the entire program necessary for a given surgery is stored in a computer, the size of the robotic accessory need not be changed. If entire robot has to go to inside the abdomen, the size of the robot has to be bigger depending upon the complexity of the surgery. As the surgeon can manipulate the tip of the instrument through a computer interfaced actuator , he can perform surgery from a distance thus has an application in Tele surgery. With relative ease with which a surgeon can reach smaller anatomical structures, newer surgical modalities can be invented. The tip of the instrument can be modified to incorporate a scanning probe. This is useful for better imaging of liver, pancreas etc. With the possibility of choosing between a manual (Glove System) or an automatic (Actuator Control) , the surgeon can actually choose whether to program his surgery or to do it manually depending on the complexity of the surgery, requirement and interest of the surgeon.

ADVANTAGES

- It reaches remote areas like securing Hepatic vein in liver resection. The conventional lap instruments cannot reach it easily.
- A cholecystectomy or Appendicectomy needs 3 or 4 ports or a single port equivalent to the length of 4 ports in the conventional laparoscopy. With this laparoscopic accessory these surgeries can be performed with single port and two punctures and with ease.
- Surgeries like hemicolectomy can be done with less number of ports, greater ease and with less positional changes of the table.
- One great advantage is its extensibility. The strings can be attached to a pulsed motor which in turn connected to a computer. A real robotic surgery programs can be written and executed. Tele robotic surgery can be performed.
- The working space of the abdominal cavity is maintained without positive intra abdominal pressure. Avoiding positive intra abdominal pressure reduces adverse hemodynamic complications.

REFERENCES

- [1] Mark E. Rentschler et al. "In vivo laparoscopic robotics", International Journal of Surgery (2006) 4, 167e171
- [2] A. Röse, H.F. Schlaak, "A parallel kinematic mechanism for highly flexible laparoscopic instruments", Technische Universität Darmstadt, Institute of Electromechanical Design, Darmstadt, Germany
- [3] Thomas Frede et al. "The Radius Surgical System", European Urology 51 (2007) 1015–1022
- [4] Yasumitsu Hirano et al. "Single-incision laparoscopic Cholecystectomy", World J Gastroenterol 2010 January 14; 16(2): 270-274
- [5] S. E. Amory, K. A. Forde, and J. L. Tsai, "A new flexible video endoscope for minimal access surgery", Springer Surg Endosc (1993) 7:200-202
- [6] <http://www.kz.tsukuba.ac.jp/~hoshino/mov/glove-hand.html#>
- [7] <http://computer.howstuffworks.com/3d-pc-glasses1.htm>
- [8] http://www.alibaba.com/product-gs/277723377/Armouring_cable_wire.html

An assessment of the physical impact of a complex surgical task on surgeons: comparison between robotic assisted, laparoscopic and open techniques.

O Elhage^a, B Challacombe^a, A Shortland^b, P Dasgupta^{a,c}

^a*Urology Centre, Guy's & Thomas' NHS Foundation Trust, London, UK*

^b*One Small Step Gait Laboratory, Guy's & St Thomas' NHS Foundation Trust, London*

^c*MRC Centre for Transplantation, NIHR Biomedical Research Centre, Guy's Hospital, King's College London, UK*

Corresponding author: oussama.elhage@kcl.ac.uk

INTRODUCTION

Open surgery provides the surgeon with direct vision of operative field and user-friendly instruments. Minimal invasive approach started with laparoscopy in the early 1990s [1]. By contrast to open surgery, the technical challenges to laparoscopic surgery may lead to specific ergonomic problems for the surgeon. 2D monoscopic camera system can cause eye strain [2], manipulation of long instruments at awkward angles leads to wrists and shoulders injuries [3], [4]. A major restriction on maneuverability is the 4 degrees of freedom (DoF) provided by laparoscopic instruments [5]. The introduction of the master-slave robot systems in particular, has brought major technical advances. The system allows 3D stereoscopic vision, more degrees of freedom (7 instead of 4 with conventional laparoscopy), elimination of tremor, and motion scaling. These features combined allow more precision than either laparoscopic or traditional open surgery [6]. Until now, there has been little work comparing the ergonomics of Robot Assisted Surgery (RAS), Laparoscopic surgery (LAP) and Open Surgery (OPEN). In RAS the surgeon is seated at a console, with the forearms resting on a padded bar. Whereas, during LAP the surgeon is standing, often with arms outstretched away from the body in positions believed to put significant stress on the back, arms and shoulder girdle. Recent work by Berguer et al[4,7] has demonstrated that over a short period laparoscopic surgical simulations result in greater muscular effort than open techniques. This may in part be due to the design of the instruments, the anterior-position of that the upper limbs and the erect position of the trunk [8]. Laparoscopic surgery may lead to an increased incidence of digital neuropraxia and other musculoskeletal injuries [9-11] to the surgeon. A comparison of LAP RAS and open surgery on the surgeon's ability to complete an extended realistic in vitro simulation has not to date been evaluated. Experiments have been conducted where variants of the LAP technique have been compared [12,13] (e.g. stereoscopic, monoscopic with digital enhancement and monoscopic visualization). Simulations amongst different grades of surgeons have demonstrated lesser variability of motion (estimated using planar video) during LAP with increasing experience [14]. Computerised 3D motion analysis allows quantification

of body position and range of movement during workplace tasks. Surface electromyography allows recordings of muscular effort and fatigue to be made during repetitive work [15,16]. Employed together, they can be used to analyse the efficacy and ergonomics of particular tasks. The discomfort or fatigue experienced by the surgeon can also be measured by self-report such as a modified Borg scale. The aim of this study is to quantify the physiological and psychological determinants of fatigue, in an in-vitro simulation of a surgical procedure, using 3 competing surgical technologies (open, lap, robotic).

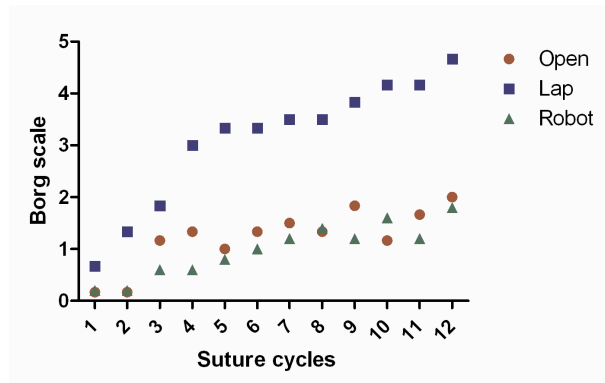
METHODS

We recruited 6 urological surgeons (41+/- 5 years). All the surgeons had 10 years experience in open surgery. The surgeons performed two vesico-urethral anastomoses in a session (each anastomosis consisted of 6 interrupted suturing cycles) under dry in vitro conditions using a robot, a laparoscope or as an open procedure. Subjects rated their level of discomfort using a modified Borg scale for each suture cycle. Movement data was captured using a 3D system (Vicon;PlugInGait). We quantified the mean posture over alternate suture cycles. We recorded muscle activity from the wrist extensors, wrist flexors, deltoid, upper trapezius, longissimus and multifidus (left and right sides) using surface electromyography (EMG). Video recordings of each procedure were made. We quantified the number of mistakes made by each surgeon. Results for level of discomfort, number of surgical errors were analysed using repeated measure ANOVAs.

RESULTS

LAP caused greater discomfort than the other two techniques ($p < 0.001$, Figure) and produced the greatest number of surgical errors. Discomfort increased significantly with suture number in each technique ($p < 0.001$) but the number of errors did not increase with suture number. Body posture was maintained during the 12 suture surgical task but there were large differences in body posture adopted by the surgeons for each technique with increased trunk flexion during RAS; increased neck extension during open surgery and increased shoulder abduction during LAP. Mean EMG

amplitude was maintained for each suture cycle during each surgical task except for the right deltoid muscle, the amplitude of which fell dramatically towards the end of each session.



DISCUSSION

LAP results in greater levels of discomfort in the surgeon, and a higher number of mistakes, than open surgery or RAS. Shoulder pain in LAP appears to be associated with a failure of recruitment of the right deltoid muscle. Most surgeons experienced increasing pain in their right shoulder during LAP which was associated with loss of deltoid muscle activity. Provision of support for the upper limbs during LAP or changes in the design of the laparoscopic instruments may improve the surgeon's level of fatigue and performance by offloading this muscle group.

REFERENCES

- [1] Schuessler W, Kavoussi L, Clayman R, Vancaille T. Laparoscopic radical prostatectomy: initial case report. *J Urol* 147, 246A. 1992.
Ref Type: Abstract
- [2] Hemal AK, Srinivas M, Charles AR. Ergonomic problems associated with laparoscopy. *J Endourol* 2001; 15(5):499-503.
- [3] Nguyen NT, Ho HS, Smith WD, Philipps C, Lewis C, De Vera RM et al. An ergonomic evaluation of surgeons' axial skeletal and upper extremity movements during laparoscopic and open surgery. *Am J Surg* 2001; 182(6):720-724.
- [4] Berguer R, Gerber S, Kilpatrick G, Beckley D. An ergonomic comparison of in-line vs pistol-grip handle configuration in a laparoscopic grasper. *Surg Endosc* 1998; 12(6):805-808.
- [5] Patkin M, Isabel L. Ergonomics, engineering and surgery of endosurgical dissection. *J R Coll Surg Edinb* 1995; 40(2):120-132.
- [6] Lee E, Rafiq A, Merrell R, Ackerman R, Dennerlein J. Ergonomics and human factors in endoscopic surgery: a comparison of manual vs telerobotic simulation systems. *Surgical Endoscopy* 2005; 19(8):1064-1070.
- [7] Berguer R, Chen J, Smith WD. A comparison of the physical effort required for laparoscopic and open surgical techniques. *Arch Surg* 2003; 138(9):967-970.
- [8] Berguer R, Rab GT, bu-Ghaida H, Alarcon A, Chung J. A comparison of surgeons' posture during laparoscopic and open surgical procedures. *Surg Endosc* 1997; 11(2):139-142.
- [9] Horgan LF, et al. Neuropraxia following laparoscopic procedures: An occupational injury. *Minim Invas Ther Allied Technol* 1997; 6:33.
- [10] Ganga RV, et al. Pressure Sore and Digital Neuropraxia of the thumb in laparoscopic cholecystectomy. *Surg Laparosc Endosc Percutan Tech* 2004;14(3):178-179.
- [11] Van der Zee DC, et al. Digital nerve compression due to laparoscopic surgery. *Surg Endosc* 1997; 9:740.
- [12] Minnich DJ, Schell SR. Evaluation of face mounted binocular video display for laparoscopy: outcomes of psychometric skills testing and surgeon satisfaction. *J Laparoendosc Adv Surg Tech A* 2003; 13(5):333-338.
- [13] Tendick F, Bhojru S, Way LW. Comparison of laparoscopic imaging systems and conditions using a knot-tying task. *Comput Aided Surg* 1997; 2(1):24-33.
- [14] Smith SG. Motion Analysis. *Surgical Endoscopy* 2002; 16(4):640-645.
- [15] Green ND, Brown L. Head positioning and neck muscle activation during air combat. *Aviat Space Environ Med* 2004; 75(8):676-680.
- [16] Emam TA, Hanna G, Cuschieri A. Ergonomic principles of task alignment, visual display, and direction of execution of laparoscopic bowel suturing. *Surgical Endoscopy* 2002; 16(2):267-271.

First Surgical Procedures under Camera-Augmented Mobile C-arm (CamC) guidance

S. Weidert¹, MD, L. Wang², J. Landes¹, MD, A. von der Heide¹,
N. Navab², E. Euler¹, MD

¹Chirurgische Klinik und Poliklinik Innenstadt, LMU Munich

²Chair for Computer Aided Medical Procedures, TU Munich

simon.weidert@med.uni-muenchen.de, navab@cs.tum.edu

INTRODUCTION

The Camera-Augmented Mobile C-arm (CamC) is an X-ray imaging device, which includes an optical camera and provides real-time co-registered X-ray and optical images. This system, introduced by Navab et al [1,2], allows the X-ray and optical imaging systems to share the same projective geometry thanks a simple single or double mirror construction (see Fig. 2). Here, we report on the introduction and use of this system within the operating room for the first time. While there is already experimental evidence that presumes a radiation sparing effect in several workflow steps [3], we believe that the presentation of co-registered optical and X-ray images to the surgeon will result in safer operations by making patient access and surgical act become more intuitive. The introduction of this novel technology into the operating room could allow surgeons to take advantage of the additional information provided by CamC to invent new techniques and methods changing the way in which many surgeries are carried out today.



Fig.1 X-ray augmented real-time video image of the first surgery done under CamC.

The number of surgeries within our on-going patient studies is not yet sufficient to provide a detailed statistical analysis of the results. Here, we will concentrate on presenting the first two basic applications of the CamC system augmenting live video with x-ray images and thus facilitating the positioning of the C-arm before acquiring each intra-operative X-ray shot and allowing confident, simple and intuitive planning and placement of incisions, in relation to the underlying bone fracture.

MATERIALS AND METHODS

The current CamC prototype used within the surgery room is composed of an iso-centric Powermobile C-arm from Siemens Healthcare (Erlangen, Germany), and an optical video camera, Flea2, from Point Grey Research Inc. (Vancouver, BC, Canada). Due to a custom-made mirror construction and after a one-time calibration during the construction of the system, the X-ray and video images are co-registered in real-time (see [1] for details of the one-time calibration procedure).

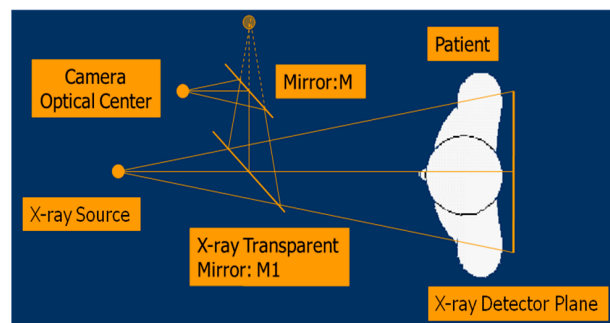


Fig.2 Schematic representation of CamC's basic concept [2].

The current prototype provides the surgeon with two monitors. The first one is the standard monitor of the mobile C-arm displaying the acquired X-ray. The second monitor positioned next to the first one visualizes the overlaid image provided by Cam-C (for an example screenshot see Fig. 1).

For documentation and postoperative analysis of the surgeries, the CamC video stream is being stored on hard disk and so are the video recordings of an external fixed camera and a head mounted wireless camera that is worn by the performing surgeon.

For each surgery, the CamC is positioned in the optimal position for the procedure. The surgeon observes the target region of the X-ray imaging system as a semi-transparent gray color circle overlaid on the optical video. This allows him to intuitively and precisely position the C-arm, achieving the best view for acquiring the desired X-ray image. Then, after the X-ray is taken, the CamC provides the surgeon with a real-time video co-registered and fused with this X-ray (see Fig. 1).

In order to avoid wrong overlay caused by patient movement after x-ray acquisition and during the CamC guided procedure, a visual marker is attached to the patient. The marker is extracted in real-time and allows the system to detect and eventually visualize the misalignment of X-ray and optical image in case of patient movement on the second monitor.

The study has been approved by the hospital's ethics committee and all patients enrolled into the study have given their consent.

RESULTS

The first set of operations performed under CamC includes foot osteotomy, elbow fracture and distal radius fracture surgeries.

Surgeons' feedback on the first CamC guided operations indicates that the new device can be smoothly integrated into the surgical workflow. The video guided X-ray C-arm positioning works intuitively and saves radiation as there is no more need for iterative acquisition of X-ray images until reaching the desired image. After acquiring the first X-ray image including the fractured anatomy, the X-ray-video overlay can further be used to plan the correct incision, placing it exactly above the fracture with what the surgeon considers as the optimal length, minimizing the wound (see Fig. 3).



Fig.3 Incision planning at a distal radius fracture: the incision line is being placed in its optimal length and position relative to the underlying fracture line. For detection of patient movement and resulting misalignment, a visual marker (see lower right) is being rigidly attached to the patient's skin. The system provides visual feedback on its main monitor, if the marker moves relative to its position since the time of X-ray acquisition.

DISCUSSION

The power and importance of CamC's image guided C-arm positioning demonstrates itself especially when imaging small parts, in which case the anatomy of interest is often placed near to the isocentre and the desired image area is small, making it hard to position the C-arm correctly and get the right image. Some commercial C-arms provide laser guidance but unlike

our solution they only point at the center of imaging area and do not visualize the total area to be imaged by the X-ray system. In our experience, apart from saving radiation dose which we expect to be up to 30% approx. in standard fracture surgeries, the CamC system provides additional information to the surgeon that helps him or her to carry out many tasks not only more intuitively but also more confidently. The participating surgeons claim that the decision-making process becomes easier with CamC and that they feel more secure when they observe their tool, their hand as well as the deep-seated anatomical target within augmented video. Basically, CamC provides more information which eventually enables surgeons to optimize their performance of tasks, while still being able to fulfill them the way they always used to, by using the basic X-ray imaging functions of the device. If wanted, it still operates like a classic C-arm but can also give access to its fusion with the real-time view of the surgical scene.

As in many cases in which a new image guided surgery system is being introduced to the real OR, the surgeons still need to explore the system and take advantage of the full potential of its functionalities. At this stage close collaboration between surgeons and engineers is extremely crucial, since joint design of the system, its functionalities and user interface could play an important role in its further development and its future clinical impact.

Many new applications could emerge from this first set of surgeries. Full video documentations of the current procedures need to be analyzed closely in order not only to identify and describe advantages and shortcomings of the system, but also to allow surgeons to eventually modify single workflow steps, optimizing the way surgeries are performed or even inventing new procedures taking full advantage of the simple and intuitive augmented reality imaging and visualization provided by CamC.

Acknowledgement: This work is partially supported by Siemens Healthcare. CamC is protected by US patents: 6229873, 6447163, 6473489, 7198404 and additional pending ones.

REFERENCES

- [1] Navab N, Heining SM, Traub J. Camera augmented mobile c-arm (CamC): Calibration, accuracy study and clinical applications. *IEEE Trans. Med. Imag.* 2010 In-press.
- [2] Navab N, Bani-Hashemi A, Mitschke M. Merging visible and invisible: two camera-augmented mobile C-arm (CamC) applications. 2nd IEEE and ACM International Workshop on Augmented Reality (IWAR'99); Oct. 1999; p. 134-41.
- [3] Wang L, Landes J, Weidert S, Blum T, von der Heide A, Euler E, Navab N. First Animal Cadaver Study for Interlocking of Intramedullary Nails under Camera Augmented Mobile C-arm. *Information Processing in Computer-Assisted Intervention (IPCAI) 2010*. Article accepted.

Realistic simulation of catheters and guidewires in vascular interventional radiology

V. Luboz¹, T. Odetoyinbo², J. Zhai³, P. Littler², T. How³, D. Gould², F. Bello¹

¹Department of Surgery and Cancer, Imperial College London, UK

{vluboz, fbello}@imperial.ac.uk

²Royal Liverpool Hospital, Liverpool, UK

³University of Liverpool, School of Clinical Sciences, Liverpool, UK

INTRODUCTION

Guidewire and catheter manipulation is a core skill in endovascular interventional radiology (IR). This skill is usually acquired while training on patient despite the risk for injury. Virtual reality simulation-based training offers an alternative for learning how to manipulate these instruments efficiently. Nevertheless, their complex behaviour and interactions require an accurate replication in the virtual environment. Based on the mass-spring model proposed in [1], this paper presents the seven guidewires and four catheters integrated in our simulation framework. The goal is to improve the behaviour of the virtual catheters and guidewires, thus the training offered by our framework. The instruments' behaviour has been derived from their real world counterparts and this evaluation is also discussed here.

MATERIALS AND METHODS

There are a number of different types of guidewires and catheters currently used in IR procedures [2]. Instruments vary widely in length, size, surface coating, material, stiffness, tip shape etc. In general, guidewires can be classified into three main groups based on their mode of use at different stages of an interventional procedure: access, selection and exchange. Catheters can be separated into two groups: for diagnostic or for treatment.

Based on the above considerations, seven commonly used guidewires were chosen for building the guidewire simulation models. They are: Fixed Core Straight (Cook Medical Inc., USA), Fixed Core Safe-T-J-Curved (Cook), Rosen-Curved (Cook), Amplatz Super Stiff (Boston Scientific, USA), Bentson (Boston), Terumo Angled and Terumo Stiff Angled wires (Terumo Corp., Japan). Among these guidewires, the Cook Fixed Core Straight, Cook T-J-curved and Bentson wires were considered representative of access guidewires. Examples of selection guidewires comprised the Angled and Stiff Angled Terumo wires. Amplatz Super Stiff, Cook Rosen-curved and Bentson wires covered properties inherent for exchange purposes. Four catheters were chosen: 4F and 5F Straight, 4F and 5F Terumo.

As presented in [1], each instrument is modelled as particles connected by links of variable flexural modulus. This coefficient is key to determine the behaviour of an instrument inside a vessel. To replicate it as accurately as possible, each guidewire and catheter was placed in three different positions (common iliac artery bifurcation, aortic bifurcation, left renal artery origin) in a silicon rubber vascular phantom (Elastrat, Geneva, Switzerland; Fig. 1) and scanned in a 128 slice CT scanner. The resulting CT datasets give the 3D position of the real instrument, which was then compared to the virtual instrument in our simulated environment. The silicon phantom was reconstructed from the CT scan using a level set method as presented in [2]. The comparison was performed by sampling both real and virtual instruments at 2mm intervals starting from the tip and computing the Euclidean distance between corresponding points along their length.

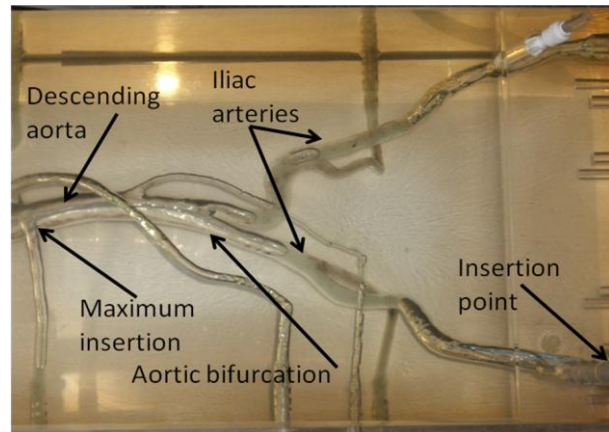


Fig. 1 The vascular silicon phantom used for the validation.

RESULTS

Numerical and graphical data demonstrated good correlation between the real 3D environment and the virtual 3D environment. Results show good correlation with an average distance of 2.27mm between the real and virtual instruments, with a standard deviation of 1.54mm. These figures highlight the accuracy and realism of our virtual instruments. A typical example (Fig. 2 and Fig. 3) showed that the distance between the

real and virtual Terumo angled guidewires was an average of 2.21mm, with a standard deviation of 1.3mm (min 0.43mm, max 5.59mm).

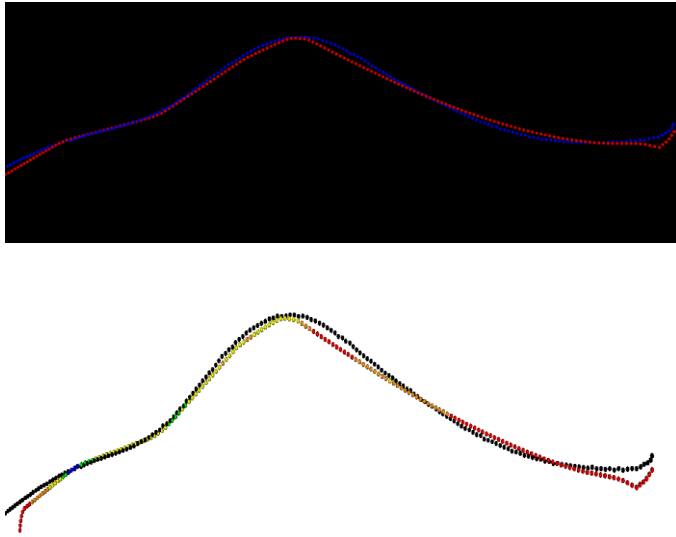


Fig. 2 Top: Comparison of the path taken by the real (in blue) and virtual (in red) Terumo angled guidewires. Bottom: Comparison of the path taken by the real (in black) and virtual (in different colors) Terumo angled guidewires. The virtual wire particles are blue when there is a very good agreement (< 0.5mm) with the real wire particles, green for a good agreement (> 0.5mm, < 1mm), yellow for an intermediate agreement (<1mm, > 2mm), orange for a poor agreement (>2mm, < 3mm) and red for a very poor agreement (> 3mm). In both pictures, the insertion point is on the left and the tips are on the right of the figure.

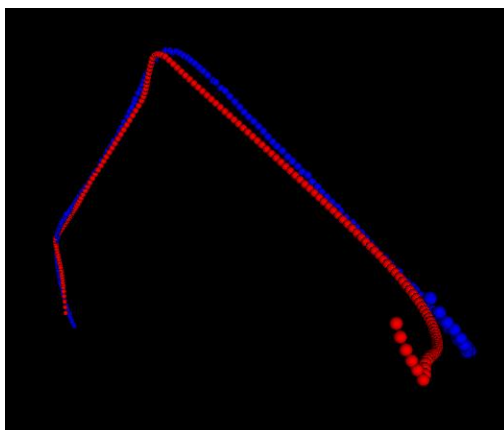


Fig. 3 Comparison of the path taken by the real (in blue) and virtual (in red) Terumo angled guidewires. The insertion point is on the left and the tips are on the right of the figure.

DISCUSSION

Use of real world physical parameters such as flexural modulus may significantly improve the behaviour of virtual IR instruments such as guidewires and catheters. Our simulation showed a good average correlation between the real and virtual instruments. Some large errors can still be observed, especially at the instrument

tip (Fig. 3), but overall there is good agreement between the virtual and real instrument behaviour. The errors are probably due to the fact that minor involuntary rotations cannot be controlled in the real environment, while these are suppressed in the virtual world.

Further work will aim at demonstrating the level of impact of these results on fidelity of IR simulations for training.

REFERENCES

- [1] Luboz V, Blazewski R, Gould D and Bello F. Real-time Guidewire Simulation in Complex Vascular Models. *The Visual Computer*. 2009, vol. 25/9, pp 827-834.
- [2] Yushkevich P. A., Piven J., Hazlett H. C., Smith R. G., Ho S., Gee J. C. & Gerig G. User-guided 3D active contour segmentation of anatomical structures: significantly improved efficiency and reliability. *NeuroImage*, 31 (3), 1116-1128, 2006.
- [3] Schneider P. *Endovascular Skills: guidewire and catheter skills for endovascular surgery*, 2008 third edition.

Dynamic Modeling of a Multispart Probe for Soft Tissue Intervention: Simulation Preliminaries

E. S.Nobari¹, F.M. Rodriguez y Baena¹

¹Imperial College London Mechanical Engineering Department

INTRODUCTION

Being able to enhance surgical tools so as to cause less damage to the tissue being operated is of immense importance. To this end, one requires reasonably accurate models, in order to be able to parameterize this damage and study it. Finite element methods, while very accurate and efficient, need very complicated modeling and are time consuming for preliminary studies. Thus, it is the aim of this paper to provide a basic and yet reasonable framework for a model, in order to be able to compare various methods of applying such surgical tools. Once the methods are compared, then one can select the most efficient method and further study its effect through an FE model.

The neurosurgical probe [1] is considered here, which is a multi-part probe. Forward motion is achieved with sequences of pushing each segment in turn and extracting all. Reciprocating motion is believed to have two main advantages, first, less brain deformation, and second, less brain shift. Indeed, reciprocal motion should amount to less brain shift since, when one part of the probe penetrates while the others are stationary, the friction between the outer surface of the stationary parts and the tissue prevents the brain from shifting as much as it would have during a direct push.

To try the validity of this belief, it is proposed to analyze the dynamics of the probe in direct push motion as opposed to the multi-part reciprocating push. In both types of motions, the amount of energy put through the probe into the material is used to compare the performance between the two motion mechanisms. As the probe is of relatively low mass and moves at constant and low velocity, the most part of the actuator energy goes to tissue deformation and friction forces, and the main differences between the two types of push lies within differences in frictional forces in the two cases. Through dynamical analysis, a relationship between the deformation of the material and the friction forces can be retrieved, and as friction forces are measurable through experimental means, deformation can be predicted.

MODELING

Dynamical modeling is done for the rig setup illustrated in Fig. 1. The probe is modeled as an axisymmetric, flat-ended cylinder of four identical sections sliding against each other (Fig. 2). All inner surfaces of the probe are of the same structure, while the external surface possesses a different friction coefficient. The probe is of finite length. The material is inside a box on

roller bearings, making it capable of sliding till it hits the sensor. This demonstrates brain shift in the form that the box (brain) slides with the probe till it is held and the probe inserts.

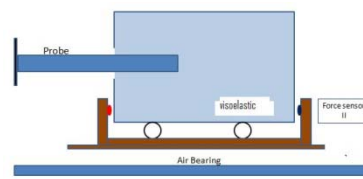


Fig.1 Rig Setup

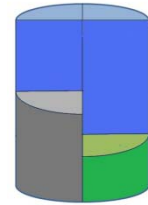


Fig.2 Probe Segments

One sequence of insertion of the four parts of the probe is modeled in this paper. The initial condition is where the four parts of the probe are embedded into the material a distance l and the final condition where all parts of the probe have displaced forward by 5 mm. In order to define the dynamical problem, the material is modeled in relative dynamical terms. Soft biological tissue can be modeled as a viscoelastic material [2]. However, while biological soft tissue is non-homogenous and demonstrates different stress-strain behavior across its structure, the material here is modeled as viscoelastic, homogenous, linear and compressible to simplify the problem.

Material stress-strain behavior is modeled via spring-dashpot models. The Maxwell model [3] is employed due to its simplicity and efficiency. The insertion process is modeled as illustrated in Fig. 3. As the dynamical analysis is in 1D, the probe is modeled to be sliding inside a tunnel in the material, compressing a cylinder identical to the probe, but of the viscoelastic material which slides (frictionless) within the tunnel as well. In effect, all three external surfaces of each part of the probe will be in contact with the probe or viscoelastic material, creating an “embedding” effect. Each of the four segments compress a responding spring as shown in Fig. 4. The model will be further exacted by introducing friction and interlocking forces between material cylinder and tunnel.

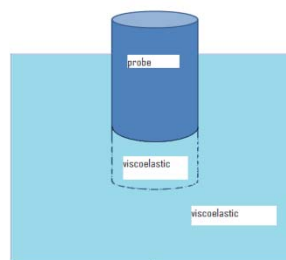


Fig.3 Probe Insertion

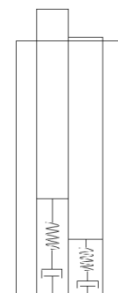


Fig.4 2D Probe

EQUILIBRIUM EQUATIONS

For each sequence of forward reciprocating motion, the movement is split into 5 stages. a) The first probe section (part A) is pushed forward, indenting and eventually causing a crack inside the material. b) The instant the crack is initiated, part A pushes through the crack and reaches final position x_f . In the next three stages, probe parts B, C and D move through the crack initiated by part A.

For each stage, the free body diagram for the box, probe and spring must be drawn. The main difference between the movements of the four parts is due to differences in the friction forces due to the changing contact surface area in each case. Equilibrium equations for probe B are shown as an example.

Forces acting on the box are: f_{sb} (the force from the sensor), f_{db} (the force from the damper to the box) and friction forces from the probe. Assuming f_{op} to be the friction per unit area between the internal sides of the probe with the viscous material, f_o as the friction per unit area between the external surface of the probe and the material, and f_p as the friction per unit area between probe segments, friction forces acting on the box from probe A are:

$$f_1 = (x_f - l) \times f_{op} \times r \quad (1)$$

$$f_2 = (x_f - x_b) \times f_{op} \times r \quad (2)$$

$$f_3 = x_f \times \frac{\pi r^2}{4} \times f_o \quad (3)$$

Probe B:

$$f_4 = (x_b - l) \times f_{op} \times r \quad (4)$$

$$f_5 = x_f \times \frac{\pi r^2}{4} \times f_o \quad (5)$$

Probe C and D:

$$f_6 = \left(\frac{\pi r^2}{4} + \frac{\pi r^2}{4} \right) \times l \times f_o \quad (6)$$

The forces acting on the probe are:

a) Friction forces from contact between probes:

$$f_7 = f_p \times \left[r \times [z - (x_f - x_b)] + r \times [z - (x_b - l)] \right] \quad (7)$$

b) Friction forces from contact with material:

$$f_8 = \left(\frac{\pi r^2}{4} \times x_b \right) \times f_o + (x_b - l) \times f_{op} \times r \quad (8)$$

c) Spring force:

$$k_b \times (x_b - x_{b1}) \quad (9)$$

The actuator force is defined as f_{ab} , where positive force is defined in the rightward direction. A point x_{b1} is defined as the point connecting the spring to the damper and its displacement represents the material deformation at the point right between the fixed wall and the probe-material contact point: the boundary conditions of both the model and the actual rig setup are the same and the material in between is uniform and linear, thus, under 1D analysis, x_{b1} represents the average movement of the modeled material. The forces acting on point x_{b1} are the spring and damper force and, as the spring is mass less, the net force on it is zero, and the damper force is equal to the spring force.

The equilibrium equations are defined as follows:

$$\sum_{n=1}^6 f_n - f_i^{sb} + c_b \times \dot{x}_i^{1b} = x_i^b \times OB_2 + OB + c_k \times (\dot{x}_i^{1b}) - f_i^{sb} = 0 \quad (10)$$

$$\sum_{n=7}^8 f_n + f_i^{ab} - k_b \times (x_i^b - x_i^{1b}) = x_i^b \times OB_3 + f_i^{ab} + x_i^{1b} \times k_b + OB_1 = m\ddot{x}_i^b \quad (11)$$

$$k_b \times (x_i^b - x_i^{1b}) = c_b \times \dot{x}_i^{1b} \quad (12)$$

where OB , OB_1 , OB_2 , OB_3 are constants. These equations are defined at every step i , converted to matrix form, then solved using a finite difference method iteratively in MATLAB. The outputs at each step i are x_i^{b+1} , x_i^{1b+1} , f_i^{sb} and f_i^{ab} .

To compute OB , OB_1 , OB_2 , OB_3 , the constants f_{op} , f_o , f_p , k_x and c_x are needed. An experiment to measure f_i^{sb} , f_i^{ab} from a prototype is currently underway. Defining constant velocity and step displacement of 5 mm per step, k_x and c_x can then be calculated from equilibrium equations.

As a point of note, each set of equations needs to hold true independently of the others, as spring/damper constants and friction force equations change for each segment. As a further point of note, in the first stage, when the probe is piercing, the respective k is non linear, as it increases during indentation, then drops sharply when the surface is breached, while, for the other stages, k is linear.

RESULTS AND CONCLUSION

As a proof of principle, values of k_b and c_b were found experimentally. Then, resolving (12) for x_i^{1b} with a step displacement of 20 mm, the following relationship is obtained:

$$x^{1b} = 0.02 - 0.02e^{-10t} \quad (13)$$

This illustrates a displacement which starts at zero at $t = 0$ and exponentially increases to 0.02 at $t = \infty$, a phenomenon which is typical of viscoelastic materials.

On the basis of this modeling framework, a complete comparative study between reciprocating and direct push is currently underway.

REFERENCES

1. L. Frasson et al. STING: A Soft Tissue Intervention and Neurosurgical Guide, IMechE Proc H, 2010, in press.
2. W. Maurel. 3D Modeling of the Human Upper Limb Including the Biomechanics of Joints, Muscles and Soft Tissue, Ph. D. Thesis 1906 – 1998, Laboratoire d'Infographie – Ecole, Polytechnique Federale de Lausanne.
3. Lucas Duffrène et al. Generalized Maxwell model for the Viscoelastic Behavior of a Soda-Lime-Silica Glass Under Low Frequency Shear Loading. Springer Berlin / Heidelberg. 2004.

Force vs. Displacement during Tool Insertion: Techniques and Modelling Approaches

T. Parittotokkarn^{1,2}, P. Degenaar^{2,3}, B.L. Davies¹, F. Rodriguez y Baena^{1,2}

¹*Mechatronics in Medicine Lab, Department of Mechanical Engineering*

²*Institute of Biomedical Engineering, ³ Centre for Neuroscience, Faculty of Medicine
Imperial College London
t.parittotokkarn07@imperial.ac.uk*

INTRODUCTION

Minimally Invasive Surgery (MIS) has become the preferred choice for the treatment of a number of pathologies. It offers several important advantages for the patient, such as reduced stress and strain to soft organs during the procedure. In order to improve upon present robotic systems for minimally invasive surgical interventions, much can be learned from biology. For instance, the ovipositor of the wood wasp [1] (*Sirex noctilio*) is an excellent example of natural microsurgical probes. Currently, we have been focusing on the development of a novel soft tissue probe for MIS, which can be used to insert into soft tissue by exploiting the unique boring motion of certain wood boring wasps. In contrast to conventional surgical instruments, which are inserted via force from outside the body, the reciprocating motion of the wood wasp would allow force projection from the tip. This then allows for non-straight line trajectories, not possible with present probes. This paper progresses the reciprocating mechanism for tissue traversal from our previous work [2]. In particular, while in that work we highlighted the experimental evidence for anisotropic friction, in this paper we model the forces to better understand how it can be used in reciprocating motion by a multi-part probe to traverse soft tissue.

MATERIALS AND METHODS

A four-segment rigid probe was fabricated from Durus White material (6.0 mm in diameter, comparable with some commercial neuroendoscopes) using rapid prototyping. The overall length of the probe was 130 mm, and ended with a conical tip. Each segment was moved either simultaneously or reciprocally by a robotic actuator. Agar gel, with a concentration of 0.5 wt.%, which Das et al. [3] reported representing human brain properties, was used to test for tissue traversal. The agar sample was placed inside a transparent box (24x54x79 mm) constructed with a hole, allowing the probe to be partially embedded 30 mm deep inside the soft tissue. The box was placed on wheel bearings mounted at the far end with a force sensor (Honeywell FSS Low Profile 1 axis Force Sensors, with operating force of 0-14.7 N) to measure the force in the plane of probe insertion into the soft tissue. The experiment was divided into two phases. Firstly, all segments of the

multi-part probe were pushed forward simultaneously by 5 mm through the sample with a speed of 1mm/s. Secondly, each segment of the multi-part probe was alternatively pushed forward into the tissue with the same displacement of 5mm during 1s, with 0.33s pause interval as show in Fig. 1. The aim of this experiment is to compare the probe-tissue interaction forces between direct pushing and reciprocating motion.

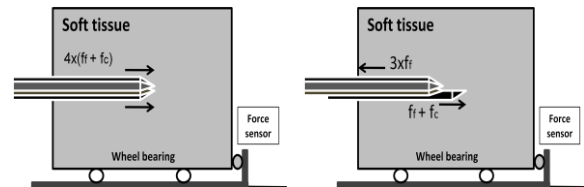


Fig. 1 The diagrams of direct insertion (left) and reciprocating motion (right) of a multi-part probe into soft tissue.

RESULTS

The force profile in Fig. 2 shows the comparative results of direct and reciprocating insertion of the probe into soft tissue. Due to the measurement of forces acquired by tissue absorption from the probe motion, the force increases rapidly during initial probe insertion followed by a lesser gradient. Thus, the direct pushing of the probe transmits the large amount of force to the tissue by as much as 0.45N. However, the soft tissue collects the minimal forces of 0.1N and 0.3N given by the reciprocating motion of the first through the fourth segment respectively. Three probes anchoring the tissue means less force is required to move the remaining probe inward. As a result, the reciprocal probe imparts two thirds of the interaction force obtained from direct pushing. The force profile of the reciprocating motion exhibits a ladder pattern because the following segment penetrates into the tissue and increases the accumulating force superimposed by the previous tissue relaxation.

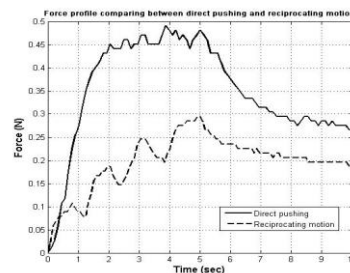


Fig. 2 Force profile comparing direct insertion and reciprocating motion of a multi-part probe.

DISCUSSION

From our analysis of the experimental results, we have generated a viscoelastoplastic model (Fig. 3) using Simscape (MATLAB 2010a). We assume that the probe is motionless and initially embedded 30mm inside the soft tissue in contact with the surface of the tissue. The probe insertion behaviour is divided into two phases in conjunction with the experiments.

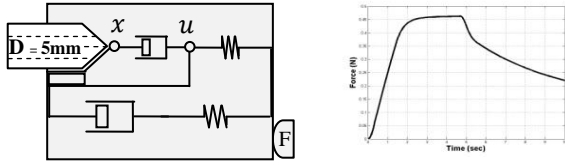


Fig. 3 Viscoelastoplastic model of direct probe insertion and force profile obtained from Simscape simulation.

Pre-sliding phase; the combined four-segment probe is pushed inward at constant velocity, with the static friction force between the probe and the tissue matching the pushing force (1). This static friction is represented as a stuck box in Fig. 3, and causes the tissue surrounding the probe to deform with probe displacement (velocity at $x = u$) corresponding to a standard linear viscoelastic model [4].

$$F_{pre\text{sliding}} = f_{static\ friction} = f_{tissue\ deformation} \quad (1)$$

Sliding phase; the combined probe is sequentially pushed deeper and turns the static to dynamic friction while the probe is sliding with difference velocity ($x > u$) relative to surrounding tissues as exhibited by the slip box in Fig. 3. At the same time, the tip of the probe cuts through the soft tissue in order to obtain irrecoverable displacement of tissue disruption as a result of tissue traversal. This behaviour is demonstrated in the following model as a viscoplastic deformation by a damper in parallel with transitional friction model [4].

$$F_{sliding} = f_{sliding\ friction} + f_{cutting} \quad (2)$$

In contrast to the combined probe, the multi-part probe is able to move reciprocally by using the same probe as direct pushing. The results in Fig. 2 show how the motion of the reciprocal probe transmits less force while penetrating the soft tissue with similar displacement and velocity. With the four-part probe sample, three-stationary segments are anchoring the contacting tissue, allowing the moving segment go forward. The tissue absorbs 0.1N of the peak force (Fig. 2) due to the summation of the cutting force and the dynamic friction force (2). Subsequently, there is a relaxation by the tissue which increases with the number of probe insertions. This may be due to a continuation of ongoing

relaxation. The relaxation to peak force remains constant at 0.1N. From this experimental data we have developed a simple model of viscoelastoplasticity for reciprocating motion and a force profile from simulation, shown in Fig. 4.

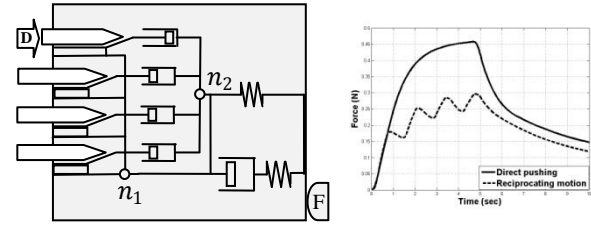


Fig. 4 Viscoelastoplastic model of a 4-part probe employing reciprocal motion and force profile from Simscape simulation.

This behaviour can be modelled by the combination of four elements of viscoelastoplasticity for each probe segment. The viscoelastic model links four sliding elements via a n_1 node and exhibits soft tissue characteristics such as relaxation, creeping and hysteresis [4]. n_2 represents cutting deformation at the tip of the probe as a set of parallel dampers. When the first segment moves a distance to traverse the tissue, the other three segments hold the tissue model in place. Thus the moving segment overcomes the resistance due to static friction and thus penetrates the soft tissue. Finally, this segment reaches an end point and stops, thereby compressing the viscoelastic element and displacing the damper in front of it. This phenomenon can cause tissue relaxation, which in turn causes a lesser amount of force to be needed for the next probe to be inserted (and the damper to be compressed). In addition, this probe-tissue interaction model is able to demonstrate the force profile from the Simscape simulation (Fig. 4), which is explicable and compares well with the real data.

CONCLUSION

This paper introduces a model of probe-tissue interaction for soft tissue intervention which can aid comparisons between direct insertion and reciprocating motion of a multi-part probe. In summary, the reciprocal mechanism of our novel soft tissue probe is able to minimize force during insertion, which is expected to reduce tissue deformation and damage. The next stage is to scale the probe further and perform measurements in-vivo, while refining and further validating the model.

REFERENCES

- [1] J. F. V. Vincent, M. J. King. The Mechanism of Drilling by Wood Wasp Ovipositors. *Biomimetics*. 1995: 3: 187-201.
- [2] L. Frasson, T. Parittotokkaporn. Early Developments of a Novel Smart Actuator Inspired by Nature. *Int. J. Intelligent Systems Technologies and Applications*. 2010: 8:1-4.
- [3] R. Das, D. Gandhi. A Benchtop System to Assess Cortical Neural Interface Micromechanics. *IEEE Transactions on Biomedical Engineering BME*. 2007:54(6):1089-1096.
- [4] A. H. C. Gosline, V. Hayward. Dual-Channel Haptic Synthesis of Viscoelastic Tissue Properties using Programmable Eddy Current Brakes. *Robotics Research*. 2009:28:1387-1399.

Design of a Magnetically Activated Stereoscopic System for Single Port Laparoscopy

M. Silvestri, M. Simi, C. Cavallotti, M. Vatteroni, P. Valdastrì, A. Menciassi, P. Dario

CRIM Lab, Scuola Superiore Sant'Anna, Pisa 56100, Italy

m.silvestri@sssup.it

INTRODUCTION

Single Port Laparoscopy (SPL) is an advanced laparoscopic surgical procedure grown in the last few years. SPL requires a single incision approximately 25-30 mm long, inside the umbilical scar, where a single multichannel port is inserted. The technical feasibility of this technique was clearly demonstrated for a wide range of surgical procedures [1] and different access ports are available on the market [2]. However, the single-access involves the need of an in-line viewing. The consequent technical difficulties are the limitation of the field of view and the not desired motion of adjacent instruments, due to conflicts and interferences among many different tools. Nowadays, there is only one commercial laparoscope designed for SPL by Olympus [3], but it has a poor image quality and an excessive encumbrance. Other solutions consist of monocamera system prototype exploiting magnetic fixation and positioning for SPL procedures [4], a manually moved steering camera [5] and a stereoscopic insertable pan/tilt imaging device, hand held or sutured into the abdomen [6].

In this paper the authors present an innovative Magnetic Internal Mechanism (MIM) for precise camera steering and orientation in SPL procedures. The first developed prototype had a 2D camera and a diameter of 12 mm in order to fit inside a standard trocar [7]. The new MIM prototype for SPL described in this work has a stereoscopic 3D vision system and two internal active degrees of freedom (DOFs).

MATERIALS AND METHODS

A stereoscopic imaging system require two main parts: an acquisition system and a visualization one. The former is composed by two cameras with two separated optical channels. Cameras of the current prototype are commercial VGA CMOS colour imagers, 8mm × 8mm × 9mm in size, with a pin-hole lens. Each camera has a field of view of about 60° in horizontal and 52° in vertical. The latter is based on a 19" autostereoscopic monitor. It has an electro-optic panel with vertical, regularly spaced slits attached to the surface of a LCD, that obscures part of the two images coming from the cameras [8]. This construction guarantees the projection of two different images on the left and right eyes. Consequently, the difference of an object's projection on the cameras due to their horizontal separation,

defined disparity (measured in degrees or mm), is captured by the user's eyes, producing the stereoscopic effect.

The aim of this design was to guarantee a stereoscopic effect within the range 5-15 cm in depth, taking into account the maximum physiological disparity limits to properly fuse the images without ocular fatigue.

According to this specification the two cameras are arranged so that their central axes are parallel to each other. Such configuration has a larger region where the binocular images are properly merged and it avoids a number of stereoscopic distortions [9].

The dimensioning of the stereoscopic vision system was carried out by applying the following equations:

$$\begin{cases} D_{\min} = Mtf \left(\frac{1}{d_0} - \frac{1}{d_{\min}} \right) \\ D_{\max} = Mtf \left(\frac{1}{d_0} - \frac{1}{d_{\max}} \right) \end{cases}$$

where D_{\min} and D_{\max} are, respectively, the minimum and the maximum disparity value, M is the value of frame magnification, d_{\min} and d_{\max} are the minimum and the maximum required scene depth values and d_0 is the zero-disparity-depth [10]. We considered the minimum and maximum physiological disparity limits of $\pm 1,5^\circ$ [11] (corresponding to ± 21 mm), a depth of stereoscopic field from 40 mm to 150 mm, a focal length f of 3,1 mm and a frame magnification M of 93,75. Considering these constraints, the distance t between the camera centres must be 8 mm.

As an endoscope, the device requires an illumination system. This is made by 8 high efficiency LEDs placed around the cameras. This configuration was optimized by mathematical modelling to obtain the maximum uniformity for the scene lightning.

All the mechanical parts of the robot were designed considering the size of the stereo vision module (23 mm in diameter and 12 mm in length) and the diameter of the umbilical port (25-30 mm) which the complete system must fit. The result is a cylinder, 25 mm in diameter, 95 mm in length and 57 g in weight (fig.1 left). The robot incorporates the stereovision system, two brushless motor, an internal permanent magnet (IPM) and two sets of gears. A flexible wired connection to the external units guarantees a real time signal transmission, control and powering, providing also an effective retrieval from the abdomen especially

in case of failure. The two internal DOFs (Roll and Tilt) of the robotic stereocamera guarantee a precise steering and orientation of the surgeon point of view whereas other 3 rough external DOFs manually activated provide the right placement of the device inside the abdomen (fig.1 right).

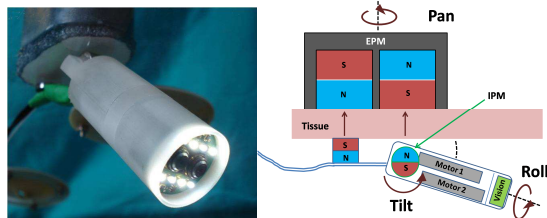


Fig. 1 The robotic stereo camera prototype (left). Schematic representation of the robotic system (right).

The MIM consists of a motor connected to an IPM by a set of gears. The device, immersed in an external magnetic field generated by a set of permanent magnets (EPMs), tends to maintain a precise alignment defined by the IPM polarization. When the motor is activated, the entire device rotates with it, while the IPM remains oriented according to the external field. Thanks to this principle of operation, the MIM enables a tilting of the device (span 60°) relatively to the surrounding tissue, without moving the EPMs [12].

The roll internal mechanism (span 180°) is being integrated in order to adjust the horizon of the stereo vision system during the surgical procedure. The motor was connected by means of a set of cylindrical gears to the head of the robot, where the two parallel cameras were fixed precisely in order to verify the geometrical requirements for the stereovision.

Another permanent magnet is then fixed at the bottom of the robot in order to couple the device with the two EPMs providing the external pan motion and translation. The chassis of the prototype was fabricated by stereo-lithography technique, guaranteeing stability of the mechanical components and correct protection of the electronic parts. A dedicated track was obtained inside the robot in order to permit the rotation of the cables.

RESULTS & DISCUSSION

The overall system was assembled and tested on a laparoscopic simulator by twelve doctors with medium-high surgical experience (fig. 2). They have performed a number of standardized exercises in both 2D and 3D visual condition by switching the autostereoscopic monitor. The parameter evaluated was the mean time to perform each exercise. Such parameter improves of about 20% for tasks requiring medium-low motor dexterity, like grasping or touching an object. Instead, for complex tasks, like suturing, the mean time decreases of about 16%. Furthermore, the EPMs-IPM magnetic link demonstrate a good stability of the robot, while the internal mechanism permitted to easily direct the surgeon point of view with a high resolution ($> 0.01^\circ$) and speed (1 rps). In conclusion, this vision platform could enhance the surgeon dexterity during

SPL procedures by limiting conflicts among instruments, still providing a stereoscopic view. As soon as the robot is inserted and fixed on the abdominal wall, space in the access port is only taken by thin cables, thus leaving space free for the access of additional instrumentation.

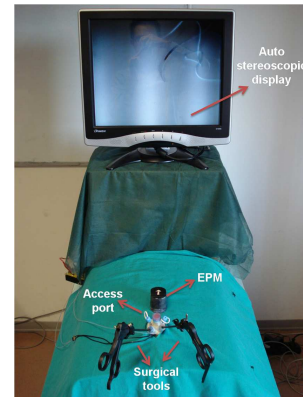


Fig. 2 The overall platform of the Magnetically Activated Stereoscopic System for SPL.

REFERENCES

- [1] Romanelli JR, Earle DB, Single-port laparoscopic surgery: an overview. *Surgical Endoscopy* 2009 Jul; 23(7):1419-1427.
- [2] Neto M, Ramos A, Campos J, Single port laparoscopic access surgery, *Techniques in Gastrointestinal Endoscopy* 2009; 11: 84-93.
- [3] Available on line: www.olympuskeymed.com
- [4] A. C. Lehman, K. A. Berg, J. Dumpoert, N. A. Wood, A. Q. Visty, M. E. Rentschler, S. R. Platt, S. M. Farritor, D. Oleynikov, *Surgery with cooperative robots. Computer Aided Surgery*. 2008, 13: 95-105.
- [5] J. Cadreddu, R. Fernandez, M. Desai, R. Bergs, C. Tracy, S. J. Tang, P. Rao, M. Desai, D. Scott, Novel magnetically guided intra-abdominal camera to facilitate laparoendoscopic single-site surgery: initial human experience. *Surgical Endoscopy*, 2009, 23: 1894-1899.
- [6] T. Hu, P. K. Allen, N. J. Hongle D. L. Fowler, Insertable surgical imaging device with pan, tilt, zoom, and lighting. *Journal of Robotic Research*. 2009, 28:1373-1386.
- [7] Menciassi A, Simi M, Buselli E, Quaglia C, Cavallotti C, Vatteroni M, Valdastris P, Arezzo A, Di Lorenzo N, Dario P, An innovative device for precise and automated camera steering in laparoscopic surgery. SMIT conference, Sinaia, Romania, Oct 2009.
- [8] Hill L, Jacobs A. 3-D Liquid Crystal Displays and Their Applications. *Proceedings of the IEEE* 2006; 94: 575-590.
- [9] Woods A, Docherty T, Koch R, Image Distortions in Stereoscopic Video Systems. *Proceedings of the SPIE* 1993; 1915: 1-13.
- [10] *Stereographics developers' handbook*. StereoGraphics Corporation; 1997
- [11] Ferre M, Aracil R, Sanchez-Uran M, *Stereoscopic Human Interfaces*. *IEEE Robotics & Automation Magazine* 2008; 15(4): 50-57.
- [12] Simi M, Ciuti G, Tognarelli S, Valdastris P, Menciassi A, Dario P, Magnetic link design for a robotic laparoscopic camera, *Journal of Applied Physics*, 2010, in press.

A Multimodal Silicone Phantom for Robotic Surgical Training and Simulation

Mirna Lerotic and Su-Lin Lee

*Institute of Biomedical Engineering, Imperial College London, UK
{mirna.lerotic, su-lin.lee}@imperial.ac.uk*

INTRODUCTION

For complex surgical procedures such as minimally invasive image guided tumour ablation [1], different modes of medical images are needed. Image guidance is used for accurate needle placement and can be performed using different imaging modalities, such as computed tomography (CT) and ultrasound (US) with magnetic resonance imaging (MRI) for validation. For these complex surgical techniques, it requires surgical phantoms for training and system validation. Surgical phantoms are also often used to test robotic surgical platforms and to familiarize surgeons with robotic environments. The currently available surgical phantoms on the market are designed for a specific procedure and often can only be used with one imaging modality.

Image guidance in surgery typically starts with 3D images, acquired using MRI or CT, which are then used to build bio-mechanical models. These deformable models can, for example, predict cardiac or respiratory motion [2, 3]. The use of these models in surgery necessitates registration which usually involves the use of different imaging technique, such as US. For this reason, a multimodal silicone phantom was built of a female subject in three-quarter size, as shown in Fig. 1a. The model is compatible with MRI, CT and US, and can simulate soft-tissue deformation.

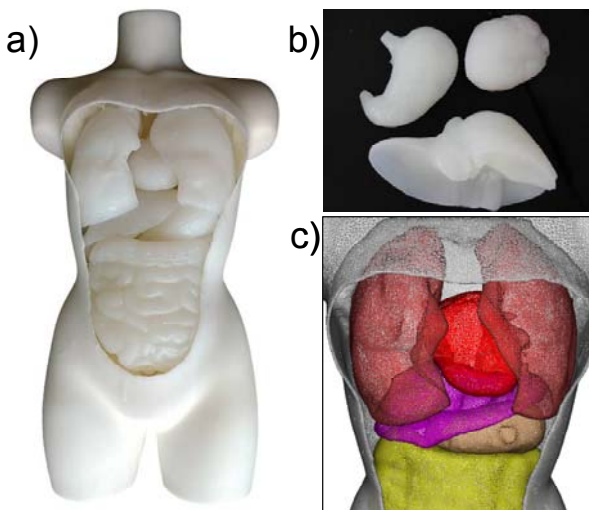


Fig. 1 The multimodal silicone phantom is shown in (a). A hollow mannequin contains silicone organ models such as stomach, heart and liver, shown in (b). (c) 3D model meshes were constructed from the CT scans.

MATERIALS AND METHODS

Materials used for ultrasound tissue phantoms have to mimic acoustic properties of human tissue. They include agar, silicone, polyvinyl alcohol gel and polyacrylamide gel [4]. We have chosen silicone for its non-toxicity, durability and ease of mould casting.

Silicone negatives of the plastic organs from a three-quarter sized teaching model were made using long lasting skin safe lifecasting silicone rubber, Body Double® and plaster for support. The deformable models were cast from these negatives using two-compound platinum-catalyzed silicone, Ecoflex® Supersoft 0030 (Smooth-On, Inc., Easton PA, USA). Several models are shown on Fig. 1b. The models were not dyed as the addition of pigment reduced the penetration depth of the ultrasound.

Glass spherical markers (approximately 6mm in diameter) were inserted into the lungs, liver and kidneys to simulate cysts or tumours. Simulated cysts can be seen on the CT scan shown in Figs. 2a and 2c. Blood vessels in the lungs and liver were simulated using wire models. The wires were removed from the casts after the silicone had cured resulting in vessels in the casts. Examples of simulated pulmonary vessels can be seen in Fig. 2b.

For the main body, a hollow plastic mannequin was procured. The legs were sealed using plastic sheeting and plastic sealant while the front of the chest was removed. The mannequin cavity was padded using two-component flexible polyurethane foam, FlexFoam-iT! (Smooth-On, Inc., Easton PA, USA) to create a body cavity fitted to the organs.

RESULTS

A CT scan of the phantom was acquired with $0.77\text{mm} \times 0.77\text{mm}$ in plane resolution and 1mm slice separation. Four transverse slices of the CT scan in Fig. 2 show different views of the phantom body; multiple organs with tumours simulated by the glass beads can be seen, as well as the blood vessels in the liver and lungs.

The phantom body and organs were segmented from the CT images using Analyze (AnalyzeDirect, Inc., Overland Park, KS, USA). The data was used to build the 3D mesh model of the phantom that can be used for surgical simulation or training. The meshes are shown in Fig. 1c.

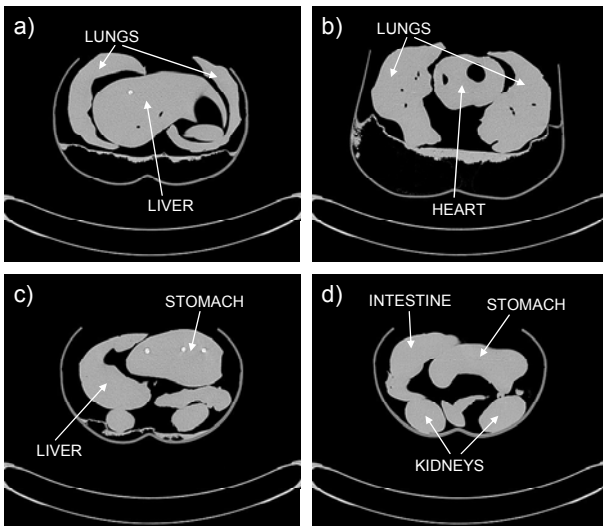


Fig. 2 Transverse slices of the CT scan of the phantom show different organs with simulated tumours and blood vessels.

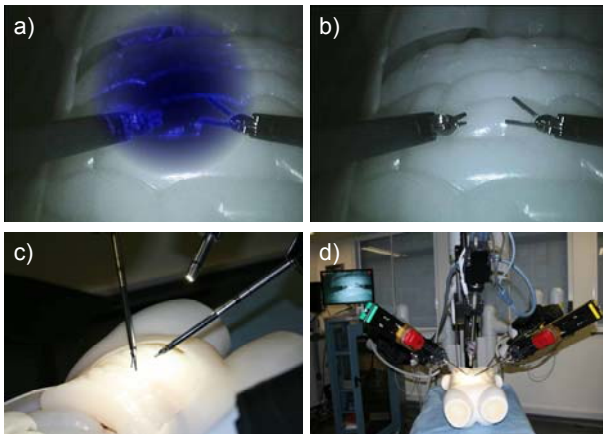


Fig. 3 The phantom was used in a robotic surgery simulation using a robotic surgical console. a) Augmented reality views of the phantom.

The phantom was used in a robotic surgery simulation using a da Vinci robotic surgical console (Intuitive Surgical, Inc., Mountain View, USA). Fig. 3 shows the simulation with the augmented reality views created by inverse realism method [5] in Fig 3a.

An ultrasound scanner, Aloka Prosound Alpha 10 Premier, was used in an image guided surgery simulation. The liver model was aligned to the captured ultrasound images as an aid in navigation. The system is illustrated in Fig. 4. The phantom body was filled with water during the simulation to facilitate the US wave propagation.

DISCUSSION

A multimodal silicone phantom was developed for robotic surgical training and simulation. The deformable organs make it an ideal phantom for validation of

robotic systems. Moreover, it can be used in situations where different imaging modalities are required to track tissue deformation. In the future we would like to add consistent respiratory and cardiac motion while maintaining its suitability for multimodal imaging as well as evaluate the material properties for each of the organs.

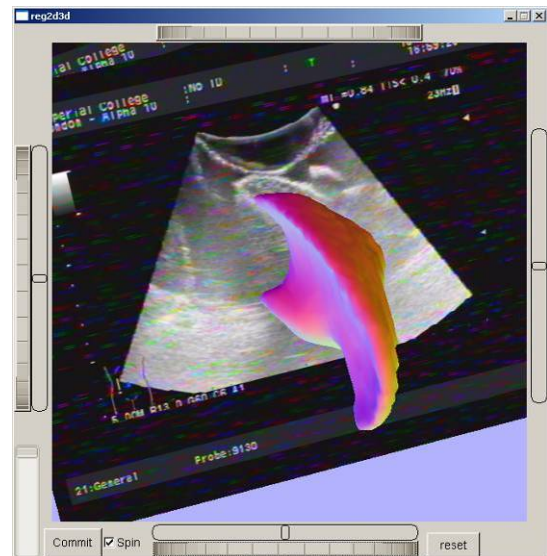


Fig. 4 An ultrasound scan aligned to the model of the liver in an in-house surgical navigation tool.

ACKNOWLEDGEMENTS

The authors would like to thank Trupti Patel for the CT scan of the phantom and Adrian J. Chung for the surgical navigation tool image.

REFERENCES

- [1] A. R. Gillams, "Image guided tumour ablation," *Cancer Imaging*, vol. 5, pp. 103-109, 2005.
- [2] N. A. Ablitt, G. Jianxin, J. Keegan, L. Stegger, D. N. Firmin, and G.-Z. Yang, "Predictive cardiac motion modeling and correction with partial least squares regression," *Medical Imaging, IEEE Transactions on*, vol. 23, pp. 1315-1324, 2004.
- [3] M. Lerotic, S.-L. Lee, J. Keegan, and G.-Z. Yang, "Image constrained finite element modelling for real-time surgical simulation and guidance," in *Biomedical Imaging: From Nano to Macro, 2009. ISBI '09. IEEE International Symposium on*, 2009, pp. 1063-1066.
- [4] K. Zell, J. I. Sperl, M. W. Vogel, R. Niessner, and C. Haisch, "Acoustical properties of selected tissue phantom materials for ultrasound imaging," *Physics in Medicine and Biology*, vol. 52, p. N475, 2007.
- [5] M. Lerotic, A. J. Chung, G. Mylonas, and G.-Z. Yang, "pq-space Based Non-Photorealistic Rendering for Augmented Reality," in *Medical Image Computing and Computer-Assisted Intervention MICCAI*. vol. 2, 2007, pp. 102-109.

Health Economics in Robotic Knee Replacement Surgery

S.A. Hurst¹, J.P. Cobb¹

¹*Department of Orthopaedics, Imperial College Academic Health Science Centre, Charing Cross Hospital, London, UK*

simonhurst8@googlemail.com

INTRODUCTION

Total knee replacement arthroplasty (TKA) is now the single most expensive operation within the NHS. It is performed over 60,000 times annually at a tariff of approximately £7,000 each. However it is only around half as effective in QALY terms as hip replacement which also costs less, making TKA far less cost-effective, at an estimated £4,111/QALY (1). Unicompartmental knee arthroplasty (UKA) is a currently underused procedure in orthopaedic surgery. The only long term level one evidence comparing UKA with TKA shows that after 15-years at no time was TKA ever superior to UKA in a randomised controlled trial(2). UKA has already been shown to offer significant financial advantages over TKR (3).

However the procedure remains underutilised not least because insurance companies pay surgeons less for the smaller operation, which is also less profitable for both hospitals and implant manufacturers.

Robotic technology has transformed productivity in the industrial world, improving standards of production and reducing costs. It has also been applied in orthopaedics, and in particular in UKA where it has been shown to be more effective in both technical and clinical terms(4-6). In a recent radiographic study (6) the variance using the manual procedure was 2.6 times greater than with the robotic arm. Evidence therefore exists to suggest both that UKA is as effective as TKR in treating arthritis, and that robotic arm assistance improves accuracy and reproducibility in this procedure. Improved accuracy leads to improved joint alignment, wear and ultimately longer life spans of implanted prosthetics.

Cost-effectiveness remains the single most powerful factor in the delivery of health care today. It is not sufficient for a technology to be effective, it must be cost-effective. Robot assisted arthroplasty must be considered in these financial terms, in order to help determine its role within a healthcare system.

This study therefore sets out to assess the health-economic impact of robotic technology on the arthroplasty industry within the NHS.

MATERIALS AND METHODS

Cost effectiveness for was assessed by GBP per quality adjusted life year, '£ per QALY.' QALYs gained by UKA were taken. The 'EuroQol Group' (EQ5D) health outcome measure was used in a cohort of patients pre-operatively and one year post UKA. Age and sex-matched groups that had undergone UKA were

compared against a matched control population with no history of knee pathology using EQ5D. The financial costs considering instrumentation were determined for both conventional UKA and *Acrobot* UKA in our institution and quality adjusted life years (QALY) and costs per QALY calculated. As the gain from treatment is expected to last for many years, whereas the costs accrued during the study period, the number of QALYs are also reported using a discount rate of 5%.

RESULTS

Cost	Conventional instrumentation	<i>Robotic Assistance</i>
Capital cost	£40,000 (4 sets @£10k/set)	£150,000
Capital cost per patient based upon 200 cases/year and a 3 year life cycle of equipment	£66	£250
Maintenance contract based upon £10k/year		£50
Sterilisation costs (per set of instruments)	£250	
Total costs of instrumentation per patient	£316	£300

Table 1 Instrumentation costs associated with conventional UKA vs *Robot Assisted* UKA (*Acrobot*).

	EQ5D Score
Pre-operation	0.544
Two-year follow-up	0.949
Mean QALY changes from baseline	0.405

Table 2. Utility in UKA (assessed from UKAs performed using conventional instrumentation)

The average pre-operative EQ5D score was and at one year post UKA with an average quality of life (QOL) gain of 0.405. The average implant cost per UKA in our institution was £1520 with a range from £1059 to £2004. The average total cost per case including aftercare totalled £4640.

Cost effectiveness of Robot Assisted UKA at 1-year:

$$\begin{aligned}\text{Cost effectiveness} &= \text{£ per QALY} \\ &= \text{Treatment costs} / \text{QALYs gained} \\ &= 4640 / 0.405 \\ &= \underline{\underline{\text{£11,457/QALY}}}\end{aligned}$$

Cost effectiveness of Robot Assisted UKA at 10-years:

$$\text{Discount rate 5\%} = \underline{\underline{\text{£1,427/QALY}}}$$

Cost effectiveness of Robot Assisted UKA compared to standard UKA:

$$\begin{aligned}\text{Cost effectiveness} &= \text{Difference in instrumentation costs} / \\ &\text{QALYs gained} \\ &= \text{UKA}_{\text{standard}} - \text{UKA}_{\text{robot}} / \\ &0.405 \\ &= \text{UKA}_{\text{standard}} - 300 / 0.405 \\ &= 316 - 300 / 0.405 \\ &= 16 / 0.405 \\ &= \underline{\underline{\text{£39.50/QALY}}}\end{aligned}$$

DISCUSSION

We have found that the costs of robot assisted arthroplasty using Imperial technology are equivalent to the costs associated with conventional instrumentation. Robotic assistance is cost-effective at £1,427/QALY. Our analysis also suggests that robotic assistance using the *Acrobot* system is £39.50/QALY less expensive than the standard procedure. The outcome of this advanced technology however, is not so straightforward, with several factors that may delay or prevent its widespread adoption, namely hostility to change, capital costs and the paradox of excellent outcomes.

UKA has perhaps proved a victim of its own success. The paradox of excellent function: someone whose knee feels uncomfortable will do little, but will be slow to complain or seek further painful surgery. Such a person will not wear out this joint, or any other. On the other hand, the excellent joint will make the patient feel good they will therefore do more. The quality of their life will be higher, but further problems associated with wear may be more prevalent.

Robotic arm assistance becomes even more attractive when compared to the *Da Vinci* robotic system currently used in the general surgical setting which has capital costs of \$1.5 million, and service contract costs of \$115,000 per year (8).

Unlike other expensive technology platforms, the *Acrobot* robotic arm system promises to deliver productivity with improved clinical results, at the same time as reducing costs to both the hospital and the purchaser of healthcare. A long-term prospective study examining the cost-effectiveness of robotic arm UKA is needed to further determine its role within the NHS.

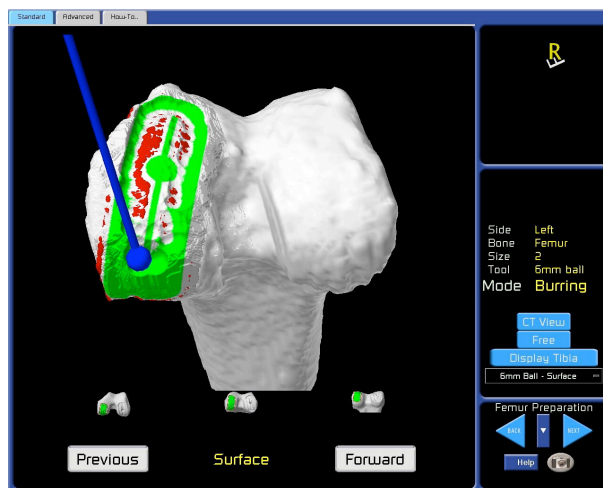


Fig. 1 Virtual image demonstrating the preparation of the femoral bone with the robotic-arm tactile guidance system (5)

REFERENCES

1. Bozic KJ, Saleh KJ, Rosenberg AG, Rubash HE. Economic evaluation in total hip arthroplasty: analysis and review of the literature. *J Arthroplasty*. 2004 Feb;19(2):180-9.
2. Newman J, Pydisetty RV, Ackroyd C. Unicompartamental or total knee replacement: the 15-year results of a prospective randomised controlled trial. *J Bone Joint Surg Br*. 2009 Jan;91(1):52-7.
3. Willis-Owen CA, Brust K, Alsop H, Miraldo M, Cobb JP. Unicompartmental knee arthroplasty in the UK National Health Service: an analysis of candidacy, outcome and cost efficacy. *Knee*. 2009 Dec;16(6):473-8.
4. Cobb J, Henckel J, Gomes P, Harris S, Jakopec M, Rodriguez F, et al. Hands-on robotic unicompartamental knee replacement: a prospective, randomised controlled study of the acrobot system. *J Bone Joint Surg Br*. 2006 Feb;88(2):188-97.
5. Conditt MA, Roche MW. Minimally invasive robotic-arm-guided unicompartamental knee arthroplasty. *J Bone Joint Surg Am*. 2009 Feb;91 Suppl 1:63-8.
6. Lonner JH, John TK, Conditt MA. Robotic arm-assisted UKA improves tibial component alignment: a pilot study. *Clin Orthop Relat Res*. 2010 Jan;468(1):141-6.
7. Jameson SS, Bottle A, Malviya A, Muller SD, Reed MR. The impact of national guidelines for the prophylaxis of venous thromboembolism on the complications of arthroplasty of the lower limb. *J Bone Joint Surg Br*. 2010 Jan;92(1):123-9.
8. Steinberg PL, Merguerian PA, Bihle W, 3rd, Heaney JA, Seigne JD. A da Vinci robot system can make sense for a mature laparoscopic prostatectomy program. *JLS*. 2008 Jan-Mar;12(1):9-12.

Maintaining Constant Tissue Contact Force for an Imaging Probe during Confocal Laser Endomicroscopy

D.P. Noonan^{1,2}, C.J. Payne¹, J. Shang¹, R. Newton^{1,2}, A. Darzi², G.-Z. Yang¹

¹*Institute of Biomedical Engineering, Imperial College London,*

²*Division of Surgery, Imperial College London*

INTRODUCTION

Probe-based confocal laser endomicroscopy (pCLE) is one of several 'optical biopsy' technologies where real-time acquisition of high-resolution *in vivo* videos and still images requires strategic manipulation of a narrow diameter probe deployed via the operating channel of an endoscope (Figure 1). Motion-free perpendicular apposition of the pCLE probe tip is often required to obtain clear still images. Constant gentle pressure is subsequently required to avoid tissue distortion. For example, during peripheral lung endomicroscopy, the probe induces a variable compression effect which disrupts the geometry of the acinus [1]. A constant contact force between the probe abutting the tissue serves to ensure consistency of the confocal tissue plane imaged, and therefore the structures visualised. The resultant stills have a field of view of less than 1mm². Whilst this can be improved by 'stitching' images together using mosaicing software [2], in order to obtain an accurate mosaic, the probe must capture the sequential images by gliding over the tissue slowly and without changing the contact force. Maintaining this constant contact force while manipulating the confocal probe manually is challenging during endoscopic interventions.

Depending on the organ being optically biopsied, these ergonomic challenges of obtaining still images and mosaics are compounded by cardiorespiratory, peristaltic and patient movement, as well as by limitations in the fine control of the pCLE probe tip using the wheels of an endoscope. The device presented in this paper aims to reduce a portion of these challenges by automatically controlling the translation of the pCLE probe tip to ensure a constant tissue force via a closed-loop force controller. It is anticipated that automating this part of an endoscopic procedure could ease and improve pCLE tissue imaging.

MATERIALS AND METHODS

This section describes the key mechatronic components of the system – an actuated, force sensitive, linear feed mechanism and a closed-loop motor control scheme.

Force sensitive linear feed mechanism

The confocal imaging probe is clamped to a force-torque sensor (ATI Nano17, calibration SI-12-0.12, resolution F_x,F_y 0.003N) from which the axial load on the optical probe can be measured directly. Naturally,

inaccuracies in the absolute force measurement will be introduced the further the sensor is clamped from the probe tip and the more tortuous the configuration of the endoscope (due to non-linear frictional interference effects along the length of the probe). However, since the aim of the system is not to provide the operator with an accurate absolute force measurement between the probe and the tissue, but rather to maintain a constant force during image acquisition, it is assumed that the force measured along the central axis of the probe is sufficiently representative of the tip interaction force to drive the force controller to maintain a constant tissue interaction force. Additionally, the probe is only expected to undergo a linear translation of 3-4mm during operation which significantly reduces the negative effects of the long transmission distance.

The force-torque sensor is clamped to a rack and pinion based linear actuator mechanism, this is shown in Figure 2. The pinion (24t, MOD 0.25) is actuated via a brushed DC geared motor (Maxon RE10 6V, 16:1 gearhead, MR Type Integrated 256cpr Quadrature Encoder). The rack (MOD 0.25) is seated in a groove which constrains all but a translational degree of freedom along the centreline of the imaging probe. A rack-pinion system was adopted for back-drivability, ease-of-use and so as to provide a fast response time which would not be possible from other forms of linear actuation. The probe is fed directly into the biopsy channel so as to prevent undesirable deflections or buckling of the probe as it is loaded axially.

Closed-loop Force Control

A closed-loop force control scheme was developed in the *LabView* development environment, a block diagram of this is shown in Figure 3. The force along the centreline of the probe was measured from the force-torque sensor is acquired using a NI-6221 acquisition card at 500Hz. This signal is then subtracted from a specified set-point value to give an error signal which is multiplied by proportional, integral and derivative gain constants. The output signal is processed by a differential operational amplifier (so as to allow bipolar control of the motor) which then forms the input of a pulse-width modulation-based speed controller for the DC motor (Maxon, LSC 30/2 linear 4Q Servoamplifier). The speed controller has an internal feedback loop which uses the integrated quadrature encoder to regulate the motor speed according to the input signal described above.

RESULTS

To demonstrate the initial feasibility of the system an experiment was conducted to demonstrate the principle whereby the probe was driven into a rigid surface until it reached the desired compressive force and held there for a number of seconds. The desired force setpoint was then adjusted in step increments of 0.1N up to a total of -1.0N and then back down to 0.0N. Figure 4 illustrates the results of this experiment, with the desired force shown in red and the measured force in blue. The plot clearly shows the ability of the system to maintain a constant pressure on the probe during stages of both increasing and decreasing force.

DISCUSSION

The results demonstrate the potential for utilizing such a system to maintain a constant tissue contact force at the probe tip. However, the current system only illustrates preliminary results for small angles of deflection of the endoscope tip (approx. $\pm 30^\circ$) and further work is required to fully characterize the system. This will include identification of realistic probe-tissue interaction forces, evaluation of the accuracy of the force measurement obtained at the distal end of the probe (through the use of a second force-torque sensor), analysis of the friction effects between the probe and the endoscope channel and evaluation of the effect of endoscope articulation on the overall measurements.

REFERENCES

- [1] Thiberville L, Salaun M, Lachkar S, Dominique S, Moreno-Swirc S, Vever-Bizet C, et al. Human in vivo fluorescence microimaging of the alveolar ducts and sacs during bronchoscopy. *Eur Respir J* 2009;33(5):974-85.
- [2] Vercauteren T, Perchant A, Malandain G, Pennec X, Ayache N. Robust mosaicing with correction of motion distortions and tissue deformations for in vivo fibered microscopy. *Med Image Anal* 2006;10(5):673-92.
- [3] von Delius S, Feussner H, Wilhelm D, Karagianni A, Henke J, Schmid RM, et al. Transgastric in vivo histology in the peritoneal cavity using miniprobe-based confocal fluorescence microscopy in an acute porcine model. *Endoscopy* 2007;39(5):407-11.



Fig. 1 Schematic illustrating an articulating endoscope (grey) and a typical confocal laser endomicroscopy imaging probe (blue). Maintaining a constant tissue contact force with such probes manually is challenging during endoscopic optical biopsy

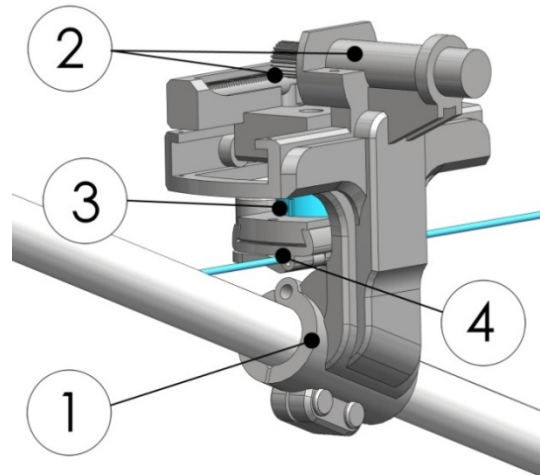


Fig. 2 Schematic illustrating Contact Force Detection System. It consists of four key components: a clamp (1) which attaches to the endoscope shaft, a Maxon RE10 Brushed DC motor driving a rack-pinion linear slider (2), a Nano17 F/T sensor (3) and a housing to clamp and thus translate the confocal imaging probe (4)

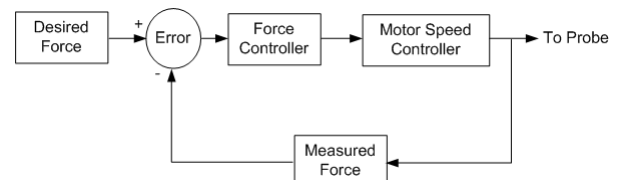


Fig. 3 Block diagram of the closed-loop force control scheme

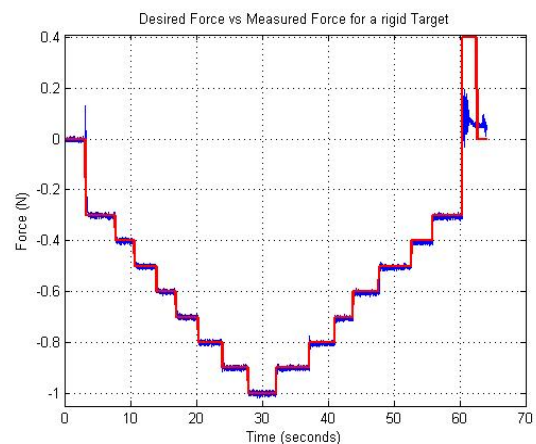


Fig. 4 Plot showing the desired force (red) versus measured force (blue) for increasing and decreasing levels of force. The high frequency oscillations at approx. 60 seconds are due to the probe disengaging from the surface

Design of a Flexural Transmission for a Dexterous Telesurgical Robot for Throat and Upper Airway: A Preliminary Result

Chin-Hsing Kuo¹, Russell H. Taylor², Jian S. Dai¹, Iulian Iordachita²

¹Department of Mechanical Engineering, King's College London, UK

²Engineering Research Center for Computer-Integrated Surgical Systems and Technology (CISST ERC), The Johns Hopkins University, USA
chin-hsing.kuo@kcl.ac.uk

INTRODUCTION

It has been perceived by the community that one of the future significant challenges for designing surgical robots is the enhancement of robot's mobility subject to the confined environments. Recently, Simaan, Taylor *et al.* [1-5] have developed a telesurgical robot for this kind of concerns. Their purpose is to design a high-dexterous surgical robot which can effectively work in a confined environment such as the throat and upper airway.

The aforementioned robotic system uses the master-and-slave concept as its structure. It basically consists of a *da Vinci* master, a stereoscopic capture and display subsystem, and a dual-arm robotic slave [5]. The master console is maneuvered by the surgeon to control the slave robotic arms, and the two slaves are supposed working together in a narrow space, like the throat and airway, to carry out the surgical operation cooperatively. Subject to the confined environment, the workspace of the slave robotic arms is limited by a long, narrow and irregularly shaped throat which can be described by a 50mm long cylinder with 40mm in diameter located 180-250mm axially down the throat [5]. Limited by the long and narrow channel, the slave arms are expected to do dexterous surgical operation such as suturing and tying knot via its end-effectors which are located in the confined working space.

Based on the design requirements and specifications as described above, the slave robotic arm has been so-designed with a lengthy structure, Fig. 1(a). Basically, it is composed of a gross actuation unit, a hollow transmission tube and a distal dexterous unit (DDU) at which the surgical operation will be performed. The hollow transmission tube attaches the actuation unit and the DDU at its both ends, and it houses four superelastic wires for delivering the motor motion from the actuation unit to the DDU. The DDU adopts a multi-backbone snake-like robot [1] as shown in Fig. 1(b), from which the pitch-and-roll motion of the moving platform is controlled by the three outer wires (Element 3) and the grasping of the gripper is controlled by the central wire (Element 4). The whole robotic arm is engaged with a screw mechanism called the "z- θ stage" which is attached to the frame and is used to provide the yaw motion and the top-and-down motion for the DDU.

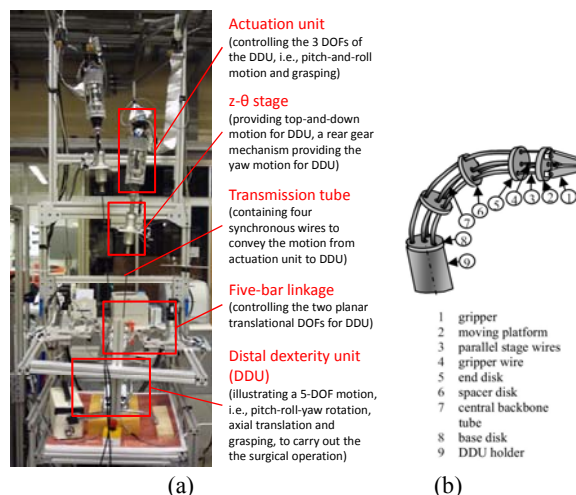


Fig. 1 (a) The composition of the slave robotic arms; (b) The DDU (Distal Dexterity Unit) [1]

From above, we can realize that when the DDU is illustrating a continuous movement that may incorporate top-and-down, roll-pitch-yaw and grasping motions as a whole, the transmission tube will experience an axial translational motion associated with a spin rotation, and the four embedded wires will follow the spin rotation of the tube but will also be bended and selectively pushed and/or pulled simultaneously. Notice that each slave robotic arm here is equipped with a five-bar linkage for controlling the quasi-planar 2-DOF motion of the DDU derived from the bending of the transmission tube. However, this set-up may be eliminated when the tube adopts a relatively rigid material for the purpose of precise control.

The above design for a single robotic arm has been successfully implemented as presented in [1-5]. However, when the two robotic arms are to be collaboratively operated in a confined environment, a crucial problem appears that, due to the relatively large actuation units (74.60mm in diameter), the two slave robotic arms cannot work in-parallel within a satisfied distance to each other (<40mm). Without modifying the actuation unit, the design of a feasible transmission that can deliver motion from the far end to the two DDUs which are working closely at a long and narrow channel therefore becomes a great challenge to be overcome.

MATERIALS AND METHOD

A novel flexural transmission for the slave robotic arm is proposed in this paper (see Fig. 2(a) and (b)). The basic design idea is as follows. First, the straight, long transmission flow is decomposed into three parts: the upper, intermediate and lower tubes. The upper and lower tubes are placed in parallel with a satisfied offset for avoiding the collision between the two actuation units. Then, two special hollow flexible joints (see Fig. 3(b)) are used to connect the upper and intermediate tubes as well as the intermediate and lower tubes, respectively. In order to assure the four wires staying at the same relative locations after a finite spin rotation, a tube cover with four centrally-distributed holes is attached to both ends of each three tubes (see Fig. 3(c)). Then, the four wires are guided to pass through the holes one-to-one for each cover, from the upper tube, intermediate tube to lower tube. Finally, the upper segments of the wires are connected to the motors in the actuation unit, while the lower segments are connected to the DDU.

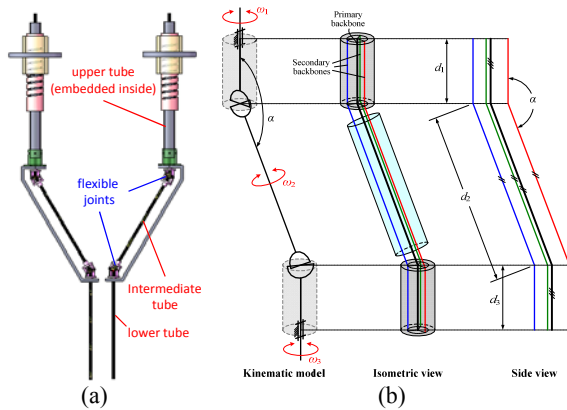


Fig. 2 The proposed concept: (a) the robotic dual-arm; and (b) the geometrical interpretation of the wire arrangement

RESULTS

A simplified SolidWorks model, which replaces the flexible joints by Hooke's joints, was built. Under this computer-aid test-rig, our new design shows that the distance between the two parallel lower tubes of the dual-arm can be potentially reduced to 28mm, measured from the symmetrical axes of the tubes, and even less (depending on the strength of the material of the housing). Also, the simulation result shows that, thanks to the use of double Hooke's joints, the spin motion between the upper and lower tubes can be transferred without any speed reduction, i.e., a 1:1 speed ratio. To further examine the actual transmission between the tubes and wires, a prototype of the flexural transmission is constructed as shown in Fig. 3. Based on a manual testing, it proves that (1) the transmission between the upper and lower tubes possesses a 1:1 speed ratio; (2) the four wire segments embedded in the upper and lower tubes can completely follow the spin rotation of their associated tubes without any speed reduction and length compensation during transmission; and (3) each wire can be independently pushed and pulled when the tubes are rotating.

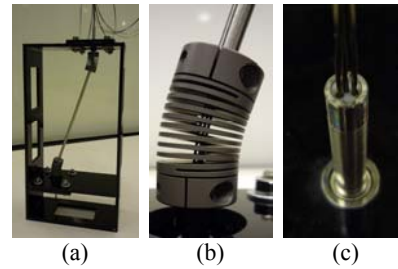


Fig. 3 Prototype of the flexural transmission: (a) overall assemblage; (b) hollow flexible joint; and (c) tube cover

DISCUSSION

The proposed transmission has demonstrated its feasibility in kinematics; however, the surface contact between the wires, tubes and tube covers might incur an unexpected friction force that will request more actuation powers for manipulating the DDU or will stop the transmission itself. The future work of this study will be concentrating on this potential problem.

ACKNOWLEDGMENTS

This work was supported in part by the CISST ERC under NSF Grant EEC 9731478, in part by Johns Hopkins University internal funds, and in part by the National Science Council, Taiwan, R.O.C. under Grant NSC-095-SAF-I-564-017-TMS. Especially, the first author would like to express his great acknowledgement to Prof. Prokar Dasgupta at the Department of Urology, King's College London for the inspiration and encouragement of developing this paper. Many thanks also go to Paul Thienphrapa at Johns Hopkins University for his help on building up the prototype.

REFERENCES

- [1] N. Simaan, R. Taylor, P. Flint. A Dexterous System for Laryngeal Surgery: Multi-Backbone Bending Snake-like Slaves for Teleoperated Dexterous Surgical Tool Manipulation. Proceedings of IEEE International Conference on Robotics and Automation. New Orleans, Louisiana, USA. 26 April-1 May, 2004; 351-7.
- [2] N. Simaan, R.H. Taylor, P. Flint. High Dexterity Snake-like Robotic Slaves for Minimally Invasive Telesurgery of the Upper Airway. Proceedings of Medical Image Computing and Computer-Assisted Intervention. Saint-Malo, France. 26-29 September, 2004; 17-24.
- [3] A. Kapoor, N. Simaan, R.H. Taylor. Suturing in Confined Spaces: Constrained Motion Control of a Hybrid 8-DoF Robot. Proceedings of the 12th International Conference on Advanced Robotics. Seattle, Washington, USA. 18-20 July, 2005; 452-9
- [4] N. Simaan. Snake-Like Units Using Flexible Backbones and Actuation Redundancy for Enhanced Minaturization. Proceedings of IEEE International Conference on Robotics and Automation. Barcelona, Spain. 18-22 April, 2005; 3023-8.
- [5] N. Simaan, K. Xu, W. Wei, A. Kapoor, P. Kazanzides, R. Taylor, P. Flint. Design and Integration of a Telerobotic System for Minimally Invasive Surgery of the Throat. The International Journal of Robotics Research. 2009; 28(9): 1134-53.

Robotic- assisted Parathyroidectomy

N Tolley¹, A Arora¹, F Palazzo¹, G Garas¹, E Edwards², R Dhawan¹, J Cox¹,
A Darzi²

¹ Dept. of Endocrine and Thyroid Surgery, Imperial Healthcare NHS Trust

² Dept. of Biosurgery and Technology, Imperial College London
asitarora@doctors.org.uk

INTRODUCTION

Telerobotic technology has successfully been applied in several surgical specialties to address the limitations of endoscopic and open minimal access surgical techniques[1]. The application of telerobotic assisted neck surgery in targeted parathyroidectomy has not been investigated. The aim of this study was to develop and prospectively evaluate a robotic assisted technique which permits a non-insufflation, 'scar-less in the neck' approach.

MATERIALS AND METHODS

An ethically approved prospective pilot cohort study of 10 patients with Primary Hyperparathyroidism was conducted between May 2009 and April 2010. Triple modality pre-operative localisation was a pre-requisite. Seven patients underwent robotic assisted parathyroidectomy (RAP) and three patients had a conventional mini-cervicotomy. Intra-operative outcome measures included procedure time and blood loss. Post-operative measures included biochemical and histopathological assessment. Patient-reported outcome measures (PROMs) included subjective assessment of pain and scar cosmesis using visual analogue scores (0-100), Voice Disability Index 2 and EQ-5D quality of life assessment performed 1 day, 2 weeks, 3 and 6 months post-operatively. Mean length of follow up was 4.5 months.

RESULTS

In all cases the parathyroid adenoma was successfully removed with negligible blood loss and no RAP conversions. The recurrent laryngeal nerve was identified, preserved and subjective voice assessment demonstrated no postoperative voice change. Robot docking and exposure times plateaued to 20 minutes after 2 and 4 cases respectively. The mean robot console time was 65 minutes (range 25-105 minutes). Factors determining this included body habitus, size of the lesion and surgical access. The mean VAS for scar cosmesis was 71% in both cohorts on the first post operative day and improved in the robotic cohort at 2 weeks, 3 and 6 months compared to the control group (91% vs. 74% at 6 months). Post-operative pain was initially similar in both cohorts and decreased to 9% in the robotic cohort whilst in the control group it increased to 41% at 2 weeks. All EQ-5D quality of life

parameters significantly improved following surgery with no significant difference between cohorts at 6 months. Mean time to daily activities was 3.4 days in the robotic cohort and 6.5 days in the control group.



Fig. 1 Surgical approach for Left RAP; ipsilateral 2.5cm infraclavicular incision and three 8-12mm trocars inserted in the anterior axillary line

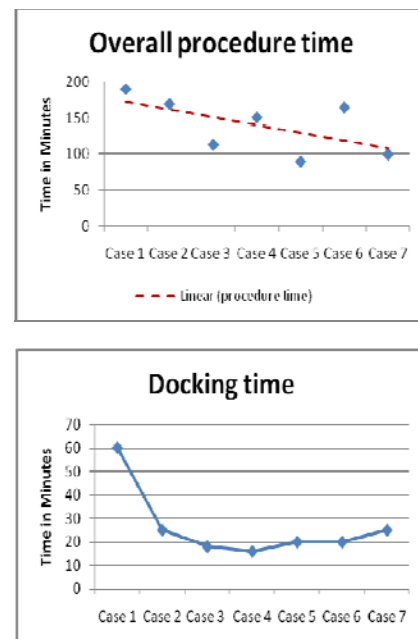


Fig. 2 Learning Curve for RAP

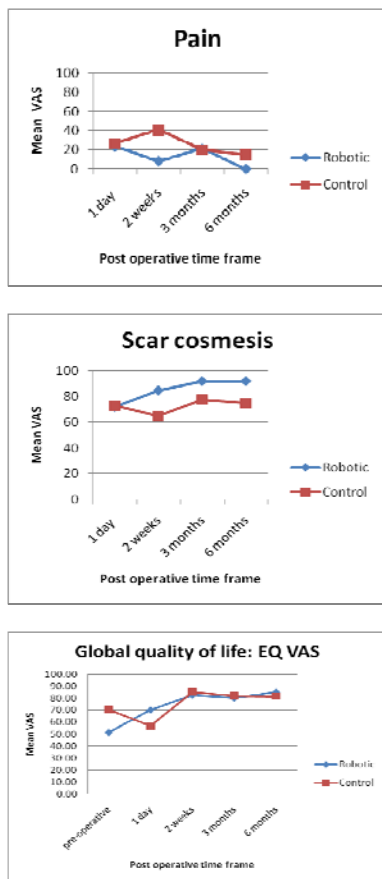


Fig. 3 PROMS for Pain (100 represents worst imaginable pain), Scar Cosmesis (100 represents completely satisfied) and Quality of Life (100 represents best imaginable health state).

DISCUSSION

Targeted parathyroidectomy represents the co-standard of treatment in at least 65% of patients with PHPT with cure and complication rates equivalent to the conventional open approach [2]. Parathyroid adenomas are ideal candidates because they are usually small, benign and can be accurately localised with ultrasound and sestamibi studies. However, existing approaches all require one or more cervical incision. The widespread adoption of the targeted endoscopic approach has also been limited by concerns such as restricted freedom of instrument movement, suboptimal depth perception, imprecise tissue manipulation and assistant dependence[3].

RAP overcomes these limitations and the primary advantage for the patient is that it avoids a scar in the neck and permits precise, minimal subcutaneous dissection. This translates to reduced post-operative pain within the first 2 weeks of surgery and a rapid return to work/daily activities. The mean time to return to work/daily activities in the robotic cohort was 3.4 days compared to 6.5 days in the control group. All patients were discharged within 24 hours which is comparable to existing approaches.² The improvements

in quality of life are at least comparable to conventional minimally invasive techniques.

Scars in easily visible parts of the body such as the anterior neck can have detrimental effects on body image and are perceived as worse than those that can be hidden by clothing.⁴ RAP avoids a neck scar by using an infra-clavicular incision which is concealed even by low cut tops. The mean length of this incision was 2.5cm compared to a 3cm cervical incision in the control group. The 6 month post-operative mean VAS scores for scar cosmesis in the RAP cohort was over 90% compared to 74% in the control group.

The harmonic scalpel was successfully utilised in all cases and resulted in minimal blood loss. Intra-operative recurrent laryngeal nerve (RLN) stimulation was performed and vocal cord function was assessed with fiberoptic laryngoscopy both pre- and post-operatively. The RLNs were identified and stimulated normally (1mA) in all cases. No nerve injury was recorded and all patients reported no voice change post operatively. No complications occurred in the RAP patient cohort (bleeding, hypocalcaemia, wound infection) and there was no need for conversion to open surgery. The parathyroid adenoma was completely excised in all cases which was confirmed both histopathologically and biochemically.

The learning curve associated with robotic surgery has been well described in other surgical fields.⁵ With the RAP technique, docking and closure times rapidly plateaued after the 2nd and 3rd cases respectively to approximately 20 minutes whilst exposure times plateaued to a similar timeframe after the fourth case. The main factors which determined exposure and console times were body habitus, the size and location of the abnormal parathyroid lesion and access to the operative site.

This preliminary report demonstrates that RAP is safe, feasible and represents a novel targeted 'scar-less in the neck' surgical approach for treating patients with PHPT in which the abnormal gland has been convincingly localised preoperatively.

REFERENCES

- [1] Tewari A, Srivasatava A, Menon M. A prospective comparison of radical retropubic and robot assisted prostatectomy. *BJU* 2003;92:205-10.
- [2] Henry J. Minimally invasive thyroid and parathyroid surgery is not a question of length of incision. *Langenbecks Arch Surg* 2008;393:621-6
- [3] Chung YS, Choe JH, Kang KH et al. Endoscopic thyroidectomy for thyroid malignancies: comparison with conventional open thyroidectomy. *World J Surg.* 2007;31:2302-06
- [4] Lawrence JW, Fauerbach JA, Heinberg L, Doctor M. Visible vs hidden scars and their relation to body esteem. *J.Burn Care Rehabil.* 2004;25:25-32.
- [5] Kaul S, Shah N, Menon M. Learning curve using robotic surgery. *Endourol* 2006;7:125-29

Author Index

A

Abi-Nahed, J. 31
Abulaban, B. 31
Alleemudder, Adam 15
Anstee, Ann 35
Arbeille, P. 1
Arora, A. 73
Athanasίου, Thanos 21

B

Baumann, M. 47
Beatty, John 29
Bell, B. 11
Bello, F. 57
Bicknell, C.D. 3

C

Can, S. 23
Canou, Joseph 1
Cavallotti, C. 63
Caversaccio, M. 11
Challacombe, Ben 13, 29, 43, 53
Chen, Dongbin 35
Cheshire, N.J.W. 3
Clancy, N.T. 49
Clark, James 21, 39
Cobb, J.P. 67
Cohen, Daniel 33, 35
Coker, B. 13
Corbishley, C. 33
Cox, J. 73

D

Dai, Jian S. 71

Dario, P. 27, 63
Darzi, Ara 21, 33, 35, 39, 69, 73
Dasgupta, P. 13, 41, 43, 53
Davies, B.L. 5, 9, 61
Degenaar, P. 61
Dhawan, R. 73
Dombre, E. 19
Donnez, J. 19
Dudderidge, Tim 15, 29

E

Edwards, Philip 35, 73
Elhage, O. 13, 41, 43, 53
Elle, Ole Jakob 25
Elson, D.S. 49
Ernst, F. 37
Essomba, Terence 1
Euler, E. 55

F

Feussner, H. 23
Fichtinger, G. 7
Fiolka, A. 23
Fonte, Aicha 1
Fraisie, P. 1
Frasson, L. 5

G

Garas, G. 73
Gerber, N. 11
Gondhalekar, A. 9
Gould, D. 57
Grandhi, Uttam 51
Grieve, A. 13
Guion, P. 7

H

Hall, E. 33
Hamady, M. 3
Hannaford, Blake 25
Hawkes, D. 41
Hegarty, N. 43
Herman, B. 19
How, T. 57
Hrouda, David 15
Hurst, S.A. 67

I

Iordachita, Iulian 71

J

James, David R.C. 21, 39, 49

K

Karimyan, Vahe 39
Kaushal, A. 7
Kerr, K. 33
Khan, M.S. 13
Khoubehi, Bijan 15
Knoll, A. 23
Ko, S.Y. 5
Krieger, A. 7
Krupa, Alexandre 1
Kuo, Chin-Hsing 71
Kósa, G. 45

L

Landes, J. 55
Lasso, A. 7
Lavan, Lisa 29
Lee, D. 17
Lee, Su-Lin 65

Lerotic, Mirna 65
Lewis, R. 33
Littler, P. 57
Luboz, V. 57

M

Mayer, Erik 33, 35
Menciassi, A. 27, 63
Morel, G. 47
Mozer, P. 47
Murphy, D. 13

N

Naerum, Edvard 25
Navab, N. 55
Neal, D.E. 17
Newton, R. 69
Nielsen, E. 11
Nobari, E.S. 59
Nolte, L.P. 11
Noonan, David 21, 69
Nuyens, J. 31

O

Odetoyinbo, T. 57
Ogden, Chris 29
Orihuela-Espina, Felipe 39

P

Palazzo, F. 73
Papadopolous, A. 17
Parittotokkaporn, T. 61
Payne, Christopher 21, 69
Penney, G. 41
Petroni, G. 27
Piccigallo, M. 27
Piercy, D. 33

Q

Quaglia, C. 27

R

Rao, Amrith 15

Rashid, Tina 29

Raucent, B. 19

Reddi, Bhavani Rao 51

Riga, C.V. 3

Rimington, P. 13

Rodriguez y Baena, F.M. 5, 9, 59, 61

S

Salzmann, J. 11

Sauvage, V. 49

Scarfogliero, U. 27

Schlaefer, A. 37

Schneider, A. 23

Schweikard, A. 37

Schwingshackl, C. 9

Shah, N.C. 17

Shang, Jianzhong 21, 69

Sharma, N.L. 17

Shortland, A. 53

Silvestri, M. 63

Simi, M. 63

Slawinski, C. 43

Sodergren, Mikael 21, 39

Stender, B. 37

Stieger, C. 11

Stoyanov, Danail 35, 49

Székely, G. 45

T

Taylor, Russell H. 71

Teare, Julian 21

Tenzer, Y. 9

Thompson, S. 41

Tolley, N. 73

Torterotot, C. 47

V

Valdastri, P. 27, 63

Vale, Justin 15, 33

Vatteroni, M. 63

Vieyres, Pierre 1

Vikal, S. 7

Vitrani, M.-A. 47

von der Heide, A. 55

Vowler, S. 17

W

Wan, Elaine 29

Wang, L. 55

Weber, S. 11

Weidert, S. 55

Whitcomb, L.L. 7

X

Xu, H. 7

Y

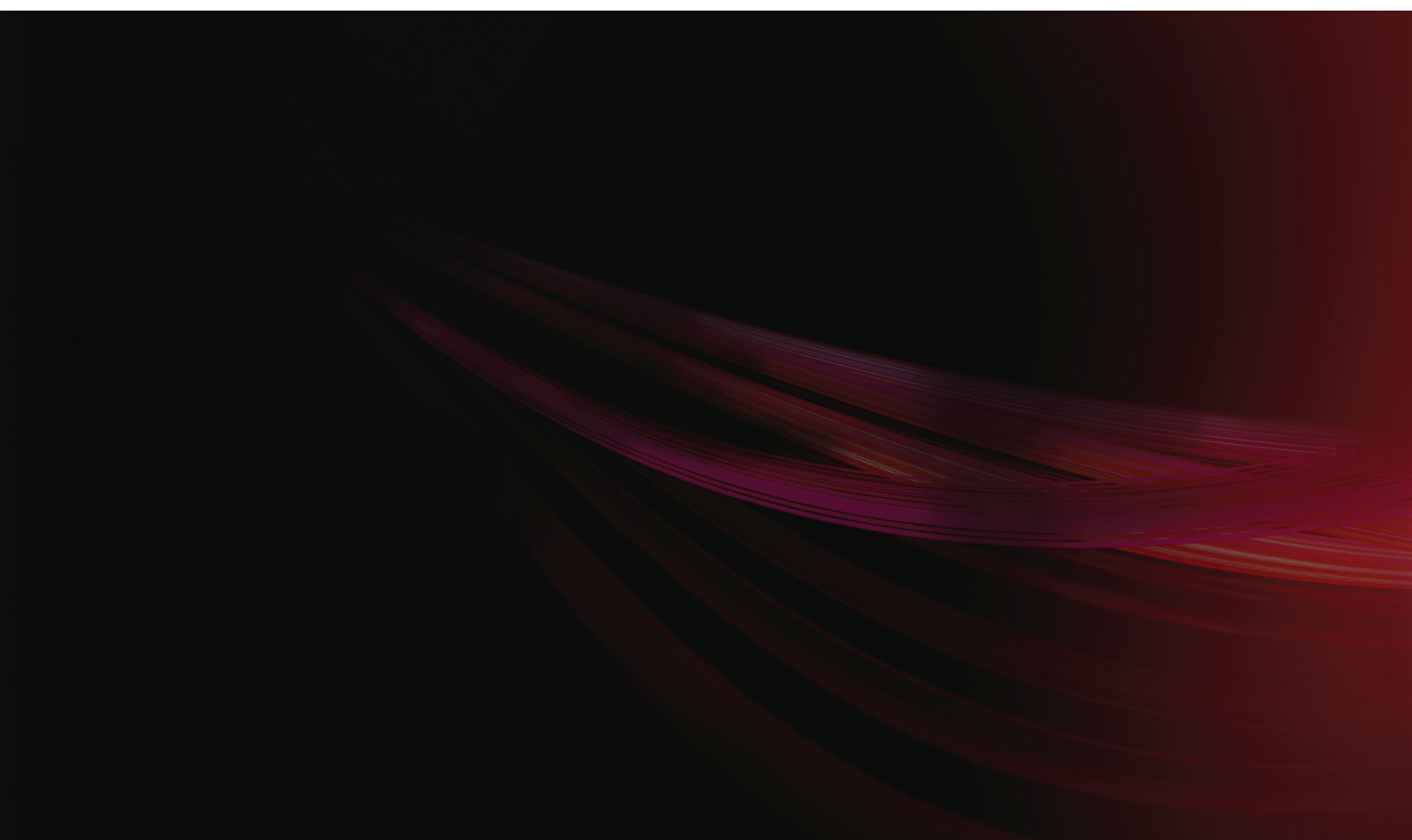
Yang, Guang-Zhong 21, 35, 39, 49, 69

Z

Zegloul, Said 1

Zhai, J. 57

Zheng, G. 11



Proceedings of
The Hamlyn Symposium on Medical Robotics
25 May, 2010, The Royal Society
London, UK
ISBN: 978-0-9563776-1-6